Aeolian Transport and Vegetative Capture of Particulates

by
John W. Glendening

P.I. Peter C. Sinclair

Department of Atmospheric Science
Colorado State University
Fort Collins, Colorado

Colorado State University

Department of Atmospheric Science

Paper No. 310

AEOLIAN TRANSPORT AND VEGETATIVE CAPTURE OF PARTICULATES

By

John W. Glendening

Preparation of this report
has been financially supported by
AEC (ERDA) Grant #5594605
monitored by the Lawrence Livermore Laboratory

Department of Atmospheric Science
Colorado State University
Fort Collins, Colorado

May, 1979

Atmospheric Science No. 310

ABSTRACT

AEOLIAN TRANSPORT AND VEGETATIVE CAPTURE OF PARTICULATES

Aeolian (wind-blown) transport of soil particles to which plutonium is attached is responsible for the escape of radioactivity beyond the boundaries of the Nevada Test Site. This thesis concerns the horizontal aeolian erosion of the large particles, which travel close to the ground. They are captured by desert creosote bushes, building radioactive wind hummocks around the shrub bases.

The airflow above and below the average shrub height and inside a bush is investigated. The drag coefficient above the vegetation is found to decrease with increasing wind speed. Below the shrub height, the development of an internal boundary layer results in a logarithmic velocity profile. The bushes are widely spaced and aerodynamically very porous, producing a flow more typical of individual roughness elements than of a plant canopy. Partitioning the total drag above the vegetation into ground drag and bush drag contributions illustrates the dominant role of the vegetation in producing drag and thereby controlling soil erosion.

The yearly horizontal erosion flux below bush height is estimated to be 40 grams per year per cm width, based upon monthly wind and soil moisture data and field erosion measurements. The ground stress needed to initiate movement is close to the minimum stress determined by Bagnold. Under these low erosion conditions the bush hummocks cannot grow large enough to significantly affect the ground stress inside the bush, so the limit to hummock growth is the creosote bush life span. It is concluded that the larger eroding

particles are trapped by the bushes as they build hummocks, thus this mode of radioactive transport is negligible compared to the resuspension transport.

John W. Glendening
Department of Atmospheric Science
Colorado State University
Fort Collins, Colorado 80523
Fall, 1977

ACKNOWLEDGEMENTS

The author expresses his sincere appreciation to his advisor, Professor Peter C. Sinclair, for his support and advice throughout the prepartation of this thesis. Thanks are also expressed to Dr. Robert N. Meroney, for his suggestions and encouragement, and to Drs. Jack E. Cermak and Elmar R. Reiter for reviewing this work. Messrs. Norm Kennedy, Ralph Quiring, and Don Homan provided data which was incorporated into this thesis. Appreciation is also extended to Drs. C.W. Ferguson, A. Klute, R. Moses, and F. Went for their helpful discussions. I am indebted to Ms. Julie Wilson for typing this manuscript.

This research was sponsored by AEC (ERDA) Grant #5594605 which was monitored by the Lawrence Livermore Laboratory.

TABLE OF CONTENTS

TABLE OF CONTENTS (cont'd)

LIST OF TABLES

LIST OF FIGURES

LIST OF FIGURES (cont'd)

LIST OF SYMBOLS

Symbol	Definition	Dimension
A_s	Ground area covered by shrub	L^2
A_f	Shrub frontal silhouette area (= DH)	L^2
C (z)	Saltation mass concentration at height z	M/L^3
C_d	Surface meteorological drag coefficient (= U_*^2/U^2)	
C_{da}	Surface aerodynamic drag coefficient	
c_d	Meteorological drag coefficient of individual shrub	
D	Shrub diameter	L
D_o	Zero plane displacement height	L
d	Particle diameter	L
E	Empirical constant in erosion flux equation	MT^3/L^3
F	Horizontal erosion flux	M/LT
F_d	Drag force	ML/T^2
F_m	Vertical momentum flux	ML^2/T^2
g	Gravitational acceleration	L/T^2
H	Shrub height	L
K_h	Eddy heat transfer coefficient	L^2/T
K_m	Eddy momentum transfer coefficient	L^2/T
k	von Karman constant	
L	Monin-Obukhov scaling length	L
M	Moisture content of soil	M/L^3
M (15 atm)	Soil moisture content at 15 atm suction	M/L^3
n	Frequency	T^{-1}

LIST OF SYMBOLS (cont'd)

Symbol	Definition	Dimension
n_i	Frequency of SYSTRAC winds	T^{-1}
P	Mean atmospheric pressure	M/LT^2
Q	Erosion wind factor $[= \Sigma_i n_i U_i^2 (U_i - U_t)]$	L^3/T^4
q	Mean kinetic energy of turbulence	L^2/T^2
R	Gas constant	$L^2/\theta T^2$
Ri	Richardson number	
RH	Relative humidity of air	
S	Specific area per bush	L^2
S_u (n)	Spectral density function	L^2/T
T	Mean air temperature	θ
U (z)	Mean horizontal wind at height z	L/T
U_i	Mean of SYSTRAC velocity interval	L/T
U_{meas}	Total velocity measured by hot wire anemometer	L/T
U_t	Saltation threshold velocity	L/T
U_*	Surface friction velocity ($= \tau_o/\rho$)	L/T
$(U_*)_g$	Surface friction velocity of ground ($= \tau_g/\rho$)	L/T
$(U_*)_t$	Saltation threshold friction velocity	L/T
$\Delta(U_*)_t$	Threshold friction velocity increase due to non-zero soil moisture	L/T
u	Fluctuating horizontal velocity	L/T
u_*	Friction velocity ($= \tau/\rho$)	L/T
V	Mean transverse velocity	L/T
W (z)	Mean vertical velocity at height z	L/T

LIST OF SYMBOLS (cont'd)

Symbol	Definition	Dimension
W_{max}	Estimated maximum of vertical velocity	L/T
w	Fluctuating vertical velocity	L/T
x	Horizontal distance	L
Z_o	Characteristic roughness length above vegetation	L
z	Vertical distance	L
z_o	Characteristic roughness length of ground	L
α_1	Kolmogorov one-dimensional constant	
Γ	Adiabatic lapse rate	θ/L
γ	Diabatic correction to equilibrium equation	
δ	Height of internal boundary layer	L
ε	Viscous dissipation of turbulence	L^2/T^3
ζ	Monin-Obukhov dimensionless height (= z/L)	
θ	Fluctuating air temperature	θ
λ	Roughness element concentration parameter (= A_f/S)	
ν	Kinematic viscosity of air	L^2/T
ρ	Density of air	M/L^3
ρ_p	Density of particle	M/L^3
σ	Standard deviation	
σ_u	RMS velocity variation (= $\sqrt{\overline{u^2}}$)	L/T
τ	Shear stress	ML^2/T^2
τ_o	Total surface shear stress above vegetation (= $\tau_b + \tau_g$)	ML^2/T^2
τ_b	Surface stress due to vegetation	ML^2/T^2

LIST OF SYMBOLS (cont'd)

Symbol	Definition	Dimension
τ_g	Surface stress due to ground	ML^2/T^2
Φ	Moisture potential of soil	L
ϕ	Shrub porosity	
Ψ	Diabatic correction to logarithmic wind profile	
Ω	Foliage area per unit volume	L

Any other symbol not listed here is explained whenever it appears.

1. INTRODUCTION

Releases of radioactive plutonium have contaminated soil on the Nevada Test Site (NTS). Aeolian (wind-blown) transport of particulates with attached plutonium is responsible for the escape of this toxic element beyond the NTS boundaries. The transport is believed to occur mainly through resuspension, small (diameter < 80 μm) contaminated particles being lifted vertically and then moving with the wind. This thesis examines the horizontal transport of the larger contaminated particles which cannot be resuspended by turbulence, i.e. wind erosion.

On the Nevada Test Site the wind loosens, picks up, and transports contaminated soil particles comprising the desert pavement. Creosote bushes capture the eroding particles, building hummocks up to 20 cm high under the bushes. These wind hummocks are more radioactive than the surrounding soil.

This thesis considers the yearly erosion flux and the capture of loosened material by the vegetation, as well as the airflow so important to both processes. Wind profiles above and below bush height and inside a bush are obtained. This allows the partitioning of the total drag into the drag on the bushes and the drag on the ground. The latter causes wind erosion, and this partitioning measures the effectiveness of the vegetation in reducing erosion. The threshold surface stress needed to dislodge the soil particles is determined. The magnitude of the desert erosion flux is estimated from wind data, based upon actual field measurements with corrections for soil moisture factors. Finally the effectiveness of the shrubs

in capturing the eroding particles, the resulting mound growth rate, and limitations to hummock growth are discussed.

2. NEVADA TEST SITE DESCRIPTION

The Nevada Test Site (NTS) encompasses an approximately rectangular area 50 miles (N-S) by 30 miles (E-W) in southern Nevada, 65 miles northwest of Las Vegas (Fig. 1). The terrain is extremely irregular, consisting of generally north-south ridges and valleys with a north to south downward slope. The valleys consist of gently to moderately sloping alluvial fans and terraces. The climate is typical of the Great Basin desert with high midday temperatures and low precipitation, producing typical desert vegetation.

The U.S. Atomic Energy Commission conducted nuclear explosions at NTS between 1951 and 1963 using plutonium (Pu^{239}) in both critical and subcritical configurations. Some of this radioactive plutonium has moved outside the NTS boundaries (Bliss and Dunn, 1971). The primary source of this escaped plutonium is believed to be the so-called "safety" explosions designed to test the effects of an accidental detonation of the high explosive trigger of a nuclear bomb. These explosions scattered large amounts of plutonium. Neither the accidental ventings of underground explosions nor the release of unfissioned plutonium from above ground full scale nuclear explosions are considered to be major sources of escaped plutonium. The movement is mainly by aeolian (wind-blown) transport with water transport playing a secondary role (Eberhardt and Gilbert, 1974). The escape of plutonium, a very hazardous toxic element with an extremely long half life, beyond the confines of federally controlled land is important because it raises the possibility of human health

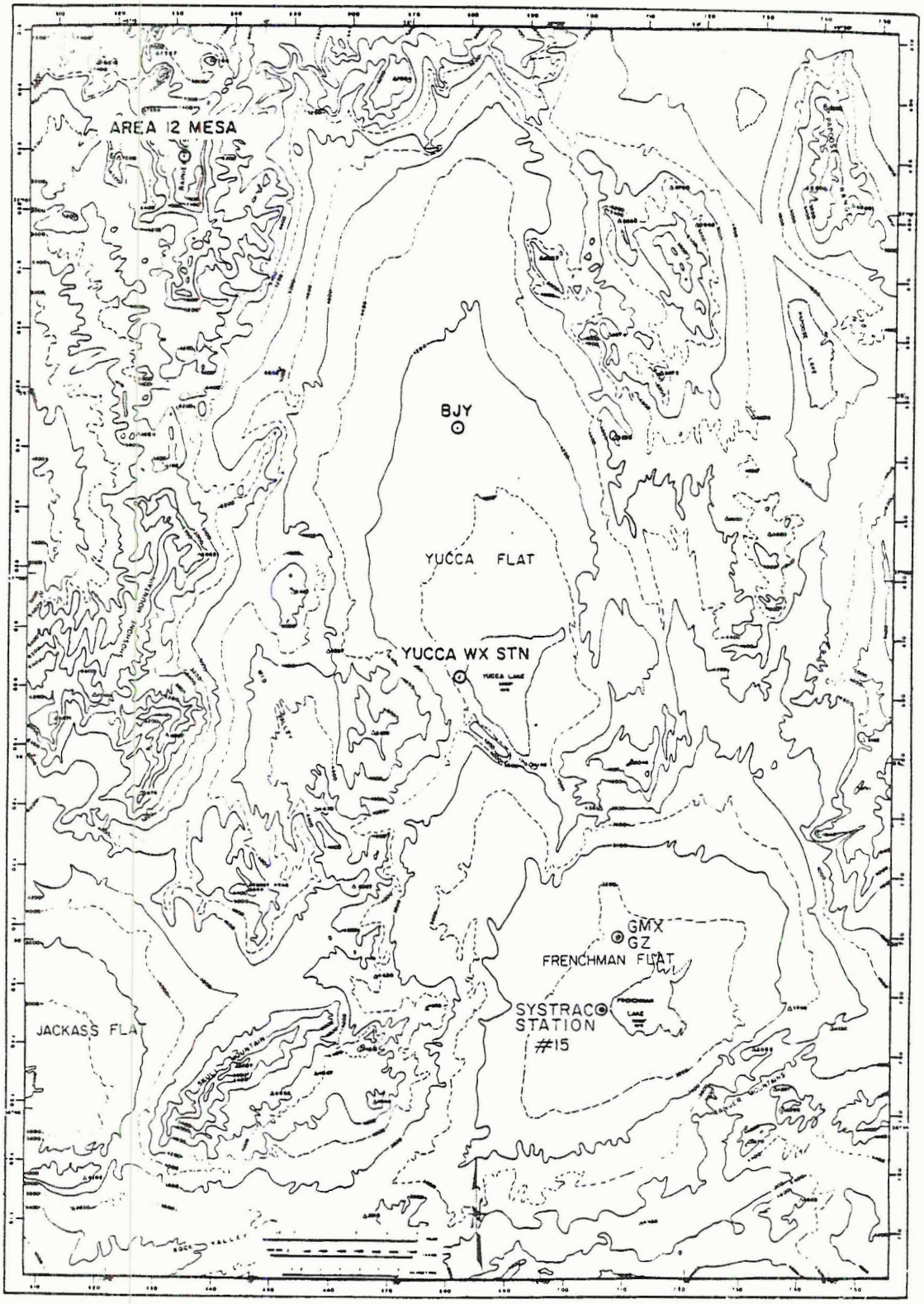

Fig. 1. Nevada Test Site (NTS) Locations (after Quiring, 1968)

damage from inhalation of resuspended plutonium or from injestion of plutonium picked up by plants or animals in the food chain.

2.1 Climatology

The climate of the NTS area is typical of a high desert basin with large temperature variations, predominately clear skies, and low relative humidities (Table 1). The average daily temperature range is about 50°F on a clear dry day in summer or autumn. The temperature can reach an extreme of 110°F. The annual average precipitation is about six inches. The rainfall maximum occurs in January and February, tapering off to a pronounced minimum in June. It then rises to a secondary maximum in July and August, followed by a rapid decline to a secondary minimum in October and a rise to the winter maximum. The wind regime is typical of mountain-valley terrain. Southerly winds predominate during daylight hours during the warm half of the year. In winter, by mid-day there is sufficient heating on the mountain slopes to introduce a southerly component. Westerly to northeasterly winds prevail at night during all months. The strongest winds occur during the spring. The wind speed shows a strong diurnal effect, peaking at 1500 hours (Fig. 2).

2.2 GMX Area

The experimental observations for this thesis were made in the GMX area of NTS. It is a region about 1 km square located within the much larger Frenchman Flat region (Fig. 1). GMX is generally flat at an elevation of 910 meters. The elevation increases slowly to the north and the area is crossed by shallow stream channels

TABLE 1

Nevada Test Site 10 Year Climatological Summary (1962-1971)

LATITUDE 36° 57' N
LONGITUDE 116° 03' W
ELEVATION 3,924 Feet

YUCCA FLAT, NEVADA – NEVADA TEST SITE

NEVADA COORDINATE SYSTEM (Central)
E680,875
N803,600

MONTH	TEMPERATURE (°F) Averages: Daily Maximum	Daily Minimum	Monthly	Extremes: Highest	Year	Lowest	Year	DEGREE DAYS (Base 65°): Heating	Cooling	PRECIPITATION (Inches): Average	Greatest Monthly	Year	Least Monthly	Year	Greatest Daily	Year	Snow: Average	Greatest Monthly	Year	Greatest Daily	Year
JAN	52.1	20.8	36.5	73	1971	-2	1970	877	0	.53	4.02	1969	T	1971#	1.25	1969	0.9	4.3	1962	4.3	1962
FEB	56.7	25.8	41.3	77	1963	5	1971#	662	0	.84	3.55	1969	T	1967#	1.16	1969	1.9	17.4	1969	6.2	1969
MAR	60.9	27.7	44.3	87	1966	9	1969	634	0	.29	.60	1969	.02	1966	.38	1969	2.0	7.5	1969	4.5	1969
APR	67.8	34.4	51.1	89	1962	13	1966	411	1	.45	2.57	1965	T	1962	1.08	1965	0.7	3.0	1964	3.0	1964
MAY	78.9	43.5	61.2	97	1967	25	1967	147	38	.24	1.62	1971	T	1970#	.86	1971	0	T	1964	T	1964
JUN	87.6	49.9	68.8	107	1970	29	1971#	35	154	.21	1.13	1969	T	1971	.45	1969	0	0		0	
JUL	96.1	57.0	76.6	107	1967	40	1964#	0	366	.52	1.34	1966	0	1963	.77	1969	0	0		0	
AUG	95.0	58.1	76.6	107	1970	39	1968	1	368	.34	1.04	1965	0	1962	.35	1971#	0	0		0	
SEP	86.4	46.7	66.5	105	1971	25	1971	51	103	.68	2.38	1969	0	1968#	2.13	1969	0	0		0	
OCT	76.1	36.9	56.5	94	1964#	12	1971	266	9	.13	.45	1969	0	1967#	.42	1969	0	T	1971	T	1971
NOV	61.8	27.6	44.7	82	1962	13	1966	602	0	.71	3.02	1965	0	1962	1.10	1970	0.5	4.8	1964	2.3	1964
DEC	50.7	19.9	35.3	70	1964	-14	1967	914	0	.79	2.66	1965	T	1969#	1.31	1965	2.3	9.9	1971	7.4	1971
ANN	72.5	37.4	54.9	107	AUG 1970#	-14	DEC 1967	4600	1039	5.73	4.02	JAN 1969	0	SEP 1968#	2.13	SEP 1969	8.3	17.4	FEB 1969	7.4	DEC 1971

MONTH	RELATIVE HUMIDITY (%) Hour (Pacific Standard Time): 04	10	16	22	WIND (Speeds in mph) (a): Average Speed	Peak Speed	Year	Resultant (Dir/Sp): 23-02 PST	11-14 PST	STATION PRESSURE (Inches): Averages	Highest	Lowest	(b) Average Sky Cover Sunrise to Sunset	AVERAGE NUMBER OF DAYS Sunrise to Sunset: Clear	Partly Cloudy	Cloudy	Precipitation: .01 inch or more	.10 inch or more	.50 inch or more	1.00 inch or more	1.0 inch or more of snow	Thunderstorms	Temperature Maximum: 90° F or more	32° F or less	Minimum: 32° F or less	0° F or less
JAN	67	49	35	60	6.6	58	1965	233/0.7	135/2.6	26.10	26.54	25.42	4.9	13	8	10	2	1	X	X	X	X	0	1	29	X
FEB	67	45	32	56	6.9	52	1967	275/1.1	118/2.7	26.05	26.42	25.56	5.0	11	8	9	3	2	X	X	1	0	0	X	23	0
MAR	58	31	23	44	8.4	55	1971	240/1.8	186/4.5	25.99	26.43	25.48	4.8	12	9	10	3	1	0	0	1	1	0	0	24	0
APR	52	27	21	38	9.1	60+	1970#	250/2.2	198/5.1	25.96	26.39	25.50	4.5	13	9	8	3	1	X	X	X	1	0	0	12	0
MAY	46	22	17	31	8.3	60+	1967	260/1.5	179/7.2	25.94	26.39	25.47	4.3	14	11	6	2	1	X	0	0	1	4	0	2	0
JUN	39	19	14	26	7.9	60+	1967	272/1.9	185/8.2	25.92	26.20	25.56	3.0	19	7	4	2	1	0	0	0	2	14	0	X	0
JUL	40	20	15	28	7.5	55	1971	278/0.9	185/12.0	26.00	26.19	25.68	3.0	19	9	3	3	2	X	0	0	4	29	0	0	0
AUG	44	23	16	30	6.7	60+	1968	222/1.5	182/12.0	26.00	26.22	25.71	3.0	20	8	3	3	1	0	0	0	4	27	0	0	0
SEP	43	21	17	32	7.0	52	1970	281/1.3	163/6.4	26.00	26.36	25.56	2.1	22	6	2	2	1	1	X	0	2	11	0	1	0
OCT	46	24	19	36	6.8	60	1971	286/1.3	138/3.7	26.06	26.40	25.52	2.9	20	7	4	1	1	0	0	0	X	2	0	9	0
NOV	61	39	31	52	6.1	51	1970	234/1.2	152/4.1	26.08	26.58	25.64	4.8	13	7	10	3	2	X	X	X	X	0	0	23	0
DEC	68	50	41	64	6.6	53	1970	288/1.9	109/1.0	26.07	26.59	25.49	4.6	14	8	9	3	1	1	X	1	X	0	1	29	1
ANN	53	31	23	41	7.4	60+	APR 1970#	—	—	26.01	26.59	25.42	3.9	190	97	78	30	14	3	1	3	14	87	2	152	1

X One or more occurrences during the period of record but average less than 0.5 day.

\# Most recent of multiple occurrences.

\+ Peak speed exceeded the upper limit of the anemometer recorder.

T Trace, an amount too small to measure.

(a) Average and peak speed are for the period starting with December 1964. The direction and magnitude of the resultant wind are from a summary covering the period December 1964 through [illegible] 1969.

(b) Sky cover is expressed in the range from 0 for no clouds to 10 when the sky is completely covered with clouds. Clear, partly cloudy and cloudy are defined as average daytime cloudiness of 0-3, 4-7 and 8-10 tenths, respectively.

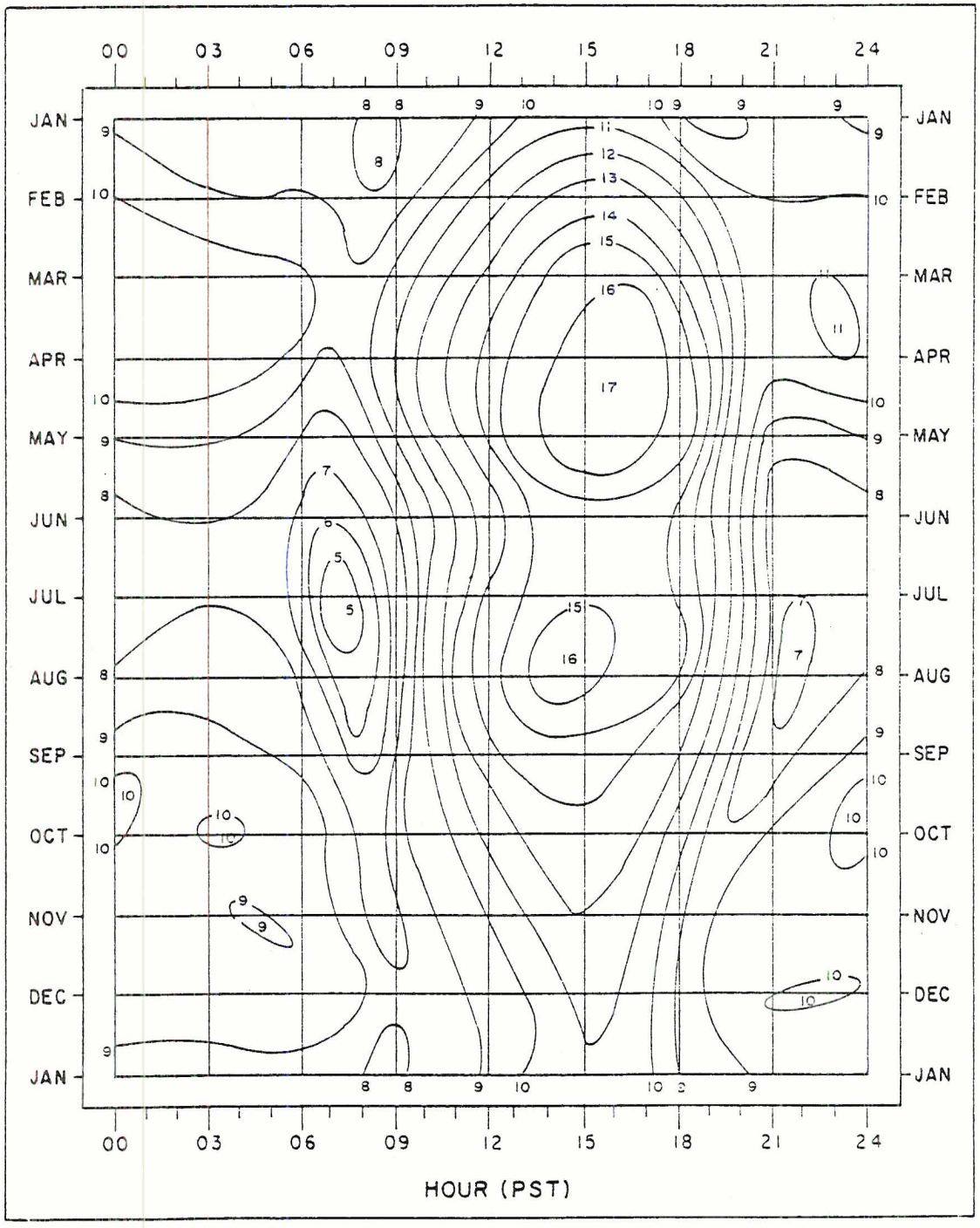

Fig. 2. NTS Wind Speed in Miles per Hour as a Function of Time of Day (from Quiring, 1968)

with a broad southward drainage. Low wind hummocks are found around the bushes.

From December 1954 to February 1956 22 small high explosive "safety" detonations released a few curies of plutonium. The area of measurable contamination is about 0.12 km^2, surrounded for several kilometers by a region of similar terrain and vegetative cover. This "safety" explosion region has frequently been used to study the plutonium escape problem. Anspaugh et al. (1976) investigated the wind-induced resuspension of plutonium contaminated soil particles, and Sinclair (1976) estimated the downwind transport due to dust devil activity. Soil (Tamura, 1974), vegetative (Romney et al., 1974), and animal (Smith, 1974) removal have all been studied in this area.

Environmental weathering over the 20 year period following the plutonium releases has intimately associated the plutonium, in the form of plutonium oxide, with host soil particles. The plutonium activity spread from ground zero downwind in the prevailing wind direction as the contaminated soil particles were dislodged and transported by wind forces, resulting in an elongated radioactive isopleth pattern (Fig. 3). Thus the radioactivity moves principally through aeolian transport of contaminated soil particles.

2.3 Test Bush Site

The primary wind measurements were made at a site on the western edge of the GMX area because of the presence of a previously established meteorological tower (Fig. 4). The site was located on an alluvial fan sloping southward with a gradient of 1-2%. It was surrounded by evenly spaced vegetation with an upwind fetch of over

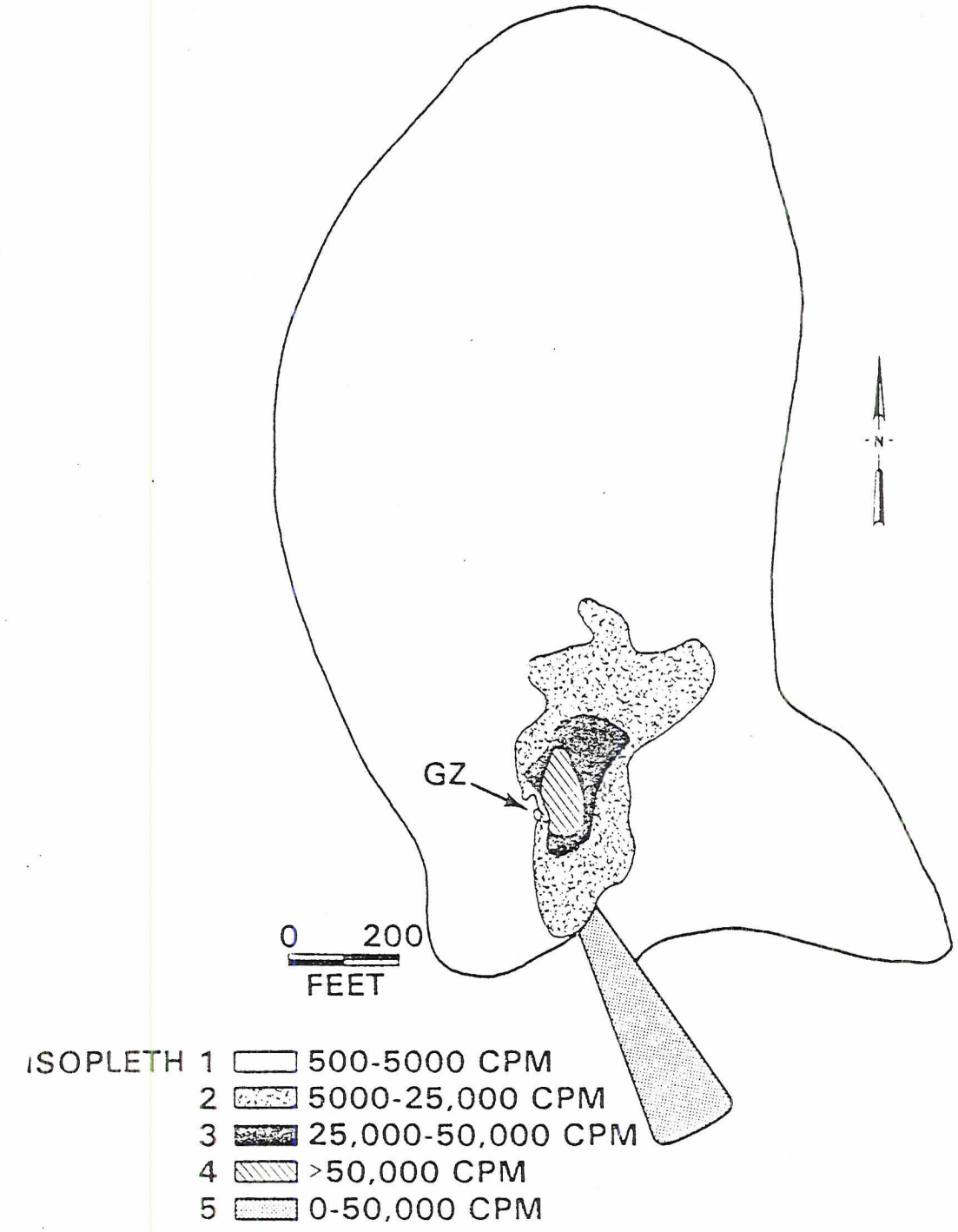

Fig. 3. Radioactivity Isopleths at GMX Area (from Gilbert and Eberhardt, 1974)

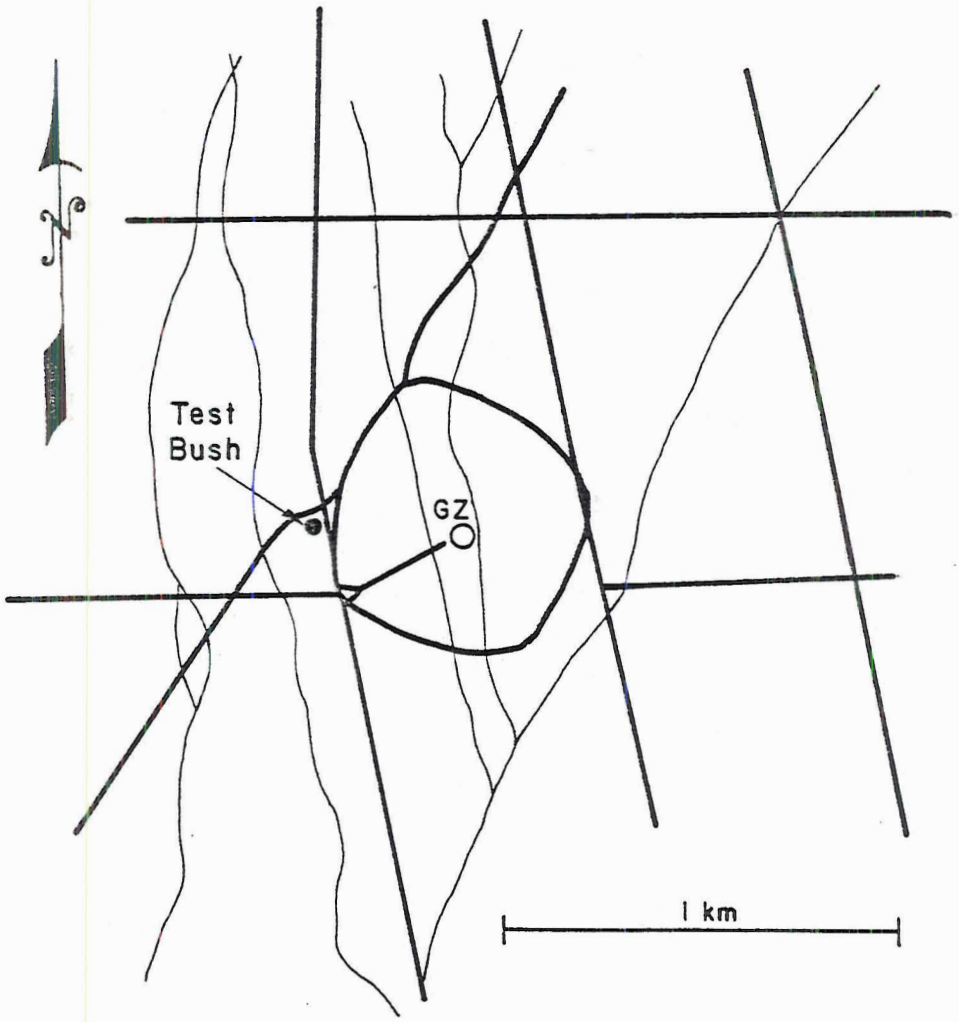

Fig. 4. Test Bush Site at GMX Area (after Rhoades, 1974)

12 km to the south-southwest. This is the prevailing wind direction for the daytime high wind periods and also for the measurement periods.

At this site a test bush was chosen for extensive air flow measurements close to and inside the bush. The criteria for choosing this bush were:

1) This test bush had a very large wind hummock built up inside it (18½ cm). Studying such a large hummock might provide clues regarding a size limit to hummock growth.

2) There was a large spacing between this bush and the closest upsteam bush. This allowed the wind incident upon the chosen bush to be in approximate equilibrium, which would not be achieved if the air flow approaching the bush was disturbed by the presence of another bush a short distance upwind.

3) The test bush was large in diameter and thus exerts a greater effect on the incident air flow than a small bush. This reduces three-dimensional effects, reduces the effects of the wind measurement probes on the air flow, and allows the hot wire anemometers to be spaced further apart inside the bush.

4) The test bush was within ten meters of a meteorological tower. It was also very close to a bivane which could be used to determine the prevailing wind direction, needed to align the hot wire anemometers.

2.4 Vegetation

The vegetation in the GMX region is predominantly creosote bush (Larrea divaricata or, in older texts, Covillea tridenta) with various coexisting species, the specific species varying in different regions of the GMX area (Rhoades, 1974). Creosote bush is a shrub with an average height of 0.6 m in the GMX area. Its main stems are woody, rising at an angle from the ground. They are limber with a one cm maximum diameter. The branches can be either simple or branched, becoming bushy at the tips where the stalk diameter diminishes greatly. Leaves are sparse, consisting of two 6-10 mm long,

3-4 mm wide broad leaflets joined at the base. Excretions of the lac scale are deposited in great quantity on the stems. It is fed upon by only a few insects, occasionally by jackrabbits, and is considered a "noxious weed." The creosote bush grows well on all soils and is the dominant plant for 30 million acres of the southwest United States.

The creosote bush growth rate is mainly determined by the annual precipitation (Dalton, 1961). The shrub grows until its size is limited by the available water. The low desert precipitation accounts for the wide spacing and even distribution of the GMX creosote bushes. Chew and Chew (1965) experimentally determined the age to reach mature growth as about 50 years. The volume of the branches increased linearly with age from 20 years until maturity (Fig. 5). Unfortunately the dependence of shrub height and diameter on age were not determined.

The average life span of a creosote bush is uncertain. No definitive studies have been made and only estimates from experienced desert observers are available. Dr. Fritz Went of the University of Nevada estimated the average lifetime to be about 100 years, but he remarked that the definition of life span is of importance since during periods of drought the branches die, leaving the root which may later grow new shoots during favorable conditions (personal communication). Dr. C.W. Ferguson of the Douglas Tree Laboratory, University of Arizona estimated the average life span as 50 to 100 years (personal communication). Shreve, a lifelong observer of creosote bushes in Arizona, estimated the average life span to exceed 100 years (Shreve and Hinkley, 1937). The average estimate is thus about 100 years.

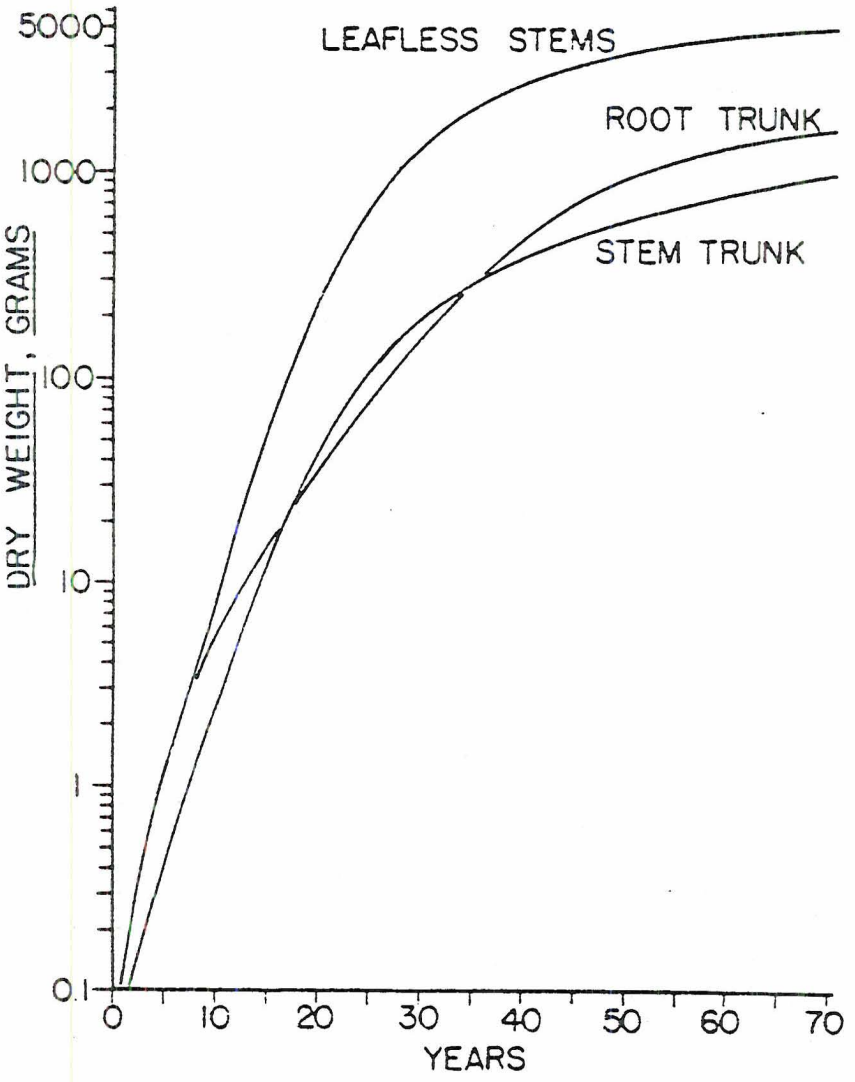

Fig. 5. Creosote Bush Growth Rate (from Chew and Chew, 1965)

Rhoades (1974) found the sizes of the creosote bushes to vary widely between different regions of the GMX area. The southeast sector had three meter high bushes, while others had bushes less than one meter high. Measurements of 20 creosote bush clumps close to the chosen test bush found the average height (H) to be 1.06 m, the variability being relatively small (σ = .22 m) (Table 2). The average "diameter" (D) was 2.07 meters (σ = 0.10 m), "diameter" being the average of the longest and shortest widths of the bush. The bush shapes ranged from circular to irregular oblongs. Most of the creosote bushes were in clumps of what appeared to be 3-4 bushes. However, the separateness of these bushes is questionable due to the ability of the creosote bush to grow a new set of branches from an older root and thus form a "new" bush. These clumps usually had wind hummocks associated with them. A typical creosote bush of the GMX area is depicted in Fig. 6.

Aerial photograph studies by Rhoades found the percentage of shrub cover to vary from 5 to 12% over the GMX area. His analysis spot closest to the test bush (330 meters away) had a shrub cover of 9.7% as measured by microscopic analysis and 8.1% when measured by a photodensiometer technique. A spot 400 meters away gave a value of 12.3% from microscopic analysis. Leavitt (1974) estimated the GMX shrub coverage to be 10%. Based upon an average of the above values, the shrub cover estimate used in this thesis was 10%.

Given the average diameter, height, and area coverage of the creosote bushes, the following parameters were computed:

A_f = Frontal silhouette area = 2.2 m^2

A_s = Bush base area = 3.4 m^2

TABLE 2

Creosote Bush Measurements

Shrub Identifier	Shrub Diameter (Min-Max) (to nearest 0.05 m)	Shrub Height Maximum (to nearest 0.1 m)	Hummock Height Maximum (to nearest 0.5 cm)	Shape Description
1	1.75		8.0	Circular
2	1.80-2.40	1.10	5.0	Oval
3	1.20	0.70		Circular
4	1.30-2.10	1.15	3.5	Oval
5	1.20-2.10	0.55	2.5	Oval
6	1.90-2.20	0.95	1.5	Oval
7	1.80	1.25	1.0	Circular
8	2.75	1.25	10.5	Ring of smaller shrubs
9	1.70	0.95	7.5	Circular
10	1.90-2.60	1.15	8.0	Oval
11	2.45-3.00	0.75-0.95	7.0	1 larger bush, 3 smaller ones
12	2.75	1.15	11.0	Circular
13	2.00-4.90	1.45	7.5	Oval
14	2.35	1.25	0.0	Circular
15	1.95	1.15	4.5	Circular
16	1.55	0.75-1.05	0.0	Weird
17	1.10-1.40	0.75-0.95	3.0	Oval
18	1.75	1.25	3.5	Circular
19	2.40-3.60	1.05	6.5	Oval
20	1.60	1.25	4.0	Circular

TABLE 2 (cont'd)

Shrub Identifier	Shrub Diameter (Min-Max) (to nearest 0.05 m)	Shrub Height Maximum (to nearest 0.1 m)	Hummock Height Maximum (to nearest 0.5 cm)	Shape Description
Mean =	2.07 m	1.06 m	5.0 cm	
σ =	0.60 m	0.22 m	3.3 cm	
Test Bush	1.60-2.80	0.90	18.5	Oval

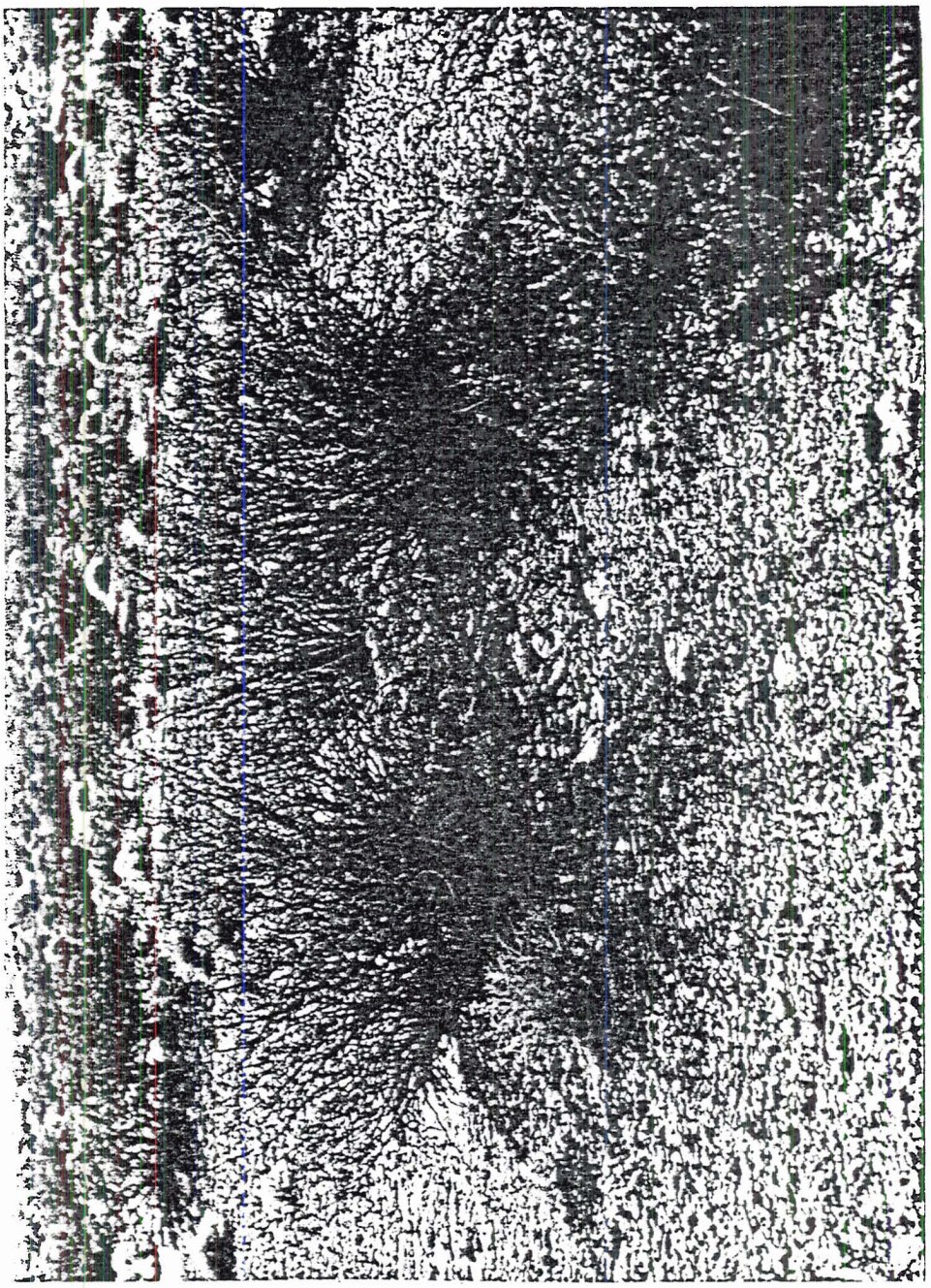

Fig. 6. Creosote Bush with Wind Hummock at GMX Area

S = Specific area per bush = 34 m^2

λ = Roughness element concentration parameter = A_f/S = 0.065.

Near the test bush the only other species of desert vegetation is the white bursage (Franseria dumosa). On the average it is one-fifth the height and one-tenth the diameter of the creosote bushes. The bursage population is relatively sparse and its branches are not densely spaced. Therefore, its effect on the air flow was considered to be negligible in comparison to the effect of the creosote bushes.

2.5 Soil

The top layer of the soil is a well developed desert pavement (Fig. 7). The soil particles are cemented together by clay particles, the surface crust forming after the soil has been wetted by rain and dried. This crust is much more mechanically stable than the underlying soil and makes the desert pavement highly resistant to wind erosion. However, the surface crust can be disturbed by the weight of vehicles or man, exposing highly erodible particles. A soil survey conducted by Leavitt (1974) assessed three sites in the GMX area down to a depth of 152 cm. He found the topmost layer to be textured gravelly or cobby sandy loam of low organic content, well to excessively drained with slow run off and rapid permeability (2½-10 inches of rainfall per hour). The soil is of volcanic origin and was formed from limestone, basalt, quartzite, and rhyolite. Moderate wind and water erosion is evidenced by the low wind hummocks around plants and the shallow stream channels prevalent. The top 15 cm is soft, friable, non-sticky, non-plastic and exhibits a weak fine platy

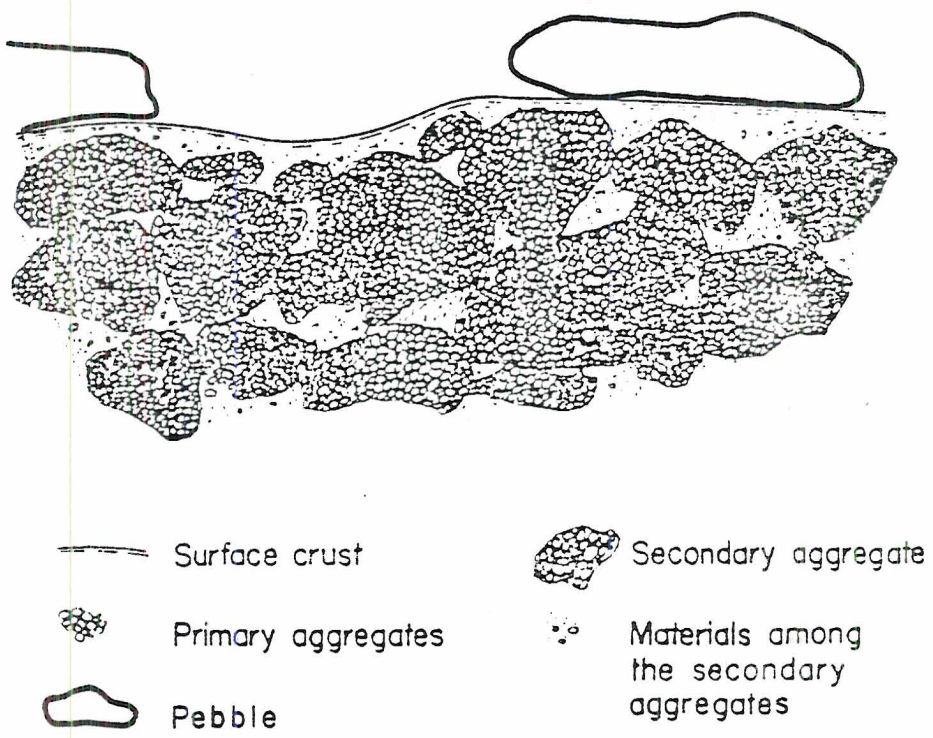

Fig. 7. Soil Structure of the Desert Pavement (after Chepil and Woodruff, 1963)

structure. Rocks and pebbles abound on the surface, with average lengths and heights of 15 mm and 8 mm respectively. They cover about 25% of the surface area.

Tamura (1974) determined the soil particle size distribution and plutonium content of the upper 3 cm soil layer (Table 3). The mean diameter of the desert pavement soil is 70 μm, if the soil particles with diameters over 2000 μm ("gravel") are neglected. Chepil (1941) has shown that the gravel particles are generally not erodible and therefore they have been excluded in computing the above mean diameter so that the particle size distribution of the desert pavement might be better compared to that of the hummock-trapped particles. This unerodible gravel comprises a large fraction (33%) of the desert pavement. The soil size distribution obeys the often cited log-normal soil distribution only for the sand sized particles. The surface layer of this soil is available for wind dislodgement and transport.

The soil was radioactive due to the presence of plutonium oxide. 80-90% of the radioactive content of the soil is in this top 3 cm layer, 95% within the top 5 cm. The major transport of radioactive particles within the soil is due to rainfall washing radioactive particles down from the surface. Because americium has a greater solubility than plotonium, it is removed more quickly from the surface layer leaving plutonium as the main component of the wind-erodible surface soil particles. Soil microorganisms are also responsible for the downward transport of radioactivity (Gilbert and Eberhardt, 1974). The radioactive particulates are less susceptible to erosion as they penetrate deeper into the soil.

TABLE 3

Desert Pavement Soil Analysis

Size Category	Size Fraction (diameter in μm)	Geometric mean Diameter (μm)	Soil Fraction (%)	Soil Fraction Cumulative	Soil Fraction Neglecting Gravel (%)	Soil Fraction Neglecting Gravel Cumulative	Activity in Fraction (dpm/g)	Activity in Soil (dpm/g)	Radioactive Contribution to Soil (%)
Gravel	>2000		30.7	100.1					
Very Coarse Sand	840-2000	1300	2.1	69.4	3.0	100.0			
Medium Coarse Sand	250-840	460	19.7	63.7	28.4	97.0	50	10	0.4
Fine Sand	125-250	180	17.1	47.6	24.6	68.6	2,632	451	17.5
Very Fine Sand	53-125	80	19.8	30.5	28.5	43.9	6,056	1,198	46.6
	20-53	33	6.6	10.7	9.5	15.4	11,850	776	30.2
Silt	5-20	10	2.6	4.1	3.8	5.9	4,032	105	4.1
	2-5	3.2	0.83	1.5	1.2	2.2	2,480	20	0.8
Clay	<2		0.67	0.7	0.97	1.0	1,698	11	0.4

Cloddiness (% > 840 μm) = 32.8%

(based upon Tamura, 1974)

Plutonium becomes intimately associated with the soil within a few months after deposition. The movement of radioactive particles is then directly related to soil erosion. The plutonium is not evenly distributed in the soil and "hot" spots are present. No apparent dependence of radioactivity upon the soil particle size has been discovered; therefore, the usual assumption is that the radioactivity is simply proportional to the soil mass (Anspaugh and Phelps, 1974).

Tamura also sampled the soil in a bush wind hummock located within ten feet of his desert pavement sample (Table 4). This soil size distribution differed markedly from that of the desert pavement soil, especially in the conspicuous absence of gravel particles. The median diameter of the soil fraction was 120 μm, again neglecting gravel. A log-normal distribution fit the sand size distribution. This "blow" sand has a higher concentration of fine sand than the pavement, due to the different natures of the soils. The pavement has developed a platy structure, whereas blow sand is very loose. Thus, the pavement size fractions often represent aggregates formed by finer sizes, while the blow sand fractions represent individual particles. The bush hummocks are more radioactive than the desert pavement. The wind hummocks gave higher surface radioactivity readings (21,000 cpm) than the bare pavement (15,000 cpm) and also showed a higher activity per unit weight of soil (3100 vs. 2570 cpm/gm).

Soil density measurements found the desert pavement soil to have a bulk density of 1.56 g/cm^3 and a particle density (ρ_p) of 2.22 g/cm^3. The bulk density of the blow sand was 1.37 g/cm^3 with a particle density of 2.44 g/cm^3. For comparison, the density

TABLE 4

Wind Hummock Soil Analysis

Size Category	Size Fraction (diameter in μm)	Geometric Mean Diameter (μm)	Soil Fraction (%)	Soil Fraction Cumulative	Soil Fraction Neglecting Gravel (%)	Soil Fraction Neglecting Gravel Cumulative	Activity in Fraction (dpm/g)	Activity in Soil (dpm/g)	Radioactive Contribution to Soil (%)
Gravel	>2000		1.3	98.7					
Very Coarse Sand	840-2000	1300	3.3	97.4	3.4	100.0	755	25	0.8
Medium Coarse Sand	250-840	460	26.2	94.1	26.9	96.6	1,008	264	8.5
Fine Sand	125-250	180	34.7	67.9	35.6	69.7	3,240	1,125	36.2
Very Fine Sand	53-125	80	24.9	33.2	25.6	34.1	4,836	1,202	38.7
	20-53	33	6.2	8.3	6.4	8.5	5,764	357	11.5
Silt	5-20	10	0.71	2.1	0.73	2.16	9,816	70	2.3
	2-5	3.2	0.58	1.4	0.60	1.43	8,400	49	1.6
Clay	<2		0.81	0.8	0.83	0.83	2,028	16	0.5

Cloddiness (% > 840 μm) = 4.6%

(based upon Tamura, 1974)

of silica sand particles is 2.65 g/cm^3. The particle density was measured using a non-polar, highly wettable liquid to fill intersticies.

2.6 Bush Hummocks

Bush wind hummocks are mainly associated with creosote bush clumps. The smaller bursage has no discernible hummock, and the occasional "single" creosote bush has either a noticeably smaller hummock or none at all. Measurements of 20 creosote clumps found the average hummock height to be 5 cm (Table 2). For these same bushes the following correlations were found:

Correlation	Correlation coefficient
Hummock height with shrub height	0.76
Hummock height with shrub diameter	0.66
Shrub height with shrub diameter	0.69

indicating that either: 1) the larger plants are older and have had more time to build a mound, or 2) the larger plants are more efficient at building mounds than the smaller bushes. Probably both mechanisms contribute to the observed correlations.

Comparison of the test bush with the 20 bush average is informative:

	Test bush	Bush average
Maximum Height	0.9 m	1.06 m (σ = 0.22 m)
Average Diameter	2.2 m	2.07 m (σ = 0.60 m)
Mound Height	18.5 cm	5.0 cm (σ = 3.3 cm)

Figure 8 shows the hummock profile of the test bush. Note that the mound edges coincide with the bush edges. There is some

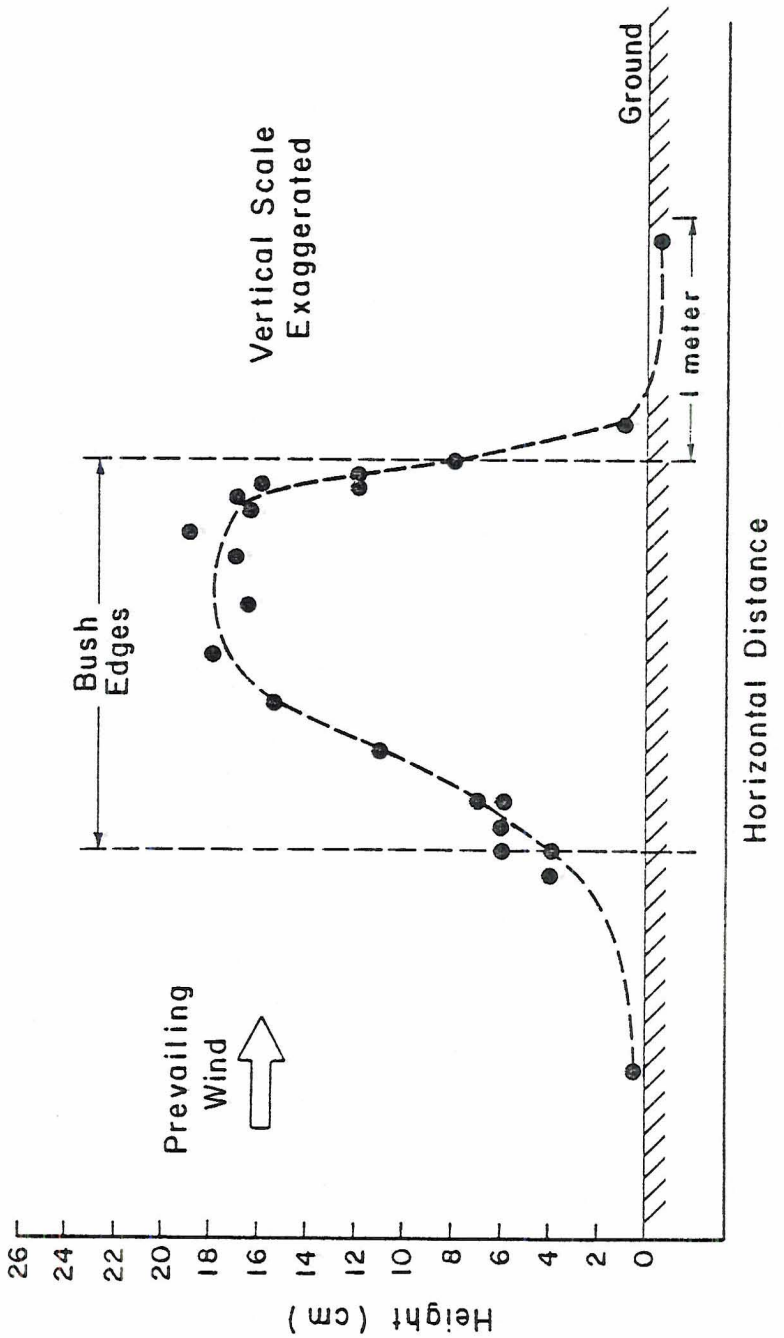

Fig. 8. Profile of the Test Bush Hummock

assymmetry in the profile. It is assumed that this is a "typical" hummock profile.

Dead organic material is prevalent inside the bush. It consists of dead leaves, flowers, fruit, and twigs.

3. EXPERIMENTAL MEASUREMENTS

3.1 Field Instrumentation

The meteorological measurements used in this study were: 1) wind and temperature readings above and below the average shrub height from instruments on meteorological towers near the test bush allowed the flow in the two regimes to be compared, 2) average and turbulent flow velocities close to and inside the test bush were measured by three hot wire anemometers, and 3) the wind data necessary to estimate the horizontal erosion flux was obtained from a climatological wind measuring station (SYSTRAC #15).

Two ten meter towers and their associated equipment had previously been established on the western edge of the GMX area at the test bush site by the Las Vegas Air Resources Laboratory of the National Oceanic and Atmospheric Administration (NOAA). A standard vane and cup anemometer continuously recorded the wind direction and speed at ten meters. Cup anemometers measured the ten minute mean horizontal wind at five levels (½, 1, 2, 4, and 8 m). A separate cup anemometer at 2 m continuously recorded the wind speed and a 2 m bivane continuously sampled the horizontal and vertical wind fluctuations. All the cup anemometers were periodically wind tunnel calibrated. Temperatures were measured every ten minutes at five levels. Two levels were below the soil surface at 1 cm and 3 cm. Above ground quartz sensors in aspirated shields measured the air temperature at ½, 2, and 8 m. A hydrothermograph, supplemented by sling psychrometer observations, provided relative humidity readings. An aneroid barometer recorded the atmospheric pressure. Soil moisture was obtained by averaging

five samples from the upper 0.5 cm soil layer. Each sample was weighed, oven dried, then re-weighed. NOAA personnel performed the data collection and recording tasks.

Three Datametrics 800-VTP constant resistance-ratio hot wire anemometers measured the mean and turbulent flow in and around the chosen bush. These battery powered instruments operated up to six hours on one charge. Because their lead length was limited to eight feet, the associated electronics were housed in chilled insulated ice chests to keep them at acceptable temperatures. The self-cleaning probes consisted of 0.5 cm long stainless steel filaments. The manufacturer specifies their accuracy to be within 2%, and their frequency response to be 100 hz. The output voltage response is non-linear and zero drift is possible. The hot wire voltages were recorded by an Incredata digital recorder at a rate of 145 readings per second per anemometer.

The three hot wire probes were suspended from aluminum tubing in either a horizontal or vertical arrangement around the test bush. Generally measurements were made at heights of 96, 45, and 4 cm. These heights were based upon the 90 cm height of the test bush. The 96 cm height was just above the bush, the 45 cm height was half the bush height, and the 4 cm height gave wind speeds close to the ground. A bivane located close to the bush was used to sight a landmark indicating the prevailing wind direction, towards which the hot wire probes were then oriented. The wind direction was also checked after each measurement. Before and after each measurement period the hot wires were covered and the zero velocity voltage was recorded.

Climatalogical winds near Frenchman Lake were measured by SYSTRAC station 15, located 3½ km south of the meteorological tower. This permanently sited cup anemometer station was periodically queried by remote control and in reply gave the ten second wind average at a height of 10 m. This station has operated from August 1969 to August 1976 with only a 15% loss of data. These breakdowns occurred randomly, usually in blocks of days or weeks. The climatalogical data is weighted towards the first two years when the sampling interval was 5 minutes, after which it changed to 15 minutes.

Besides the hot wire anemometer data, the digital recorder also recorded the output of a Meteorology Research Inc. Model 1550B nephelometer. This instrument measures the backscattered light from particulates in a control volume, thereby indicating the particulate loading of the air. The nephelometer sampled the air 10 cm above the ground at a location three meters from the test bush. It was designed to provide 10% accuracy and withstand a 0°-130° F temperature range. The inlet sampling tube introduced a time delay of 0.8 sec, the time constant of the instrument being 2 sec. Although only qualitative measurements of the atmospheric dust content were needed, nevertheless the nephelometer was calibrated, using Freon gas as a backscatter coefficient reference.

3.2 Hot Wire Anemometer Data Analysis

The hot wire anemometers were individually calibrated in a wind tunnel by comparing pitot tube velocity calculations with output voltages measured by a digital voltmeter. This voltmeter also calibrated the digital recorder which recorded the hot wire voltages

in the field. A third order polynomial was fit to each calibration curve and used to convert each recorded anemometer voltage into a corresponding velocity.

The "velocity" measured by a hot wire anemometer is actually a "mass velocity" i.e. the product of air density times velocity. Therefore all calculated velocitites, measured both in the field and in the wind tunnel, had to be corrected for density to obtain the true velocity. Air temperature and pressure data were thus needed in both cases. This presented difficulties for the field data, since velocity measurements were made at a 4 cm height while the lowest air temperature sensor on the meteorological tower was at 50 cm. To overcome this problem, a constant temperature differential between the two layers was assumed. This temperature difference was estimated to be 4°C from comparisons of the measured temperature profiles to temperature profile formulas developed by Malurkar and Ramdas (1931). Because the field measurements were all taken during the afternoon on sunny days, the air temperature on a given day was relatively constant (2°C maximum range). Since the density depends upon the absolute temperature, errors from this source were negligible compared to other errors in the velocity measurements, e.g. a 1°C temperature error would give a velocity error of only 0.3%.

In the field the hot wire anemometers were compared both to themselves and to the cup anemometers on the meteorological tower. For intercomparison of the hot wires they were placed a foot apart at a 2 m height in an "isolated" spot, i.e. one far removed from nearby bushes. The flow past each of the anemometers should be the same. An 18.3 minute test (150,000 values per hot wire anemometer)

gave velocities of 3.96, 4.00, and 4.01 m/sec for the three anemometers, showing agreement within 1%. The standard deviations obtained agreed within 5%. To compare the hot wire anemometers with the tower cup anemometers, a 40 minute test was made with a hot wire anemometer located a foot to the side of both the 1 m and 2 m tower cup anemometers. The average ratios between the four ten minute mean cup velocities and the corresponding ten minute mean hot wire velocities were 1.144 (σ = 0.017) at 1 m and 1.139 (σ = 0.029) at 2 m. The ratios agreed to a surprising degree for both heights. The source of the discrepancy between the hot wire and cup anemometer velocities is cup anemometer "overspeeding", a well-known effect resulting from the cup characteristically accelerating faster in gusty winds than it decelerates. The magnitude of this overspeeding error was consistent with the results of an intensive investigation of cup overspeeding errors made by Izumi and Barad (1970). They found the overspeeding to average 16% of the wind speed, but noted that tower influences could account for as much as 5% of this and that stability also influences the overspeeding. They suggested that the best estimate of overspeeding error was about 10%. The cup anemometer speeds obtained were corrected for overspeeding by multiplying them by a factor of 0.876, the average of the above two ratios. Using this ratio for all heights is justified by the agreement between the 1 m and 2 m ratios and by Izumi and Barad's conclusion that no strong relationship existed between overspeeding error and anemometer height.

One major source of error in hot wire anemometer measurements can be zero drift. To minimize this the anemometers were covered

before and after each measurement period and the zero velocity voltage was recorded. Because the measurement periods were relatively short (~30 minutes), this was done often enough that the change in zero velocity voltage was generally small (average drift ≈ 0.08 mv/min). A one millivolt error gives a velocity error of 0.45% at a velocity of 3 m/sec. In the data reduction the zero velocity voltage used to calculate the velocity from the recorded voltage was presumed to be a linear interpolation of the zero velocity voltages measured before and after the measurement period. Unfortunately there were two periods where an end zero velocity voltage was not obtained. Taking a "worst case" zero drift for the longer of the two periods, a maximum average velocity error of 1.2% was calculated. This is small enough to be ignored.

Hot wire anemometers respond not to wind flow in one direction only but to the flow in a plane perpendicular to the wire. Thus a horizontally oriented hot wire will also respond to vertical flow, but not to horizontal flow parallel to the wire. Practical considerations of placing a probe very close to the ground forced the use of a horizontal orientation for the hot wires. Any change between the mean wind direction and the plane normal to the hot wire would result in the measured velocity decreasing according to the cosine of the angle, a relationship verified during the wind tunnel calibration. If the angle increased beyond 15° the presence of the probe posts would further decrease the measured wind velocity. It was therefore important that the wind direction remain essentially constant. Fortunately the wind direction during the field measurements was remarkably steady. The nearby bivane inked record was checked

for wind direction before, during, and after each measurement. Two measurement periods which showed variations greater than ten degrees were discarded. Such a ten degree variation would give an error of 2% according to the cosine law.

With the hot wire element horizontally oriented, any mean vertical wind would give a measured velocity greater than the actual horizontal wind. Although there is definitely vertical flow due to the bush, estimates using the continuity equation showed it to be generally negligible (See Appendix A).

Because the hot wires also respond to turbulent fluctuations in the vertical direction, turbulence will cause the measured velocity to be greater than the actual horizontal velocity. This effect was estimated and found to be negligible except close to the ground behind the bush where turbulent intensities of up to 0.7 are found. Such high turbulence levels would produce an estimated error of 7% (See Appendix A). Since a hot wire anemometer is unable to distinguish flow direction, such large turbulent intensities raised the possibility that intermittent reverse flow might have occurred. However the velocity frequency distributions of these cases were essentially Gaussian, which would not be expected if reverse flow was significant.

4. AIRFLOW ABOVE AND WITHIN VEGETATION

Surface friction leads to the formation of a boundary layer below the geostrophic wind. In this boundary layer momentum is transferred downward by turbulent wind shear and bouyant motions to the surface layer. The surface layer is defined as that region where the fluxes of momentum, heat, and moisture are independent of height, to a first approximation. The height of this layer can extend from 10-50 m. When considering flow over a vegetated surface the momentum flux is constant only in the horizontally homogeneous flow above the wake interaction region. Below this height horizontal inhomogeneities produce stress variations with height.

The ground and obstacles above it, e.g. vegetation, exert a drag on the air flow called the total surface stress (τ_o). The surface friction velocity is defined as:

$$U_* = (\tau_o/\rho)^{\frac{1}{2}} \tag{4-1}$$

where ρ = air density. In the surface layer the vertical momentum flux (F_m) is constant, equal and opposite to the shear:

$$F_m = -\tau = +\rho\ \overline{uw} \tag{4-2}$$

where τ = shear stress

u = fluctuating horizontal velocity

w = fluctuating vertical velocity.

Momentum transfer is often described by semi-empirical relationships. One method, analogous to molecular transport in viscous flow, uses the velocity gradient and an eddy turbulent transfer coefficient (K_m):

$$F_m = -\rho K_m \frac{\partial U}{\partial z} . \qquad (4\text{-}3)$$

A second method uses a transfer coefficient in integrated form:

$$F_m = -\rho C_d U^2 . \qquad (4\text{-}4)$$

Both K_m and C_d are functions of height. The "meteorological" surface drag coefficient (C_d) used here is one-half the value of the "aerodynamic" surface drag coefficient (C_{da}):

$$C_d = \tfrac{1}{2} C_{da} = \left(\frac{U_*}{U}\right)^2 . \qquad (4\text{-}5)$$

The logarithmic wind law is known to adequately describe the velocity profile in the surface layer under neutral conditions:

$$U = \frac{U_*}{k} \ln \frac{z}{z_o} \qquad (4\text{-}6)$$

where k = von Karman constant

z_o = characteristic length of surface roughness.

U_* is a useful scaling velocity for the surface layer. z_o is often used to scale the eddies responsible for the drag on a rough surface. The logarithmic wind profile can be derived either: 1) by assuming a constant stress, neutral conditions, and mixing length theory, or 2) more generally, i.e. with fewer restrictions, by asymptotic matching of a law of the wall with a velocity deficit law of the outer flow. The logarithmic wind profile can also be valid for heights above the surface layer, up to 100 m or more.

The von Karman constant (k) has traditionally been given a value of 0.4, based upon laboratory experiments. Experiments in the

atmosphere, with higher Reynolds numbers than are typical of laboratory flows, show a large scatter. The most extensive experiments to date, conducted in a Kansas field, indicated k = 0.35 (Businger et al., 1971). This value has been accepted by many micrometeorologists because it agrees closely with the k = 0.33 value Tennekes (1968) deduced by extrapolating wind tunnel measurements to very large Reynolds numbers. Some disagreement continues, however, as Pruitt et al. (1973) found k values between 0.39 and 0.44. The von Karman constant used in this thesis was the traditional 0.4 value.

In dealing with flow over vegetation, the height where the mean wind vanishes according to the logarithmic wind profile may not be the ground itself, but some height above the ground which acts as a new surface with respect to the wind, the zero plane displacement height (D_o). Eq. (4-6) then becomes:

$$U = \frac{U_*}{k} \ln \left(\frac{z - D}{Z_o}\right) \tag{4-7}$$

where Z_o = characteristic roughness length above vegetation.

The neutral case requires that there is no heat flux from the surface to the atmosphere. In the more usual diabatic case, heat flux is present. The associated bouyancy forces may play a significant role in modifying the surface layer wind profile. The Richardson number (Ri) is often used as a measure of stability:

$$Ri = \frac{\text{bouyancy transfer of momentum}}{\text{mechanical transfer of momentum}} = \frac{g}{T} \frac{\left(\Gamma + \frac{\partial T}{\partial z}\right)}{(\partial U/\partial z)^2} \tag{4-8}$$

where g = gravitational acceleration

Γ = adiabatic lapse rate.

Another stability parameter, the scaling length L, was introduced by Obukhov (1946) using similarity arguments. L is usually called the Monin-Obukhov length:

$$L = -\frac{T}{kg}\frac{u_*^3}{\overline{w\theta}} \qquad (4\text{-}9)$$

where θ = fluctuating temperature. L is used to define the Monin-Obukhov dimensionless height, $\zeta = z/L$. The advantage of this representation is that L is approximately constant in the surface layer, whereas the Richardson number is not. In diabatic conditions Eqs. (4-6) and (4-7) must be modified, as will be described later.

Whether the roughness elements are densely spaced or not, at some height their wakes interact and are integrated into a horizontally homogeneous flow. The outer flow above the wake interaction region is the constant stress region described by Eq. (4-7) for neutral conditions. The existence of this constant stress layer above the vegetation has been well documented in both wind tunnel work (O'Laughlin and Annambhotla, 1969; Plate and Quraishi, 1965; Sadeh et al., 1971) and in field experiments (Kutzbach, 1961; Thom, 1971). The constants in Eq. (4-7) are determined by the combined effects of single roughness elements. An individual roughness element is generally characterized by a height (H), a diameter (D), and a porosity (ϕ). When considering uniformly scattered roughness elements the specific area, i.e. the ground area per roughness element (S), is an important parameter. Many empirical formulae have attempted to relate Z_o and D_o to H, D, and S. For example, Lettau (1969) suggested:

$$Z_o = \tfrac{1}{2}\, HD/S \ . \qquad (4\text{-}10)$$

This formula has been found to be most useful when the roughness elements are somewhat isolated. Other proposed formulae are more adequate when the individual roughness elements are so close that they have lost their identity, i.e for canopy flow. Empirical formulae for D_o have also been proposed for such cases. Seginer (1974) references much of this work.

In the upper flow regime the mean and turbulent velocities depend solely upon the height above D_o and the shear stress, not the parameters of the roughness elements that produce this shear stress. Morris (1955) has noted that the distance from the ground to this upper flow regime depends primarily on the frequency and size of the vortices formed by the roughness elements. Woodruff et al. (1963) found the height of the wake interaction region for actual and model windbreaks to extend to 2.0 H and 1.8 H respectively for downwind distances of 20 H. O'Loughlin and Annambhotla (1969) found wake depths of H to 1½ H for flow over roughness elements, while Sadeh et al. (1971) found depths of 1.7 H. Flow experiments over two-dimensional solid windbreaks, where the vertical flow is of necessity much greater than for porous ones, found a wake interaction region up to 2-4 H (Good and Joubert, 1968). Based upon the average bush height of 1 m, the height of the GMX wake region was estimated to be less than 2 m. Therefore, velocities at and above 2 m were considered to represent the constant stress outer layer.

The preceeding arguments have concerned the horizontally homogenous flow above the wake interaction layer. Below this height the effect of individual roughness elements must be considered. Vegetation interacts with the mean flow wind by 1) extracting the

momentum required by the aerodynamic drag of plant parts, 2) converting mean kinetic energy into turbulent kinetic energy in the wake formed behind an obstruction, and 3) breaking down large scale turbulent motions into smaller scale motions in the wake region.

The flow past an individual two-dimensional roughness element, e.g., a windbreak, will be described first. The incident flow is distorted, producing a pressure differential across the element, and separation bubbles ahead of and behind solid obstacles. A wake or shear zone extends above the near separation zone. Intense shear transfers mean kinetic energy into turbulent energy, resulting in increased mixing. The greatest velocity reductions occur in regions of greatest mixing. The velocity profile continually adjusts until the excess mixing becomes negligible. Downstream of the separation zone, a new boundary layer flow develops in equilibrium with the underlying surface (Fig. 9). This internal boundary layer grows slowly downstream, eventually displacing the wake region. Streamlines on the upwind side start to rise before reaching the obstacle, reach a maximum at a point beyond the obstacle, and then slowly drop. The drag exerted on the airflow reduces the wind velocity, as indicated by the upward rise of the streamlines. The surface stress is also reduced (Fig. 9). The sheltered zone has been estimated to extend from 5 H windward to 30 H leeward (van Eimern et al., 1964). The wind reduction at lower heights is balanced by a corresponding wind speed increase at upper levels, as required by the law of continuity.

For porous obstacles the flow features are qualitatively similar, except that the lesser pressure differential across the element usually results in the disappearance of the separation region. Flow

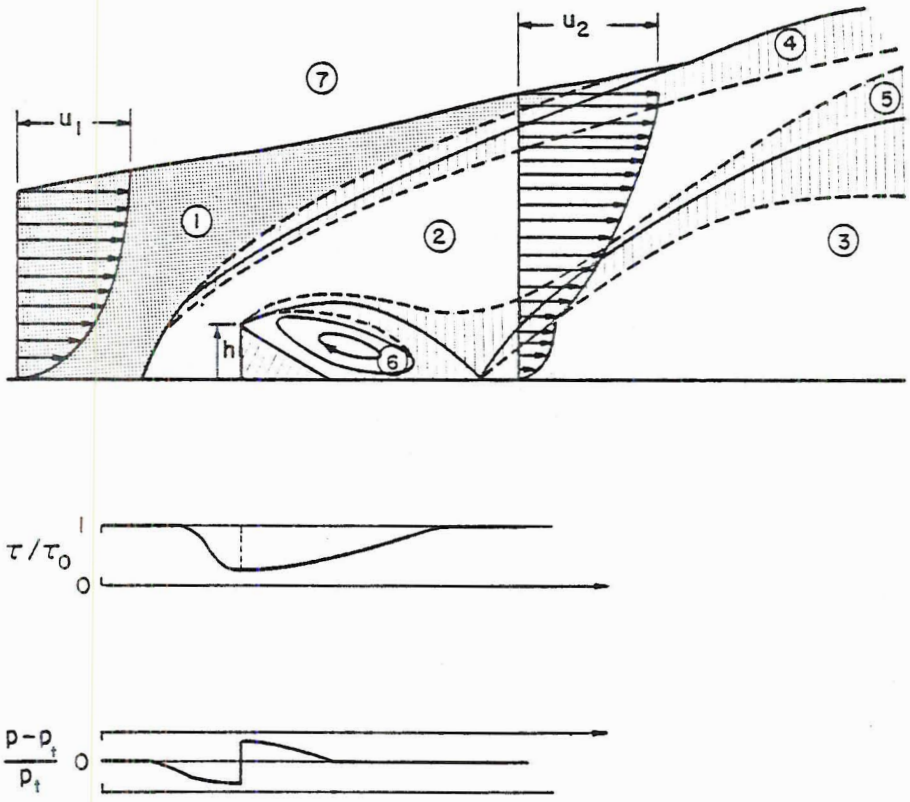

Fig. 9. Airflow Regions Behind a Windbreak (after Plate and Lin, 1965 and Seginer and Sagi, 1972)

changes are less abrupt and the turbulence is less intense. The decreased mixing allows the wind reduction zone to extend further downwind. At the front and rear of a porous screen, both the pressure and velocity are approximately constant with height. The air flowing through the screen provides the leak which reduces the pressure differential across the obstacle. This pressure drop is proportional to the velocity squared, in agreement with the drag force (F_d) equation:

$$F_d = \rho c_d A_f U^2 \qquad (4\text{-}11)$$

where the drag coefficient of the obstacle (c_d) is a function of porosity.

For porous plates in a wind tunnel, Castro (1971) found that the vortex street and reversed flow recirculation region, two characteristics associated with flow behind solid objects, both disappeared when the plate porosity increased beyond 30%. Bleed air entraining into the shear layers prevented them from interacting. The effective porosity of the creosote bushes will be found to be 70-80%. Obstacles of such large porosity can be considered to be lattices whose separate elements are of sufficiently small width that they have negligible individual effect on the flow, but which together form a uniform sheet of resistance. The main effect of such a structure is to produce a drop in the total pressure along any streamline passing through it. A summary of relevant formulae has been given by Graham (1976).

The windbreak discussed above has been assumed to be two-dimensional. Estimates of the length to height ratio required to meet

this assumption have ranged from 12 to 24. A ratio of two reduces the protective effect by one-half (Bleck and Trienes, cited by van Eimern et al., 1964). Flow past a three-dimensional object involves additional turbulent mechanisms. As the flow passes the roughness elements, the wake vortices transfer vorticity from the mean shear to the flow direction itself. The shear is greater than that of two-dimensional flow and more turbulent kinetic energy is generated. Initially this turbulence is scaled to the dimensions of the roughness element, but further downwind the distance from the surface becomes the scaling length just as it was far upstream. The lateral velocity deficit region grows linearly with distance downstream and soon becomes Gaussian (Meroney, 1968).

Plants create disturbances, whose individual effect is soon dissipated but whose aggregate effect determines the intensity and nature of the turbulence. In the region below bush height the time averaged flow is three-dimensional, and a one-dimensional model can be only partially adequate. Two types of flow have been observed, isolated roughness flow and canopy flow. The latter can be further divided into wake interference flow and skimming flow.

The "isolated roughness" type of flow occurs when individual roughness elements are far enough apart that the wake and vortex of each element have completely developed and dissipated before the next element is reached. In such a flow, Eq. (4-7) is valid above the roughness element height. Z_o is greater than it would be for the surface alone, since it is a measure of the surface drag and the projections considerably increase this drag.

"Wake interference" flow occurs when the roughness elements are close enough that the wake and vortex of an element interferes with the flow at following elements. When the roughness elements are so close that stable vortices or pockets of "dead" air are formed, the flow is called "skimming" flow. In both cases the roughness elements are packed so closely that a new uniform surface, the canopy, is formed by their tops, and the surface layer is displaced upward by the displacement height D_o. Eq. (4-7) is valid above the canopy height. Below this height a complicated, but comparatively weak, canopy flow exists. It is usually treated as a one-dimensional flow, and an exponential wind law has often been observed (Inoue, 1963; Cionco, 1972):

$$U \alpha \exp [a (z/H - 1)] \tag{4-12}$$

where a is an empirical constant.

The main difference between the flow inside vegetation and above it is that in the former case momentum can be absorbed directly by the vegetation and the equation of motion becomes:

$$\frac{\partial(\overline{uw})}{\partial z} = - \frac{1}{\rho} \frac{\partial P}{\partial x} - c_d(\frac{\Omega}{S}) U^2 \tag{4-13}$$

where P = mean pressure and Ω = foliage area per unit volume. Both c_d and Ω are usually complicated functions of height, and c_d is also somewhat dependent upon wind speed.

Three flow regimes are distinguishable in well-developed canopy flow:

1) in the upper part of the canopy the pressure term is negligible;

2) in the middle of the canopy the divergence of the momentum flux is negligible, especially for a dense canopy; and

3) very close to the surface $\partial(\overline{uw})/\partial z = 0$ and the wind profile is logarithmic. The height of this region depends upon the roughness element spacing.

Seginer (1975) has shown that turbulent mixing dominates bouyant effects close to a windbreak. Stability effects can be significant for downwind distances beyond 3 H, reducing the sheltering effect by approximately 10%. Uchijima and Wright (1964) found no large thermal effects in a corn crop canopy study covering a wide range of thermal stabilities.

In the following analysis of the flow in and above the desert chaparral of the GMX region, the following conclusions will be reached. The creosote bushes are widely spaced and aerodynamically very porous. They act as individual roughness elements, each producing a wake that is essentially dissipated by the time it reaches the downwind bushes. The flow is closest to the "isolated roughness" flow, not the "canopy" flow produced by more closely spaced elements. The wake region of a bush is similar to that of a two-dimensional windbreak, with an internal boundary layer developing downstream. These wakes combine and merge vertically within twice the bush height. A horizontally homogeneous, constant stress region exists above this wake interaction region. Due to the close and regular spacing of the branches, the flow within an individual bush has properties similar to that of flow through a canopy, although the flow has not had time to become well-developed.

5. AIRFLOW MEASUREMENTS

5.1 Flow Above the Vegetation

The airflow above the shrubs was investigated because 1) it provided clues to the type of flow below shrub height and 2) the results were used to estimate the partitioning of the total drag between the bush and the ground, an important factor in assessing the ability of vegetation to control wind erosion.

A great deal of effort has gone into developing relations between the momentum flux and the wind profile under unstable conditions. Barad (1964) gave a historical account of 30 years of work measuring surface stress in the surface layer. Under neutral conditions the surface stress can be easily determined from the logarithmic velocity profile, but diabatic conditions require consideration of bouyancy effects. The GMX velocity profiles were obtained under unstable daytime conditions. Therefore a diabatic flux relationship was used to obtain the stress above the vegetation.

In the most extensive measurements to date, Businger et al. (1971) related the dimensionless wind gradient to ζ. Paulson (1970) integrated this relationship, giving:

$$U = \frac{U_*}{k} \left[\ln (z/z_o) - \Psi \right] \qquad (5\text{-}1)$$

where Ψ = diabatic velocity profile correction

$$= 2 \ln \left[(1+s)/2\right] + \ln \left[(1+s^2)/2\right] - 2 \tan^{-1} s + \pi/2$$

$$s = (1 - 15\,\zeta)^{\frac{1}{4}}.$$

For measurements over vegetation, the zero plane displacement must be added to the above equation:

$$U = \frac{U_*}{k} \ln \left(\frac{z - D_o}{Z_o} - \Psi \right) \qquad (5\text{-}2)$$

where now $\zeta = (z - D_o)/L$.

Eq. (5-2) was employed to obtain "best fit" values of Z_o and D_o for the GMX area from 89 concurrent wind and temperature profiles measured at the meteorological towers. Since the region of interest was the constant stress layer above the wake interaction region, only the winds at 2, 4, and 8 m were used. The long upwind fetch insured that the 8 m velocity was well within the constant stress region.

The Richardson number at 4 m was computed using wind and temperature gradients determined by fitting a quadratic of (ln z) to the wind and temperature profiles. The Monin-Obukhov length was then calculated using Businger et al.'s (1971) empirical relationship:

$$Ri = \frac{0.74\ \zeta\ (1 - 15\ \zeta)^{\frac{1}{2}}}{(1 - 9\ \zeta)^{\frac{1}{2}}} . \qquad (5\text{-}3)$$

Knowing L, Ψ could be calculated for each of the wind profiles.

Munroe and Oke (1973) found no statistically significant relation between either Z_o or D_o and wind speed, contradicting the results of other investigations. They attributed the Z_o and D_o variations found by others to inadequate diabatic corrections and streamlining effects. Accordingly, Z_o and D_o in the GMX area were assumed to remain constant under all wind conditions and a U_* for each individual profile determined from a least square fit. The sum of the squared difference between each estimated and measured velocity was computed, and the values which gave the minimum squared velocity

error were Z_o = 2.7 cm and D_o = 8 cm. The average velocity error percentage was 0.52%.

To determine whether the Z_o and D_o values calculated in this manner were a function of stability, the wind profiles were separated into stability classes and the above process repeated. The calculated Z_o and D_o values exhibited no definite trend with stability, therefore the diabatic velocity profile correction used above introduced no systematic error.

It is interesting to compare these results to those which would have been obtained by assuming neutral conditions. Using the above method with no diabatic correction gave Z_o = 0.73 cm and D_o = 25 cm, the average velocity error percentage being 1.1%. As might be expected, when separated into stability classes the calculated Z_o and D_o values depended strongly on stability. The diabatic correction does not introduce an additional degree of freedom, so the decrease in the velocity error obtained by using it is significant.

In simultaneously determining Z_o and D_o, there was a strong interaction between the two and the minimum was rather broad. This should not affect the U_* values calculated for each profile.

Figure 10 gives as a function of wind speed the 8 m meteorological drag coefficient, $C_d(8\ m) = U_*/U(8\ m)$. The 8 m drag coefficient decreases for stronger winds, in agreement with field studies of a windbreak (Seginer, 1975) and of a crop canopy (Uchijima and Wright, 1964). Since the total drag is the sum of the form (pressure) drag and skin friction, the total drag should not increase in proportion to the velocity squared, so it is not unexpected that the drag coefficient varies. The total drag results mainly from bush drag,

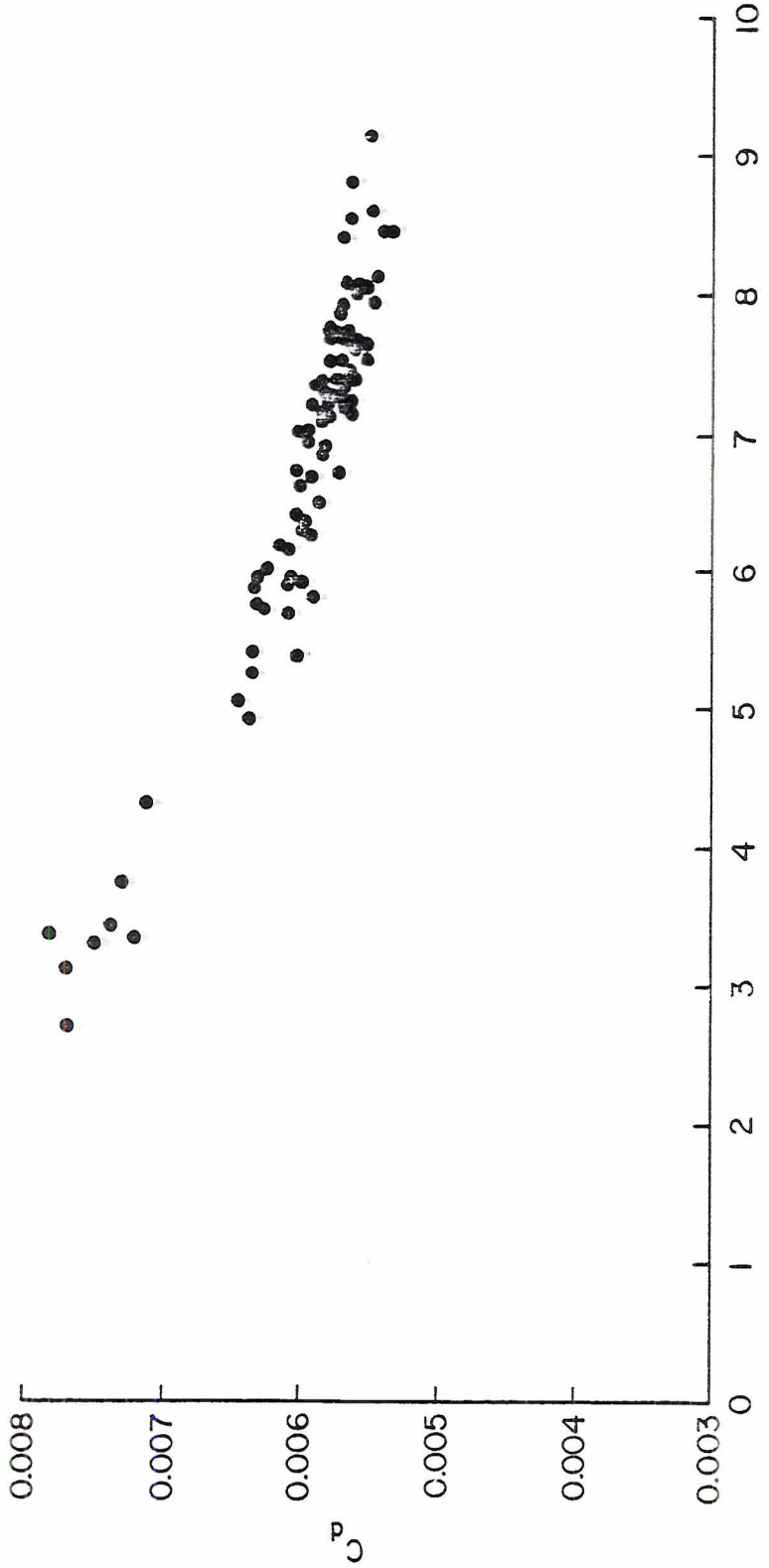

Fig. 10. Meteorological 8 m Drag Coefficient as a Function of Wind Speed

and the change of C_d with U probably indicates a change in the bush drag coefficient (c_d) with U. The plant elements are flexible and their effective resistance changes with wind speed. Also, the mutual sheltering of the elements may be a function of wind speed. A decrease of c_d with wind speed is in agreement with the measurements of Meroney (1968) and Landsberg and Thom (1971) for individual plant elements in wind tunnels.

The computed D_o is small compared to the height of the vegetation. This implies that the flow is an "individual roughness" type, since D_o's calculated using empirical formulas derived from canopy flow studies are much larger. Later results will support this conclusion.

5.2 Flow Below Shrub Height

The flow below shrub height was also investigated. A velocity profile measured at an "isolated" spot, i.e. far removed from nearby bushes, is shown in Fig. 11. This wind data implies a logarithmic profile with z_o = 0.12 cm, but since winds were obtained for only three heights this cannot be proved. Note that the apparent logarithmic profiles exhibit a consistent z_o for different time periods with different mean velocities.

A theoretical case for predicting a logarithmic profile between obstacles for isolated roughness flow will be made in the following paragraphs, and experimental results have confirmed this prediction. However, no canopy investigation has found such a profile. Thus the apparent logarithmic profile between shrubs is further evidence that the flow is of the isolated roughness type.

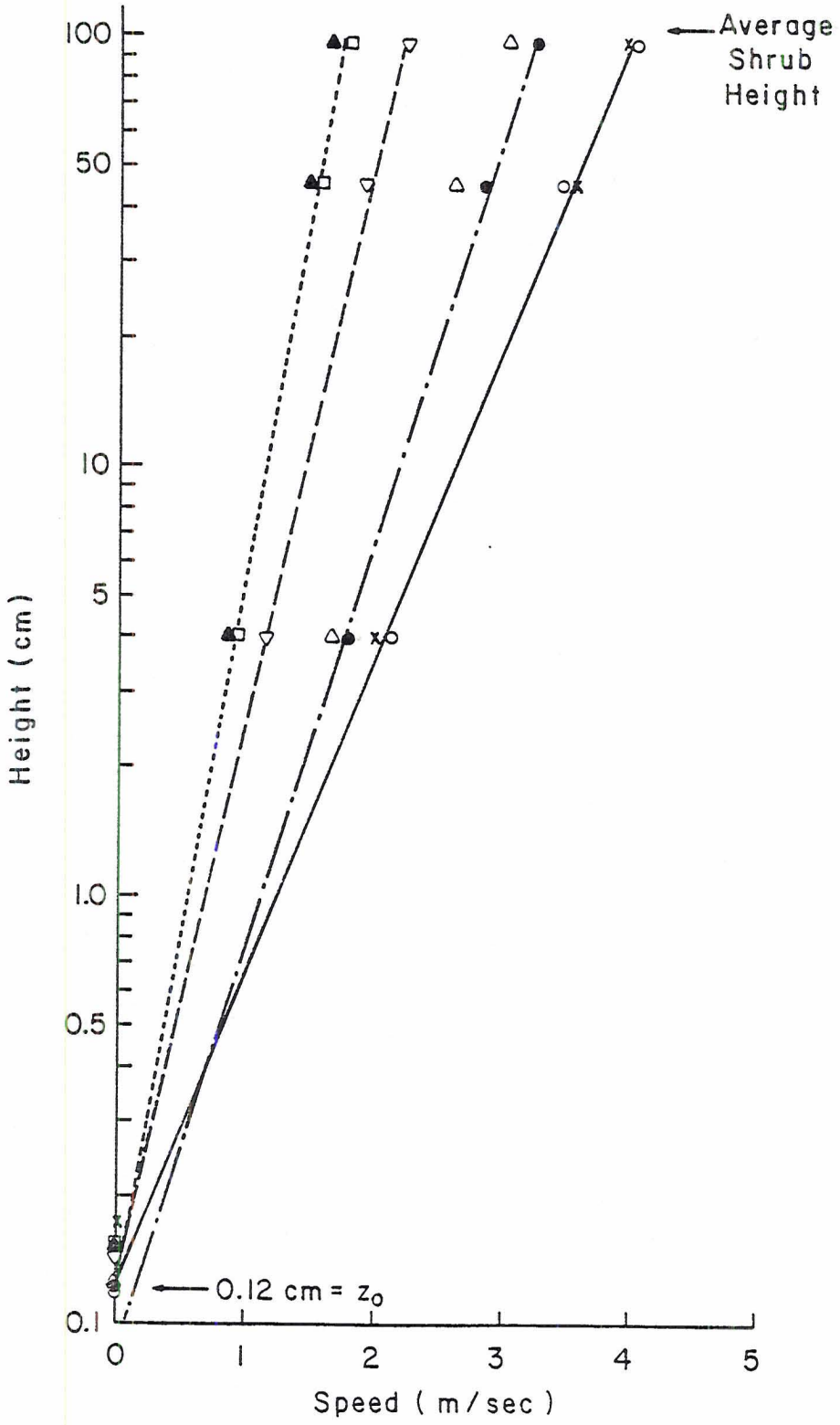

Fig. 11. Wind Profiles Between Shrubs

When an established flow experiences an abrupt change in surface roughness, the flow does not immediately adjust to the new surface at all levels. At the surface an internal boundary layer develops. This layer is in equilibrium with the new surface and has a logarithmic velocity profile. The depth of the equilibrium layer increases downstream as the flow at higher level adjusts to the new boundary conditions.

This same phenomenon, the development of an internal boundary layer, also occurs downwind of a line change of roughness such as a windbreak (Plate, 1971). Counihan et al. (1974) have developed a theory of wake flow in which this "wall" layer is assumed to be an "equilibrium" layer, as defined by Townsend. Turbulent energy production then locally balances dissipation. They argue that since the perturbation pressure gradient is negligible and the velocity approaches zero at the wall, the momentum equation requires the shear stress gradient near the wall to be zero and a logarithmic velocity profile results. Their experimental data does indicate such a region in the wake flow behind a solid object.

The upwind fetch needed to build an internal boundary layer to bush height may be estimated from Elliot's (1958) equation:

$$\delta/z_o \propto (x/z_o)^{4/5} \qquad (5\text{-}4)$$

where δ = height of the internal boundary layer

x = horizontal distance downwind of the change in roughness.

Bradley (1968) found the proportionality constant to be about 0.9. Since z_o = 0.0012 m, the internal boundary layer would reach the average shrub height at 6.1 m downwind. The average distance between

bushes is 5.8 m, and since they are staggered it is reasonable to expect a logarithmic profile between bushes. The particular isolated spot at which the measurements were made had an upwind fetch of about 12 m, so a logarithmic profile should have been established.

O'Loughlin and Annambhotla (1969) experimentally studied the "wake layer" flow below the tops of solid roughness elements. Their flow visualizations showed the existence of a "horse-shoe" vortex with horizontal diameter of 3 H surrounding and streaming from each side of a roughness element. They found logarithmic velocity profiles between the elements, profiles which were not dependent upon the boundary layer thickness. Thus the surface boundary conditions dictate a type of "inner" law, in which the shear stress does not vary greatly with height. Their inner logarithmic profile met an outer flow logarithmic profile at $z \approx 1\frac{1}{2}$ H, producing a kink similar to that observed in the GMX area where outer and inner logarithmic profiles were also found (Fig. 12).

If a logarithmic velocity profile is assumed [Eq. (4-6)], the ground friction velocity $[(U_*)_g]$ can be obtained from the velocity at 4 cm:

$$(U_*)_g = \frac{k}{\ln(z/z_o)} U = \frac{(.4)}{\ln(\frac{0.04\ m}{0.0012\ m})} U(4\ cm) = 0.114\ U(4\ cm). \qquad (5\text{-}5)$$

Under the above assumption the meteorological drag coefficient is not a function of wind speed. Although a logarithmic profile usually implies a constant stress layer, caution must be exercised in such an interpretation. Sadeh et al. (1971), for example, found a nearly logarithmic profile when the stress was not constant with height.

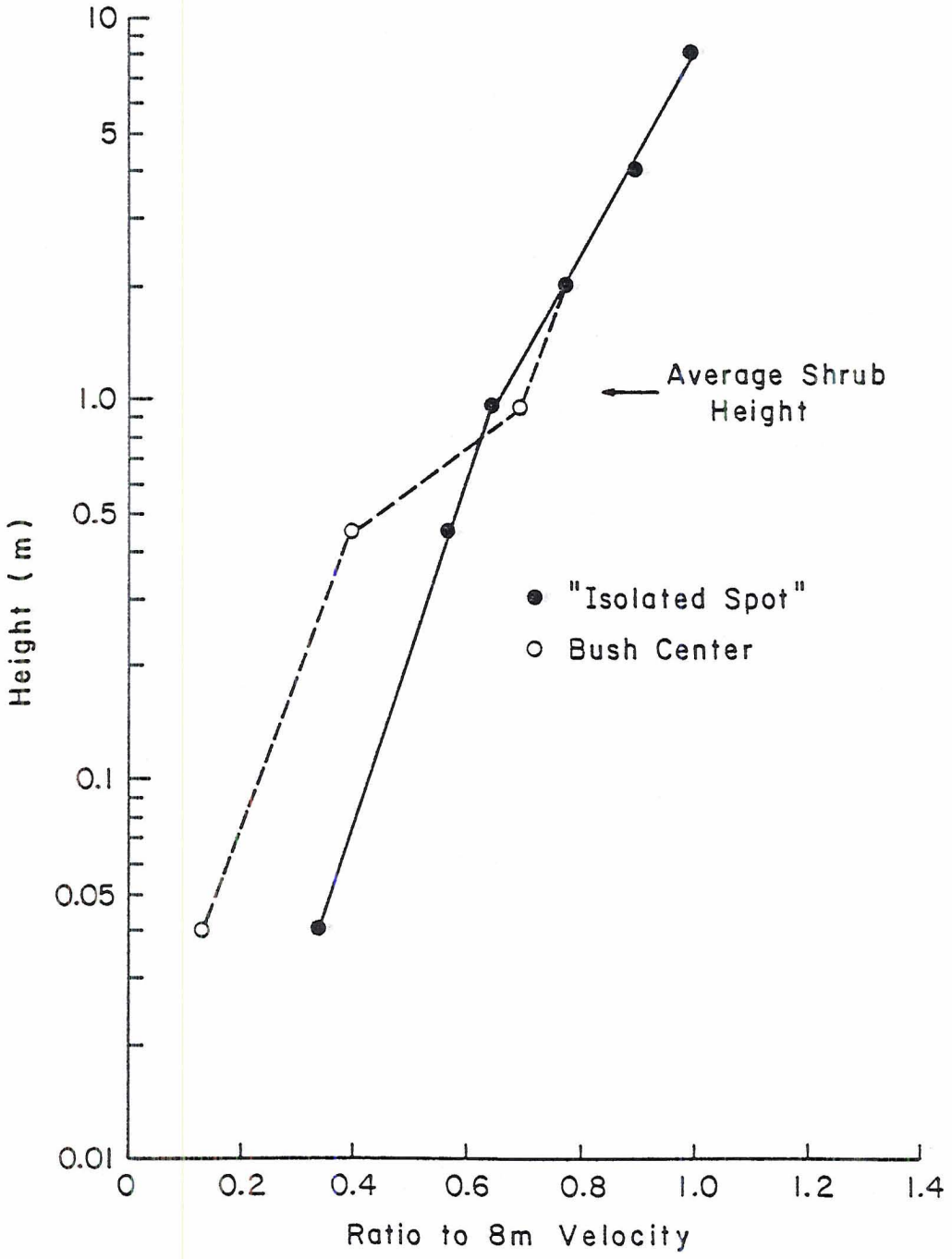

Fig. 12. Wind Profiles Above and Below Shrub Height

The above calculation of the ground stress by Eq. (4-6) omits the diabatic correction previously used to calculate the total stress above the vegetation. Similarity based diabatic corrections have been shown to be valid above a horizontally homogeneous surface, but not between roughness elements. Below the shrub height the vegetative drag dominates the momentum transfer and bouyancy effects should be negligible. The observation that the wind speed ratios below shrub height were not dependent upon the wind velocity, while the ones above shrub height were, supports this contention. Further support comes from Bradley (1972), who found the measured drag coefficient to be independent of wind speed below a 1 m height over wheat stubble, whereas at higher levels the drag coefficient decreased with increasing wind speeds.

The above drag coefficient value can be checked by assuming that an equilibrium layer exists close to the ground (See Appendix B). An analysis of 24 cases for the isolated spot implies that $(U_*)_g/U(4\text{ cm})$ is not constant, as a logarithmic profile would imply, but is dependent upon wind speed (Fig. 13). However, the equilibrium layer assumption is less valid at lower wind speeds, so this implication may be false. The important point is that at the higher wind speeds the result $(U_*)_g/U(4\text{ cm}) \approx 0.12$ is supported by both equilibrium layer assumption and logarithmic profile assumption calculations.

The velocity distributions for all heights at the isolated spot are very close to Gaussian curves within two standard deviations of the mean, but the tails were slightly heavy. The heaviness of the low speed tail results from the inability of a speed to be negative.

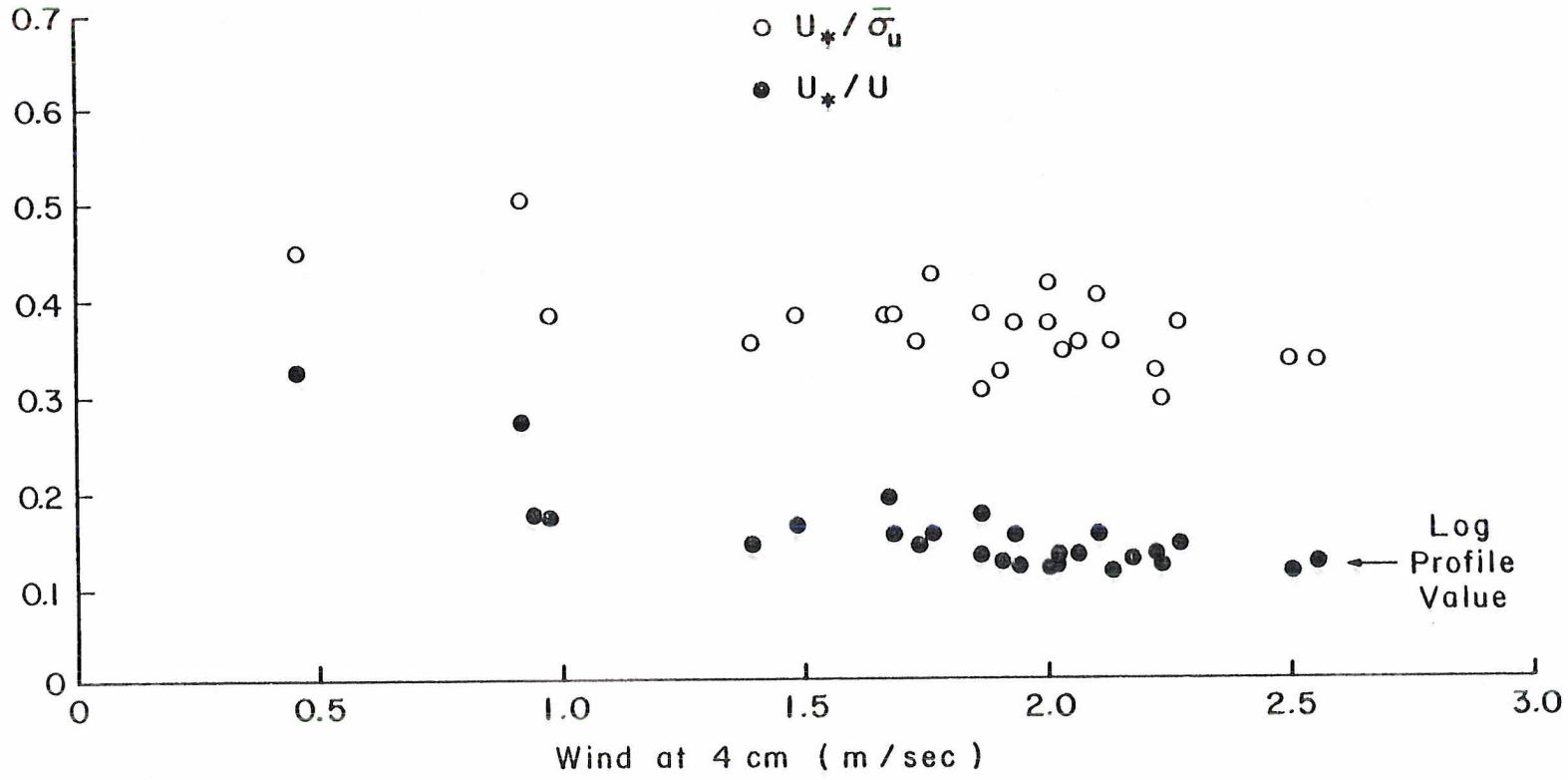

Fig. 13. $(U_*)_g/U$ and $(U_*)_g/\overline{\sigma_u}$ Between Shrubs as a Function of Wind Speed

The positive skewness of the distributions reflects the finite probability of very large velocities. Plotting the complement cumulative distribution function showed that the tail is most similar to a Gamma distribution tail. The shorter the time interval, the closer the velocity distribution approached a Gaussian distribution because the flow was steadier.

Nikuradse (cited by Businger, 1973) found an often used criteria for "fully" rough flow:

$$\frac{U_* z_o}{\nu} > 2.5 \qquad (5\text{-}6)$$

where ν = kinematic viscosity of air. It should be noted that Counihan (1975) has suggested that this criteria may be a function of surface roughness. At GMX z_o = 0.0012 m and $(U_*)_g/U(4\text{ cm})$ = 0.114. Since $\nu = 1.7 \times 10^{-5}$ m^2/sec @ 40°C and 0.92 atm, the flow is fully rough whenever U(4 cm) > 0.3 m/sec. All the measurement periods met this condition. Furthermore, the minimum friction velocity for erosion will be found to be 0.21 m/sec (at 0% soil moisture), so $\{(U_*)_g\ z_o/\nu\}$ > 15 under erosion conditions.

The criteria usually used for fully turbulent flow is $(U_*\ z)/\nu$ > 30, thus when erosion occurs fully turbulent flow extends down to and below 0.24 cm, although probably not to heights close to z_o.

5.3 Flow Inside the Test Bush

A creosote bush consists of relatively stiff branches of up to one centimeter in diameter. Each branch exerts a drag on the flow, a combination of form and surface drag. Each individual branch has a negligible effect, but together they form an effective resistance

which produces a pressure drop extracting momentum from the flow. Each branch generates a wake, producing a large turbulent intensity just behind it, but the eddies generally have such high frequencies that individually they contribute little to the shear stress. Using the relation between Strouhal number and Reynolds number for flow past a cylinder (Schlichting, 1968) to approximate flow past a branch, the eddy frequencies in a bush may be expected to range from 20 to 1000 cps under typical conditions, with the smaller frequencies found only for very large lower branches. Since spectral measurements determined that the inertial subrange exists only for frequencies less than 50 cps, the individual branch eddies contribute little to large scale shear.

Vertical velocity profiles were obtained at locations upwind, downwind, and inside the chosen bush along the wind radial passing through the bush center. Some measurements were also made to the side of the bush. Velocity profiles were obtained by the three hot wire anemometers and standardized using concurrent measurements of the isolated 2 m cup anemometer (Fig. 14).

The general features of these velocity profiles can be qualitatively described. The flow is retarded as it approaches the bush at the lower levels, but at the top of the bush it speeds up slightly. As the flow moves through the bush the flow strength decreases at all levels. Behind the bush the velocity retardation is greatest at mid-bush height. The velocity profile adjustment is similar to that found by Kawatani (1968) in the initial adjustment flow region within peg roughness elements. Plate (1971) has suggested that the velocity should be approximately constant just ahead, behind, and inside a

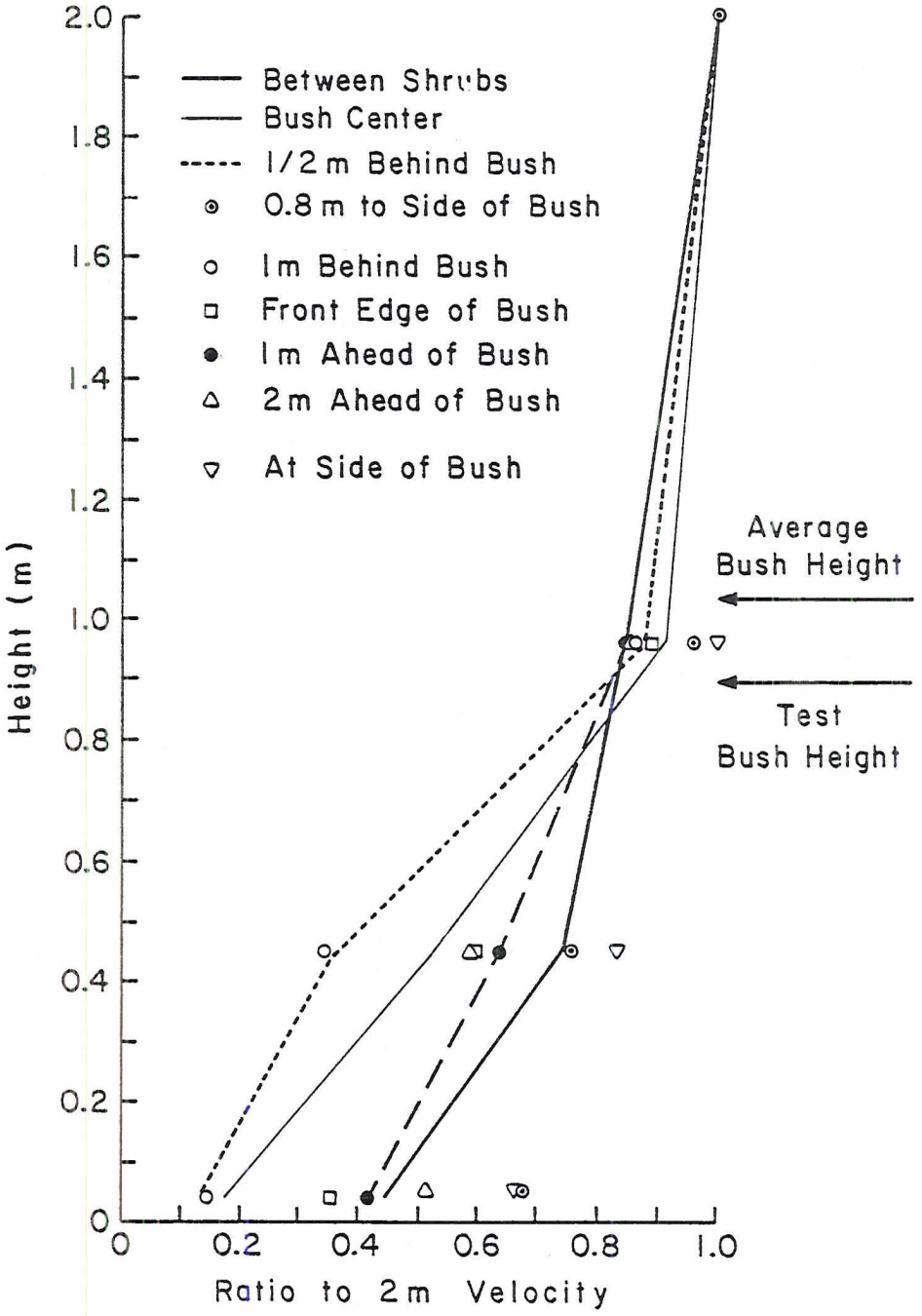

Fig. 14. Wind Profiles Near and Inside the Test Bush

porous wind break. Although Fig. 15 might indicate that the velocity profile is linear with height, an approximately constant velocity profile (dotted line) cannot be ruled out because measurements are only available at three levels.

Even though the flow through a three-dimensional object must itself be three-dimensional, for flow along the centerline parallel to the wind it was considered to be two-dimensional to a very rough approximation. Justification comes from symmetry arguments and from Edling's (1974) analysis of flow over a finite roughness element, which found the three-dimensional effects to be confined to a narrow shear plane near the edge. Towards the center of his roughness section the flow was two-dimensional to a first order approximation.

To the side of the bush the velocity increases markedly at all levels. This implies that the flow may diverge horizontally more than vertically.

The velocity frequency distributions measured inside the bush were approximately Gaussian, except for the tails, which were significantly heavier than the distribution tails measured outside the bush. They exhibited large positive skewness and a platykurtic distribution. The turbulent intensity increases close to the ground. These results agree with those of Allen (1968) and Perrier, et al. (1970) and are typical of flows found within vegetative canopies.

5.4 Drag Partition

A major difficulty in assessing the susceptibility of a soil to wind erosion is allowing for the protection afforded by vegetation. Most studies of the drag on roughened surfaces in a fully developed

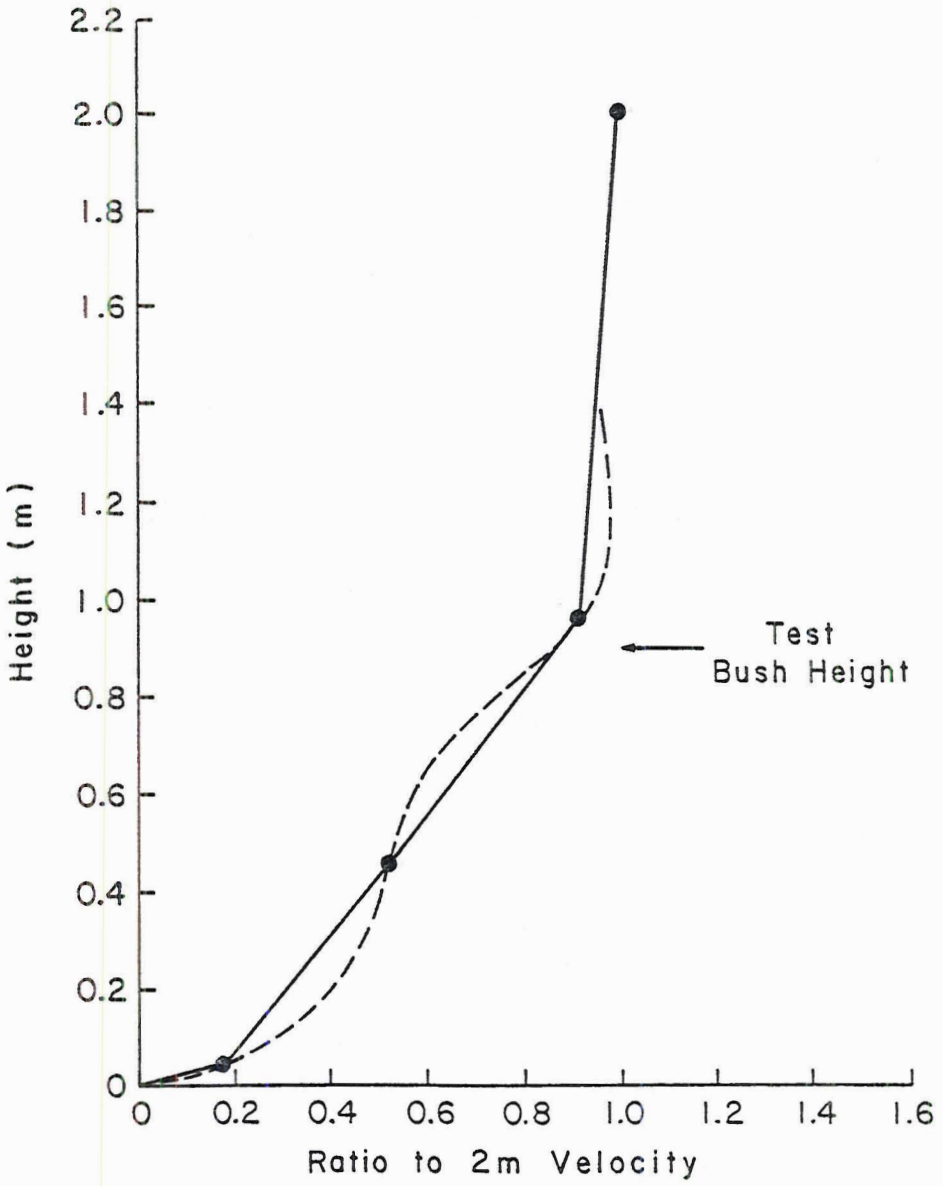

Fig. 15. Wind Profile at the Center of the Test Bush

boundary layer have assumed the surface to be homogeneous, as in Nikuradse's classic studies on sand-roughened pipes. But the flow over discrete isolated obstacles with a relatively smooth surface between them is a considerably different circumstance, since the total drag arises from both ground drag and obstacle drag. Scant attention has been paid to the question of how drag is partitioned between the two sources, but such studies are vital to estimating the shear stress on the soil from known stress above the vegetation. Wooding, et al. (1973) give a brief history of the few drag partition investigations which have been undertaken.

The total shear stress of the air flow above the bushes (τ_o) is a combination of the stress on the ground itself (τ_g) and the stress exerted by the bushes (τ_b). Their relative magnitude can be computed for the GMX area, based upon previous stress calculations for the flow above and below bush height. Using C_d from Fig. 10, the friction velocity above the bushes is found to be 0.62 m/sec for a reference wind of 8 m/sec at 8 m. The corresponding 4 cm wind is 2.42 m/sec, and since the surface drag coefficient is 0.013, the calculated surface friction velocity is then 0.32 m/sec. The definition of friction velocity [Eq. (4-1)] then gives $\tau_o = 0.41$ n/m^2 and $\tau_g = 0.11$ n/m^2. Assuming that the surface stress is constant outside the bush and zero inside it, the drag partition equation may be written:

$$\tau_o = \tau_b + \tau_g \left(1 - \frac{A_s}{S}\right). \qquad (5\text{-}7)$$

Solving Eq. (5-7) for τ_b and using the above values of τ_o and τ_g gives $\tau_b = 0.31$ n/m^2. Therefore 76% of the total stress above the bushes

results from the bushes themselves, even though they only cover 10% of the surface area. The remaining 24% of the total stress arises from stress on the soil.

The assumption that the surface stress is constant outside the bush and zero inside the bush, used to derive Eq. (5-8), is often made for the sake of simplicity. This assumption is certainly not valid for a solid, two-dimensional windbreak as the surface stress is negative for the part of the surface covered by the front and rear separation bubbles. Downstream of the reattachment point, it increases rapidly, and approximately linearly with distance to reach its unobstructed value (Plate and Lin, 1965), unless adjacent roughness elements are too closely spaced. Porous wind breaks have no separation bubble and the stress is positive inside the bush, making the assumption more valid. For three-dimensional objects the stress distribution around the object is unknown. Because of the above assumption, the average τ_g should have used to calculate τ_b from Eq. (5-7). However, because the maximum value of τ_b had been measured it was used instead. This results in a slight underestimate of τ_b.

The drag coefficient of a bush for this flow situation can be calculated from:

$$c_d = \frac{\tau_b \, S}{\rho \, A_f \, U^2} \, . \qquad (5\text{-}8)$$

Obviously the bush drag coefficient depends upon the reference velocity. Since one purpose of computing the drag coefficient is to use published graphs of porosity (ϕ) vs. drag coefficient (c_d) to estimate the porosity of the average bush, several drag coefficients have to be calculated.

Seginer (1972) compiled c_d vs. ϕ curves from several sources, using a drag coefficient based upon the velocity at bush height. The corresponding bush c_d of 0.17 implies porosities of 0.68, 0.77, and 0.80 from these curves. Hagen and Skidmore (1971) used an average velocity computed over the wake depth for their c_d. Taking this depth to be 2 m, the calculated bush c_d is 0.16 and gives a porosity of about 80% by extrapolation. Graham's (1976) wind tunnel gauze results imply a porosity of 82%.

The above results suggest that the average bush porosity is in the 70-80% range. However, this "porosity" is actually the equilvalent porosity of a two-dimensional windbreak, since the curves used to obtain the porosity values had all been derived from windbreak data. Thus the "porosity" calculated above includes the effect of the finite width allowing air to flow around the bushes.

Marshall (1971) conducted wind tunnel experiments to measure the drag partition for solid cylinders and hemispheres of various diameters and spacings. He was able to obtain a good correlation between the stress partition and the roughness element concentration parameter λ. Using his Figure 7, the calculated λ of 15.4 for the bushes at GMX predicts that the portion of total stress due to ground stress should be negligible. The discrepancy between this prediction and the above calculation showing the stress absorbed by the ground to be 24% of the total stress results from the fact that Marshall's measurements were made on solid (0% porosity) objects while the bushes have just been shown to be aerodynamically quite porous (ϕ = 70-80%). In an attempt to empirically correct for this

porosity, λ may be divided by the approximate "denseness" of the bush (25%). This new value predicts the ground stress fraction to be 24%, in considerably better agreement with measurements. Marshall (1970) used his wind tunnel results to estimate the amount of vegetative cover needed to arrest soil erosion in a semi-arid region of Australia. Because he made no allowances for bush porosity, his calculations must over-estimate the protection afforded by a given shrub concentration. Wooding, et al. (1973) combined several sets of high Reynolds number drag partition experiments, including Marshall's, into a slightly different curve of drag partition vs. λ. It also predicts that the stress is entirely due to the vegetation, while using the same porosity correction more correctly implies that only 71% of the stress will be absorbed by the plants. It is concluded that drag partition studies based solely on the roughness element concentration (λ) of solid roughness elements cannot be directly used for aerodynamically porous bushes. Some allowance must be made for the effect of bush porosity upon the bush drag coefficient.

Arya (1975) derived an expression for drag partition, his equation 10 which may be written as:

$$\frac{\tau_b}{\tau_o} = \left[1 - \frac{2(1 - m\lambda)\, k^2}{c_d\, \lambda\, (\ln H/z_o)^2} \right]^{-1} \qquad (5\text{-}9)$$

where m = parameter correcting for non-constant ground stress. Eq. (5-9) predicts the bush stress to be 78% of the total stress, closely agreeing with the calculated value of 76%. For comparison purposes m was set equal to 2 in using Eq. (5-9), which is equivalent to making the assumption used to derive Eq. (5-7). No porosity

correction was needed, since Eq. (5-9) includes the effect of a variable drag coefficient. For this reason Arya's formulation is believed to be more useful in estimating the ground stress for a surface protected by vegetation.

It is interesting to estimate Z_o for the GMZ area from a relatively complex formula also derived by Arya, the calculated value being 3.6 cm. To compare this value to a measured value, Z_o must be obtained from Eq. (4-6), i.e. a logarithmic profile with no displacement height, since this is the profile that Arya assumed in his derivation. Under this requirement, the observed Z_o was 3.1 cm, in relatively good agreement with the estimated value. However, the much simpler Lettau formula [Eq. (4-10)], one believed to be relatively accurate for widely spaced obstacles, predicts Z_o = 3.3 cm, in even better agreement.

Marshall (1971) demonstrated that for widely spaced roughness elements, the drag due to the bushes can be found by calculating the drag on each bush from the drag coefficient for a single bush and adding the drag due to the surface stress. However, as the elements become less distantly spaced a point is reached when the above approach is invalid. This is because the flow has changed from an isolated roughness flow to a wake interference flow, where the wake or separation zone from an upwind obstacle now affects the flow around downwind elements. In this regime the c_d determined for an isolated element is no longer valid, and as the elements become very closely spaced the total drag actually decreases and the surface stress becomes negligible. Marshall developed a criteria for determining whether

the obstacles behaved as individual elements. Using the same porosity correction as previously, the criteria for isolated roughness flow was found to be satisfied. Thus the bushes act as individual roughness elements, in agreement with previous conclusions.

6. AEOLIAN EROSION

6.1 Erosion Description

The severity of aeolian erosion depends upon the climate, the soil, and the vegetation. Soil erosion by wind action is a problem primarily in dry regions. In these areas high winds occur frequently, the soil texture and moisture usually permit easy detachment of the particles, and the sparse vegetation cannot shelter the soil. The greatest wind erosion occurs where the average annual precipitation is less than 20 inches.

The following paragraphs will discuss only aeolian erosion. While stream bed particulate transport is qualitatively similar to wind erosion, the vast difference in density between water and air produces different quantitative results. Specifically, the large difference between the density of air and the particle density enables particle inertial effects to dominate fluid viscosity effects for aeolian erosion, but this is not the case for water erosion.

Wind driven soil movement occurs in three modes: surface creep, saltation, and suspension. The saltation mode, in which the particles move in a series of jumps, is the initiating mechanism. Wind erosion begins when soil particles or aggregates are set into motion through wind pressure forces overcoming gravitational forces. The surface shear stress required to move the most erodible soil grains is called the threshold stress $[(U_*)_t]$.

In the field, erosion begins at knolls, ridges, and other more exposed spots. Once erosion has started, it spreads fanwise to leeward and the bombarding action of the saltating particles causes

other particles to move. The saltating particles can also abrade the large soil aggregates, disintegrating them into more easily erodible sizes. Coarse soil particles hinder the erosion by sheltering the finer, more erodible grains from the wind. Very fine dust particles also hinder erosion by increasing the cohesive forces between soil particles. Assuming an eroding surface of sufficient length, the erosion flux increases with downwind distance until it reaches the maximum that the wind can sustain.

Particles moving in saltation usually begin their motion by rolling, then they abruptly rise vertically into the airflow. Aerodynamic drag accelerates them and they reach horizontal speeds approaching those of the wind itself. After the particles reach their maximum height, gravity pulls them downward in a nearly straight trajectory at an angle of 5-12° to the horizontal. The higher the grains bounce, the more momentum they extract from the wind and the harder they impact the soil surface. Upon impingement the saltating particles may cause other particles to move, as in a chain reaction, or they may bounce upward again. Quartz sand particles in particular are very elastic. The oblique descent angle and the irregular surface result in the rebounds being nearly vertical. Lift on the particle also contributes to this vertical rise. Momentum is thereby transferred from the fluid flow to the surface, resulting in a shear stress between the two. The saltation transport depends upon the ground shear stress.

Saltating particles have diameters of 50-500 μm. They must be small enough to be moved by wind action but large enough not to remain suspended in the air. The impacts from these saltating grains

initiate the movement of both larger and smaller particles. The size distribution of the saltating particles changes with height due to the faster gravitational sedimentation speed of the larger particles.

The larger and heavier soil particles and aggregates move by sliding or rolling along the surface in the surface creep mode. Many of these particles cannot be moved by wind pressure alone, but they are moved by the impact of saltating grains. Gillette et al. (1972) found the particle size distributions of the creep particles and of the soil to be nearly identical. The diameter of particles moving in surface creep is usually less than 2000 μm.

Very small particles in the soil are extremely cohesive and are raised into the air only through the sand blasting action of saltation. If their settling velocity is less than the characteristic velocity of the turbulent fluctuations, they will be supported by the turbulence and carried horizontally in the third mode of movement, suspension. Upward eddies, such as thermals (Sinclair, 1976), can lift dust particles high into the atmosphere. Particles in suspension have diameters less than 80 μm. Alternatively, dust particles may cling to the larger grains and be transported with them.

Aeolian erosion is essentially a surface phenomenon extending to saltation height. Comparatively few saltating grains jump higher than a meter above the ground, 90% of the mass movement occurring below 20 cm. The saltation layer is about 10 cm deep for particles of 100 μm diameter. Saltation coupled with mechanical and thermal turbulent eddies may raise dust clouds three to five kilometers high, but the major movement of the soil mass is horizontal, not vertical.

Most of the eroding soil moves in the saltation mode. The relative proportions of the three movement modes varies greatly for different soils and different wind speeds. Roughly 50-75% of the soil mass is moved through saltation, 5-25% in surface creep, and 3-40% by suspension (Chepil and Woodruff, 1963). The distinction between these modes of transport is somewhat artificial, since all three result from the interaction of particles with the turbulent wind.

As the erosion continues the smaller, more erodible soil fractions are continually sorted from the larger clods and rocks, which remain in place unless they are broken down by abrasion. The eroding fraction is caught by bush hummocks, and comparison of the desert pavement and hummock soil size distributions confirms that the gravel ($d > 2000$ μm) has indeed been sorted out. The most erodible fraction appears to be the fine sand ($d = 125$-250 μm). This might seem to conflict with Bagnold's (1954) observation that the most easily disturbed particles have a 110 μm diameter, but his result was obtained for loose, cohesionless sand grains. Since cohesion forces affect smaller particles more strongly, it is logical that under field conditions the most erodible particles should have a diameter larger than 110 μm and this has been confirmed by Zingg and Chepil (1950).

Bagnold (1954) found that sand moving in saltation took up much of the momentum of the wind, reducing its velocity just above the surface. It is also believed that suspended particles can dampen turbulence and thus alter the apparent von Karman constant (Barenblatt and Golitsyn, 1974). Because the saltation flux at NTS was small, neither of these factors need to be considered.

6.2 Soil Erosion Factors

Describing the factors that affect aeolian erosion will emphasize the complexity of the subject and underscore the necessity for empirical approaches to the problem. These factors are particle size and density, wind speed and surface stress, turbulence, soil moisture, surface soil structure, non-erodible elements, and vegetation.

Particle size and density affect the threshold stress needed to initiate movement. As previously indicated, few very large or very small particles are moved directly by the wind. Thus the soil must contain a large fraction of sand sized particles to begin the saltation movement so necessary to sustain wind erosion. Relatively few particles with diameters larger than 500 μm are moved by winds, although a few up to 2000 μm may be moved by very strong winds, so soil cloddiness decreases the soil erodibility. Chepil (1946) used a 840 μm diameter cutoff to distinguish between erodible and non-erodible soil fractions.

The wind erosion rate depends upon the frequency and intensity of high wind episodes. A strong wind, greater than the saltation threshold velocity, is needed to dislodge the grains and initiate movement. Also, a strong wind imparts more momentum to the saltating particles, thereby increasing the horizontal flux.

Wind turbulence must have some effect on the threshold velocity, but presently little is known about the magnitude of its influence because most work has been conducted in wind tunnels over relatively plane surfaces. There the turbulence was determined by the surface roughness, giving turbulence levels significantly different from those found in the atmosphere above a pebble-covered surface.

Soil moisture is an important determinant in wind erosion because only relatively dry particles are wind erodible. Water film cohesion between particles make them virtually stable. The force of cohesion varies directly with the moisture content. This cohesive force raises the threshold stress needed to dislodge the particles.

A very important determinant of the soil erosion rate is the soil structure. Any change in particle cohesion or agglomeration changes soil erodibility. The desert pavement has a crust about 0.2 cm thick, recognizable by its dense platy structure. This erosion resistant crust is formed by the action of rain drops striking the surface and dispersing clay and silt particles at the surface. On drying, the soil particles are cemented together to form a crust more compact and mechanically stable than the soil below. The number of non-erodible clods is also increased. This cementing action is more common during the summer months. The surface crust can be weakened by the abrasion from saltation, which loosens the bonds between the soil particles and exposes a more erodible soil. The non-erodible clods also gradually break under these impacts. The longer the erosion continues the greater the quantity of erodible material that is formed by abrasion. The desert crust is especially susceptible to abrasion. Artificial mechanical disturbances, e.g. vehicles driving on the desert pavement, enormously increase the erodibility of the soil.

Rainfall often carries water soluble cementing materials downward, leaving on top coarser particles such as quartz sand or water stable aggregates. Some of these particles remain loose on the surface and contribute to the initiation of soil erosion. They dry rapidly

on the surface and consequently may be moved by the wind soon after the precipitation, even before the drying of the surface is apparent. Abrasion from these particles tends to wear down the surface crust, and thereby hasten the drying of the surface.

The erosion flux depends upon the unobstructed distance over which soil particles can move. The more frequently moving particles strike the surface, the greater the subsequent detachment of the soil particles. Thus wind erosion increases with upstream fetch until it achieves equilibrium at the maximum erosion rate the wind can sustain. The more erodible the soil, the shorter the distance needed to reach this maximum.

A rough surface is less erodible than a smooth one for two reasons. Firstly, it is more effective in slowing down the wind velocity close to the surface. Secondly, it allows entrapment of the moving soil particles in sheltered sites, especially when ridges or furrows are present. Non-erodible clods and plant residues on the surface both decrease erodibility for these reasons. Windbreaks, such as standing vegetation, decrease the stress on the ground and are important erosion control devices.

The quantitative effect of the above factors upon erosion flux is very difficult to estimate. The effect of soil structure in particular is especially hard to assess, yet a surface crust can greatly decrease the soil erosion rate. All erosion flux equations contain at least one empirical constant. The best method for determining its magnitude is from actual field measurements of wind erosion at a specific site.

6.3 Erosion Flux Formulae

To develop a formula relating the horizontal saltation flux (F) to wind velocity, Bagnold (1954) assumed that the moving sand grains absorbed the surface stress from the air during their saltation trajectories and transferred it to the ground upon impact. He developed the proportionality:

$$F \propto U_*^3 \tag{6-1}$$

In field experiments with sand dunes Bagnold determined values for the proportionality constant as a function of the soil size distribution. These constants gave the maximum flux sustainable by the wind, since the surface consisted of loose sand grains and the upwind fetch was long enough that the maximum flux had been achieved. Chepil (1945) has shown the general form of Eq. (6-1) to apply equally well to saltation, suspension, and surface creep of dry soils. His investigations have also evaluated the effects of soil texture (Chepil, 1946), cloddiness and vegetative residue (Chepil and Woodruff, 1954), soil moisture (Chepil, 1956), and fetch (Chepil, 1959) on erosion.

Somewhat different equations have been proposed by Kawamura (1948):

$$F \propto \{U_* - (U_*)_t\}\{U_* + (U_*)_t\} , \tag{6-2}$$

by Owen (1964)

$$F \propto U_*^3 + aU_*^2 - U_*(U_*)_t^2 - a(U_*)_t^2, \tag{6-3}$$

where a is an empirical constant,

and by Lettau (1973)

$$F \propto U_*^2 \{U_* - (U_*)_t\} . \qquad (6\text{-}4)$$

As noted by Belly (1964), any of Eqs. (6-1), (6-2), (6-3), or (6-4) could be used to relate wind speed to erosion flux, since all are third order polynomials in U_* with empirical coefficients which must be experimentally determined. Gillette (1976) found Lettau's formula to agree reasonable well with the erosion flux over a Texas field, and this formula was chosen for use with the GMX data. Assuming proportionality between the surface stress and the surface wind, Eq. (6-4) becomes:

$$F = EU^2 (U - U_t) \qquad (6\text{-}5)$$

where E = empirical flux equation constant
U = wind at a given height
U_t = threshold velocity at a given height.

7. EROSION ASSESSMENT

7.1 Threshold Stress

The wind velocity needed to initiate soil particle movement is greatly dependent upon the size of the particle. Because of their weight, large particles are not easily moved. Very small particles also resist movement because they are held by strong cohesive forces and because they remain inside the viscous sublayer for flow over smooth surfaces. Thus there is some intermediate size for which the stress needed to move the particle is a minimum.

The wind forces acting on a surface particle are the total drag, resulting from form drag and skin friction, and the lift caused by the velocity gradient across the particle. By considering these forces, Bagnold (1954) derived an equation relating the movement threshold to the particle diameter and density:

$$(U_*)_t \alpha \left[\frac{\rho_p - \rho}{\rho} gd\right]^{\frac{1}{2}} \qquad (7\text{-}1)$$

This equation ignores the effects of particle cohesion, non-erodible surface roughness elements, and turbulence. Wind tunnel studies conducted by Bagnold confirmed this equation, except for very small particles for which cohesion was a factor. These cohesive forces cannot be evaluated theoretically because the geometry of the contact surfaces is unknown. Figure 16 depicts the classic relationship Bagnold found between particle size and threshold friction velocity for quartz sand (ρ_p = 2.65 g/cm^3), showing that the 110 μm particles are the ones most easily disturbed. Iversen et al. (1973) confirmed this relationship in an extensive wind tunnel study using particles

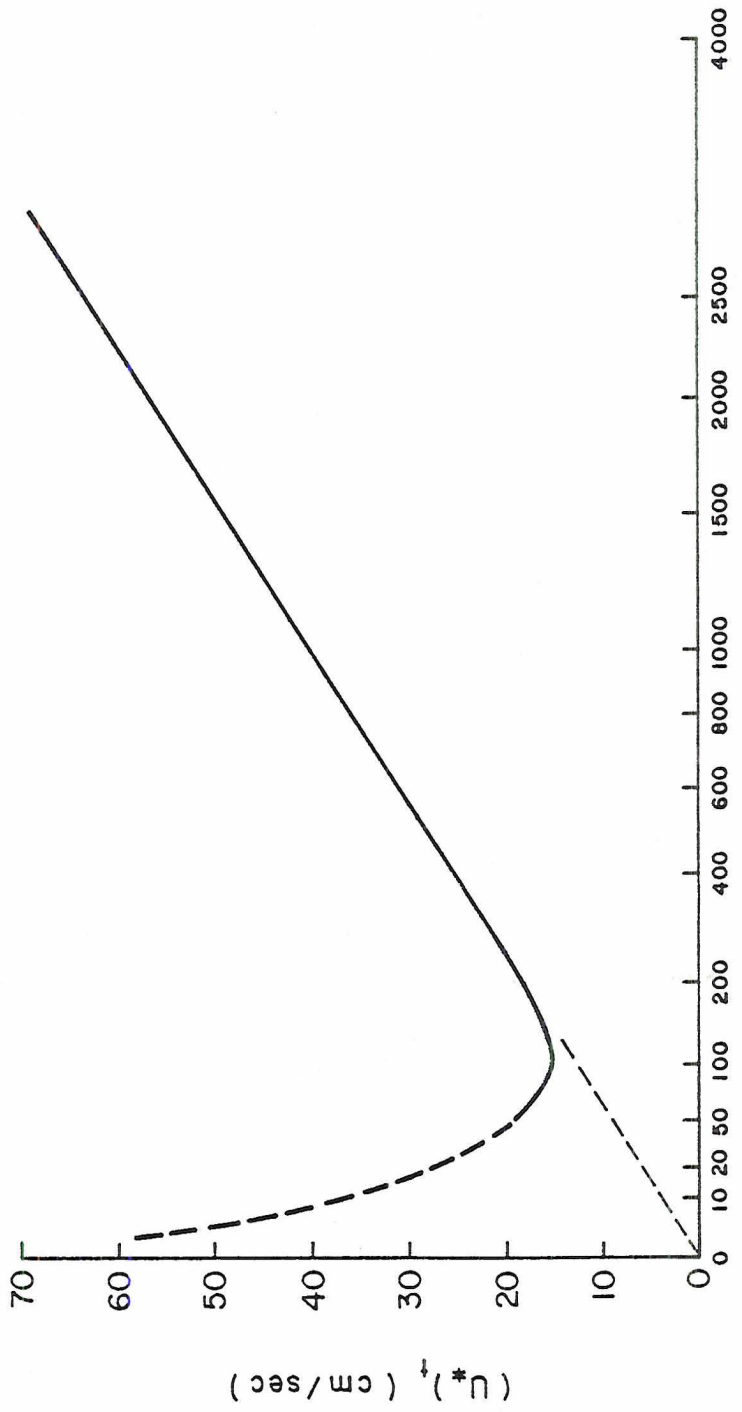

Fig. 16. Threshold Friction Velocity as a Function of Particle Diameter

of various sizes and densitites. All of the above studies involved loose particles. Moisture causes soil grains to adhere to each other, increasing the threshold stress needed to initiate saltation. Chepil (1956) found an empirical relation between soil moisture and the increased threshold friction velocity $[\Delta(U_*)_t]$:

$$\Delta(U_*)_t = 0.77 \left[\frac{M}{M\ (15\ atm)}\right] \qquad (7\text{-}2)$$

where M = soil moisture content

$M\ (15\ atm)$ = soil moisture content at 15 atm suction.

This equation will be used to correct erosion flux calculations for the effect of soil moisture. The value used for M(15 atm) is 4.4%, based upon Seller's (1965) tabulations for sandy loam. It is close to the 4.0% value used by Chepil (1956) for Pratt sandy loam.

Although wind tunnel work has successfully related threshold stress to particle diameter and density, an independent field determination was made for the GMX area. This was done because the surface structure, e.g. non-erodible clods and pebbles and the surface crust, will affect the threshold stress, this threshold value being an important factor in the erosion flux formula.

Gillette et al. (1974) have determined that dust suspension is primarily due to saltation action. Therefore, an increase of dust concentration over the background level is qualitative evidence that saltation is occurring. Figure 17 compares concurrent nephelometer and hot wire anemometer readings at 4 cm. During high velocity periods, when the surface stress exceeds the saltation threshold, the saltation-produced dust concentration rises far above background values. Concurrent ten second averages of the two are shown in

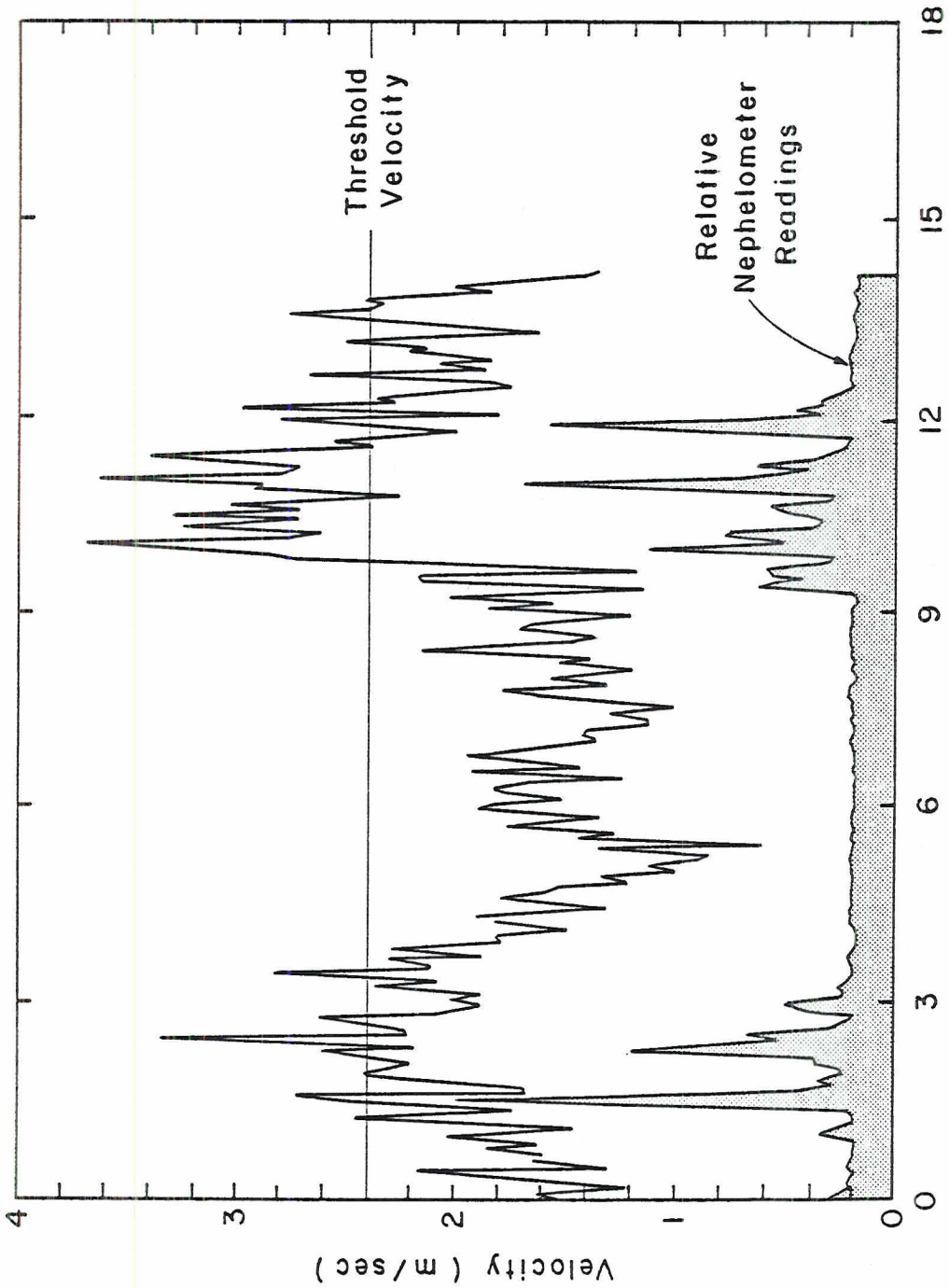

Fig. 17. Saltation-produced Dust Episodes

Fig. 18. The estimated threshold velocity is indicated. Because we are considering only average values, the cut off is not ideally sharp, but a threshold is definitely apparent. Three anomalous points, i.e. high nephleometer readings at velocities below the threshold value, all were found to have occurred after sudden wind bursts had knocked the dust into the air and before the dust had had time to settle out. Using the previously determined relationship between the wind velocity at 4 cm and surface stress, the 2.4 m/sec threshold velocity equates to a 0.27 m/sec threshold friction velocity. This agrees closely with the 0.25 m/sec value found by Gillette (1976) for soils of similar moisture content. Further, when corrected for the 0.35% soil moisture of the measurement period a $(U_*)_t$ of 0.21 m/sec is calculated for a completely dry soil. This is larger than the 0.15 m/sec obtained in a wind tunnel for individual sand particles by Bagnold (1954), which is reasonable since the GMX soil surface elements will increase the stress required to initiate particle motion.

7.2 Erosion Flux Formula Calibration

Because of the complexity of the factors involved, it is difficult to theoretically estimate the quantitative soil erosion rate, as Gillette et al. (1972) discovered in a study of a Nebraska field. This is especially true at GMX, where a surface crust exists. Experimental data is needed to determine the proper porportionality constant for Eq. (6-5). Fortunately, GMX saltation data had been gathered for the period March 20 to April 25, 1974 (Table 5). Unfortunately, only six data values were obtained, two replications

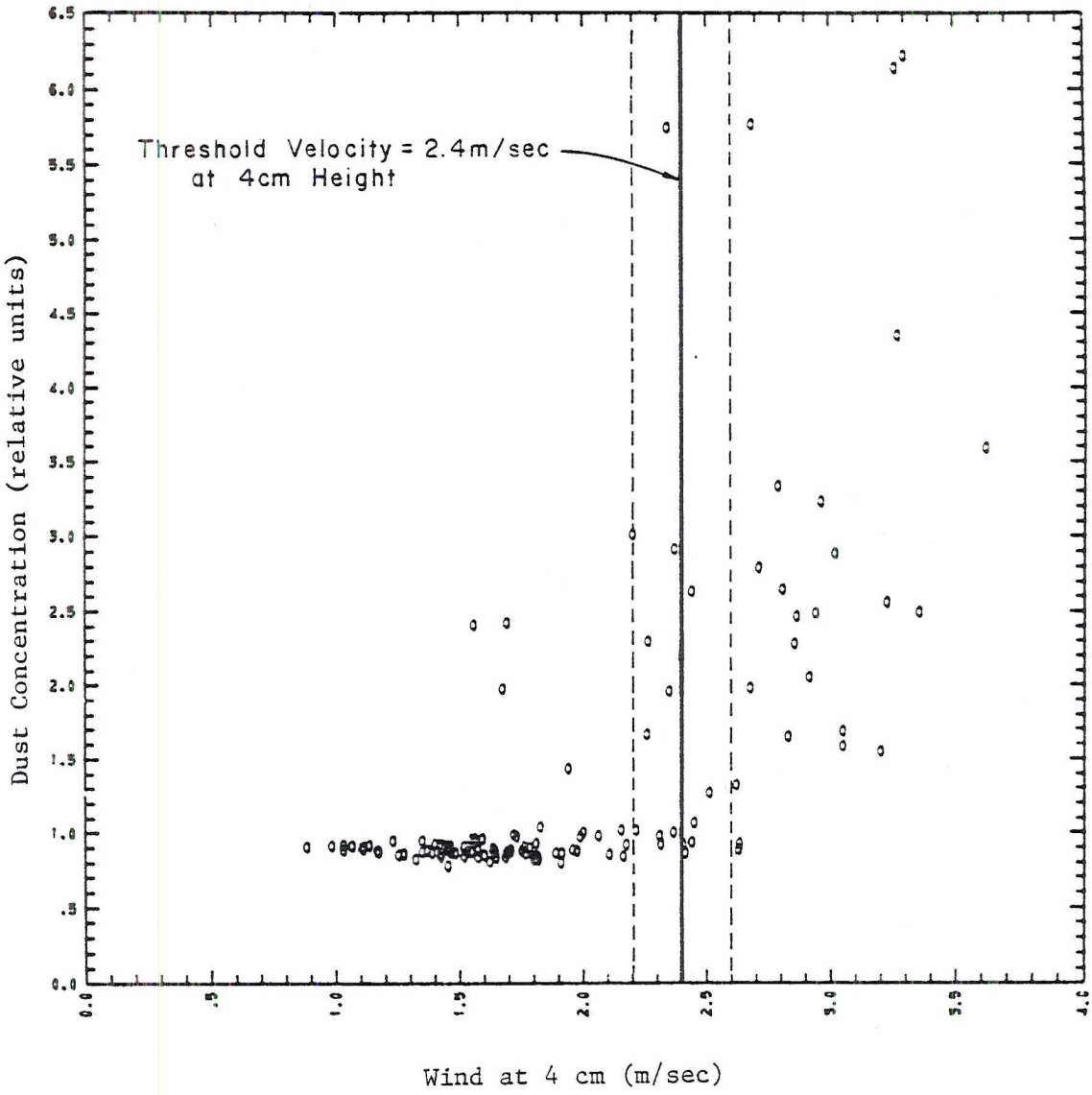

Fig. 18. Threshold Velocity Estimate from Dust Episodes

TABLE 5

GMX Aeolian Erosion Measurements

Level	Period 1		Period 2		Period 3	
	Sample 2	Sample 3	Sample 5	Sample 6	Sample 1	Sample 4
	9^{35} March 20, 1974 to 9^{35} March 28, 1974		9^{30} April 12, 1974 to 14^{25} April 25, 1974		9^{30} March 20, 1974 to 14^{25} April 25, 1974	
22.9-30.5 cm	0.002 g	0.001 g	0.134 g	0.525 g	0.175 g	0.537 g
15.3-22.9 cm	0.002	0.001	0.278	0.536	0.237	0.473
7.6-15.3 cm	0.012	0.004	1.042	1.356	1.143	1.355
0 - 7.6 cm	0.092	0.028	2.392	2.431	2.754	3.407
Surface Creep	0.046	0.022	0.686	0.773	1.010	1.198
Total Saltation	0.108 g	0.034 g	3.846 g	4.848 g	4.309 g	5.772 g
Total Erosion	0.154 g	0.056 g	4.532 g	5.621 g	5.319 g	6.970 g

(from Homan, 1976)

Period	Date	Average Erosion (below 30.5 cm)
1	3/20/74-3/28/74	0.105 g
2	4/12 74-4/25/74	5.077 g
3	3/20/74-4/25/74	6.145 g
Derived	3/28/74-4/12/74	0.963 g

of three time periods, since a certain minimum of collected soil was needed for accurate weighting, and for each measurement the low erosion flux made a long collection period necessary. However, since the three periods overlapped, subtraction allowed a fourth value to be derived for the indicated period. The 30.5 cm high erosion collectors sampled the horizontal flux in five separate fractions (Reichman, 1974). The surface creep dropped through an aperture at ground level, and the saltation flux was captured in four equally spaced vertical compartments. The units had vented collection passages to allow the airflow through the devices to approximate the air flow outside and thereby collect the smaller particles more efficiently. The vents were covered with mesh to allow no particles larger than 10 μm to escape.

The erosion samplers were fixed in position, partially buried in the ground to better collect the surface creep. Because the direction of the collector's aperture was constant, it only measured the vector flux in that direction, not the total erosion in all directions. Particles entering from slightly different directions were sampled according to a cosine law, and erosion in the reverse direction was not sampled at all. Erosion samplers which can rotate with the wind have been designed, but a fixed collector was believed to be adequate for the GMX area because there the erosion moves primarily in one direction. Since there is a particle movement threshold velocity, only the stronger velocities will produce soil movement. Further, because the erosion depends on the cube of the velocity [Eq. (6-5)], the high wind occurrences essentially determine the erosion rate. Figure 19 indicates that the wind direction

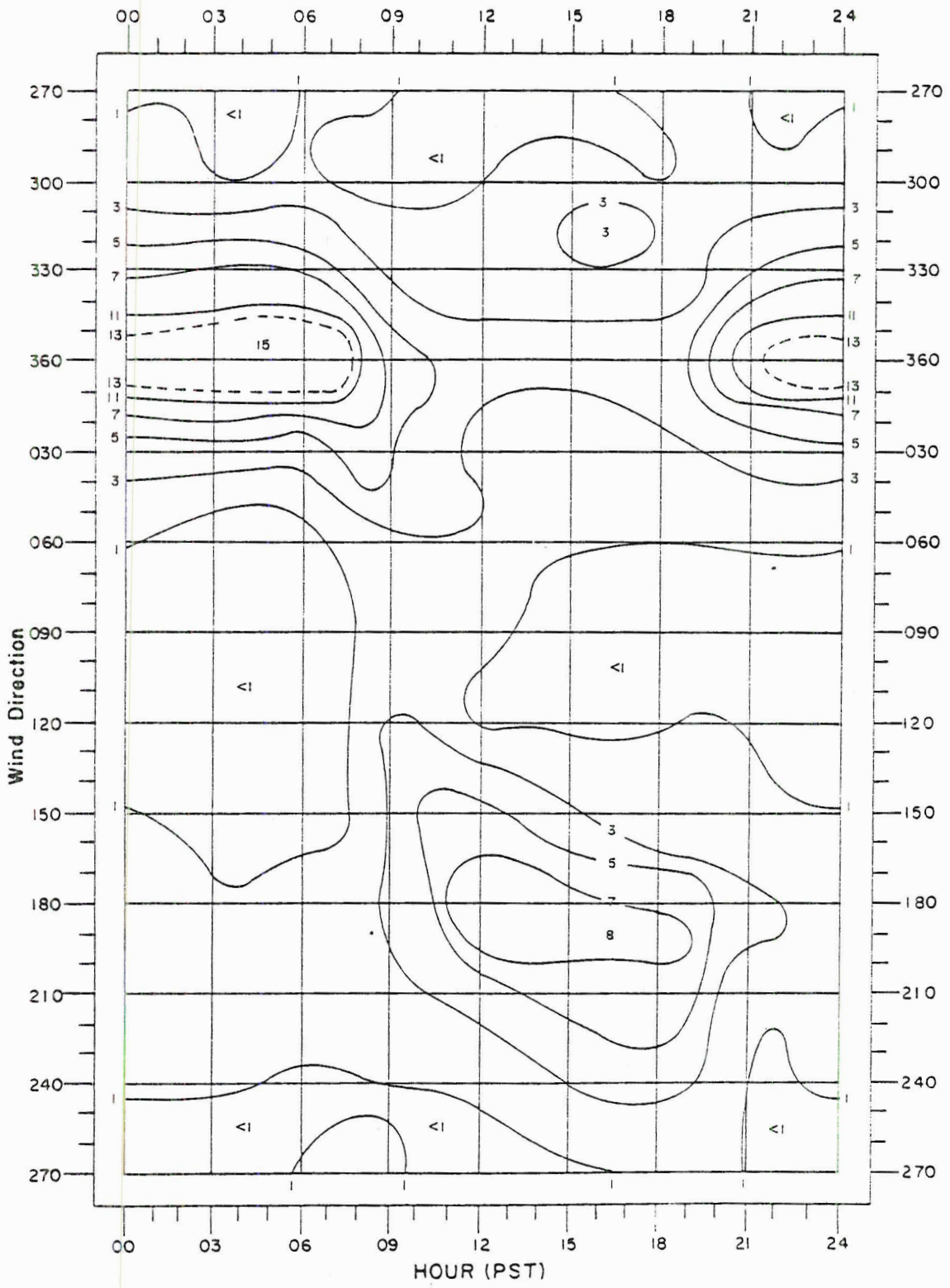

Fig. 19. NTS Wind Direction Percentage as a Function of Direction for March

is very constant for the daylight hours of highest wind speeds during March, the month with the strongest winds. This pattern also prevailed during the year. The following calculations of erosion flux would not be justified if a prevailing direction for high speed winds had not been found. The calculations give the erosion flux in the direction of these high winds (north northeast), and this erosion is believed to represent nearly all of the total erosion flux. Because far fewer high winds occur for other directions, erosion flux in these other directions will be very small.

To find the proportionality constant in the erosion flux equation, Eq. (6-5), the field saltation data must be related to wind data for the same period. For this calibration, the SYSTRAC Station 15 data is used. It would have been preferable to use winds measured closer to the ground and nearer to the erosion collector locations, but such data was not available. A meteorological tower had been erected near the collectors, but wind data was obtained from it only sporadically. More importantly, SYSTRAC winds were available not only for the four calibration periods but also on a climatalogical basis.

As described in the previous section, a threshold velocity (U_t) at 4 cm has been measured, but to use Eq. (6-5) with the SYSTRAC data, an equivalent SYSTRAC U_t is needed. The computed value, 6.1 m/sec for 0% soil moisture, is based upon the following conversions: 1) the ratio between 350,000 hot wire wind speeds at 4 cm and 96 cm for an isolated spot, a ratio found to be essentially independent of wind speed, 2) a small correction factor to adjust 96 cm wind speeds to 1 m wind speeds, 3) the ratio between 125 tower cup anemometer winds at 1 m and 8 m, a ratio found to be a function of

wind speed, and 4) the ratio between 125 8 m tower anemometer and 88 SYSTRAC average winds over the same time period. In anticipation of this conversion, the U_t at 4 cm had been determined for a ten second average velocity because the recorded SYSTRAC velocitites were known to be ten second averages. For the four calibration periods, a SYSTRAC U_t of 10.4 m/sec is used. This value is obtained by applying Chepil's soil moisture correction [Eq. (7-2)] for the measured 0.65% soil moisture to the U_t for 0% soil moisture. No rain fell during these periods, and the measured soil moisture remained constant.

Once the threshold velocity for the SYSTRAC station is known, the empirical constant in Eq. (6-5) can be obtained. To do this the equation must be expressed in the form:

$$F = E \times \sum_i n_i U_i^2 (U_i - U_t) = E \times Q \qquad (7\text{-}3)$$

where Q = erosion wind factor = $\sum_i n_i U_i^2 (U_i - U_t)$

n_i = wind frequency

and the summation is over a given time interval. The frequency values, i.e. the number of SYSTRAC winds of average velocity U_i, were determined for each of the four calibration periods from the SYSTRAC wind data (Table 6). However, since the SYSTRAC stations only measured the winds for a ten second period every 15 minutes, only 1/90 of the possible wind speeds were recorded. Just because a high wind episode had not been recorded did not mean that one had not occurred. The high wind "tail" of a velocity distribution has an important effect on the flux computed by Eq. (7-3). To examine this tail, the complement cumulative distribution functions (CCDF) was plotted

TABLE 6

SYSTRAC Station 15 Winds for Erosion Calibration Periods

Wind Speed (kt)	Frequency (%)			
	Period 1	Period 2	Period 3	Derived Period
0	9.4	10.7	8.9	7.1
1	13.2	7.9	9.4	8.7
2	15.3	8.5	11.1	11.1
3	11.5	8.4	10.0	10.6
4	8.2	8.0	8.0	8.0
5	6.5	7.8	6.7	5.9
6	4.7	5.6	5.1	4.9
7	2.9	4.7	3.8	3.6
8	2.4	4.8	3.9	3.8
9	4.0	3.7	3.3	2.5
10	2.6	3.1	2.9	3.0
11	3.7	3.8	3.4	3.0
12	2.1	2.7	2.5	2.5
13	1.8	2.1	2.2	2.4
14	1.7	2.2	2.4	2.9
15	2.2	1.2	2.2	2.9
16	2.1	2.3	2.3	2.4
17	0.9	1.4	1.5	2.0
18	0.9	1.4	1.5	1.8
19	0.7	1.5	1.6	2.2
20	1.2	1.2	1.5	1.8

TABLE 6 (cont'd)

Wind Speed (kt)	Frequency (%) Period 1	Period 2	Period 3	Derived Period
21	1.3	1.4	1.4	1.5
22	0.1	1.0	0.82	1.0
23	0.3	1.3	0.79	0.6
24	0.1	0.8	0.73	1.0
25	0.1	0.8	0.64	0.8
26		0.2	0.38	0.7
27		0.1	0.06	0.1
28		0.6	0.52	0.7
29		0.5	0.17	0.0
30		0.1	0.06	0.1
31		0.1	0.12	0.2
32		0.0	0.06	0.1
33		0.0	0.03	0.1
34		0.1	0.03	
35		0.1	0.03	
36		0.2	0.06	
Q Value $(kt)^3$	0.3×10^5	5.0×10^5	7.2×10^5	1.7×10^5

for the calibration periods (Fig. 20). The tails were found to follow an exponential distribution. Accordingly an exponential tail was fit by eye to each of the velocity distributions. In calculating values of Q, actual n_i's were used up to the velocity where the scarcity of the wind values produced an irregular distribution. Above this velocity the frequency values of the fitted exponential tail were used in the computations, up to a cut-off velocity of 60 knots. This has the effect of smoothing out the irregular statistical variations resulting from the small number of observed high winds. Figure 21 compares the measured erosion flux to the calculated Q value for the same period. The value of the empirical constant E is found to be 9×10^{-6} gm per $(cm/sec)^3$ per unit width.

7.3 Yearly Erosion Flux Calculation

The average monthly erosion flux may be estimated from climatalogical SYSTRAC Station 15 wind data, a record covering 15 years (Table 7). The procedure followed is nearly identical to that used in the last section for the four calibration periods. To calculate Q, actual monthly frequency distribution values were used up to the higher velocities, above which a fitted exponential tail was used. A SYSTRAC U_t was calculated for each month from the estimated average soil moisture, again using Eq. (7-2).

While the soil moisture was known for the calibration periods, average monthly climatalogical values were not known. Only 27 sporadic measurements were available, mostly taken during the spring months. Sellers (1965) has described methods for estimating the water content of a soil, the relevant factors being a known monthly

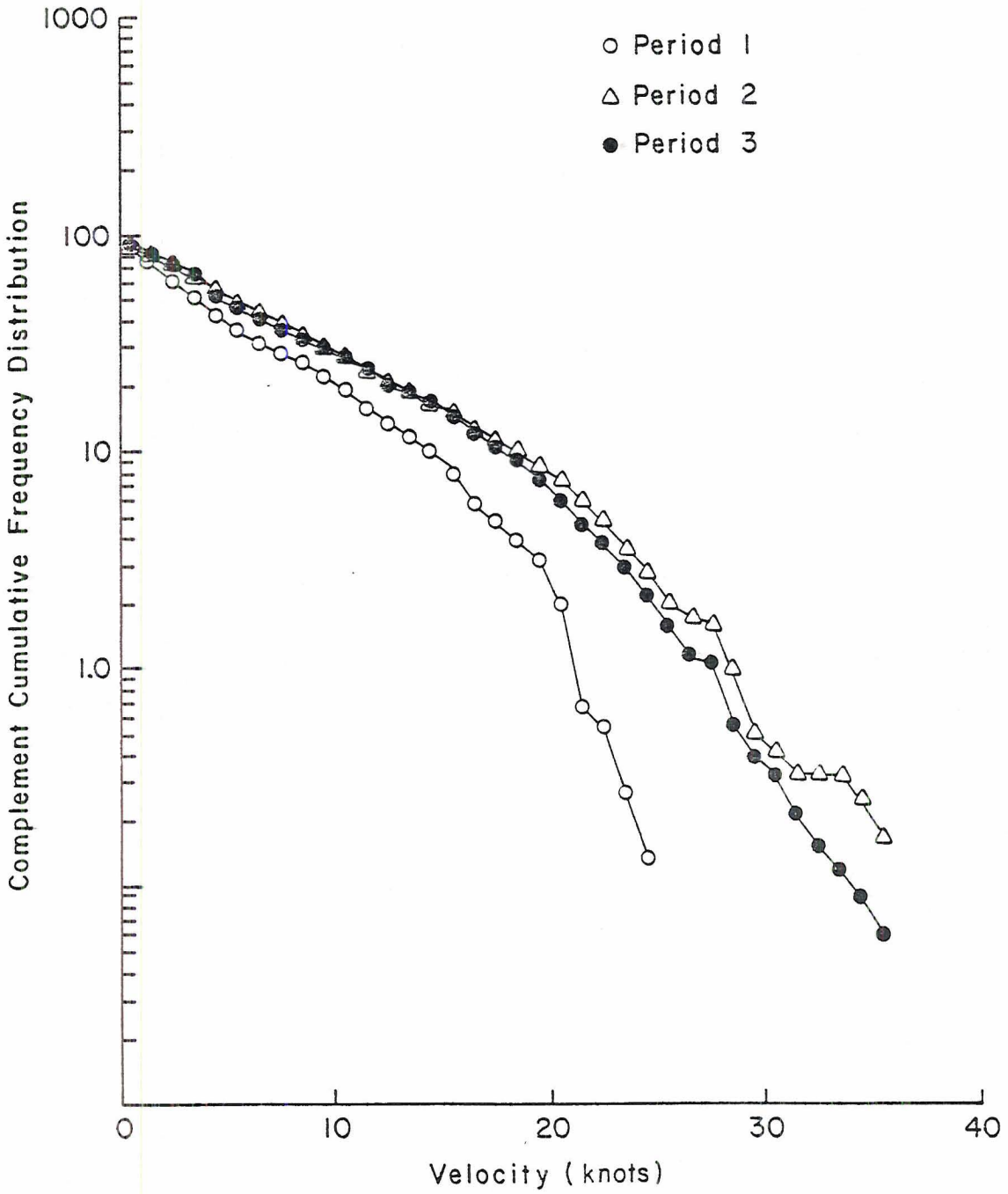

Fig. 20. SYSTRAC Station 15 Complement Cumulative Wind Frequency Distribution for Erosion Calibration Periods

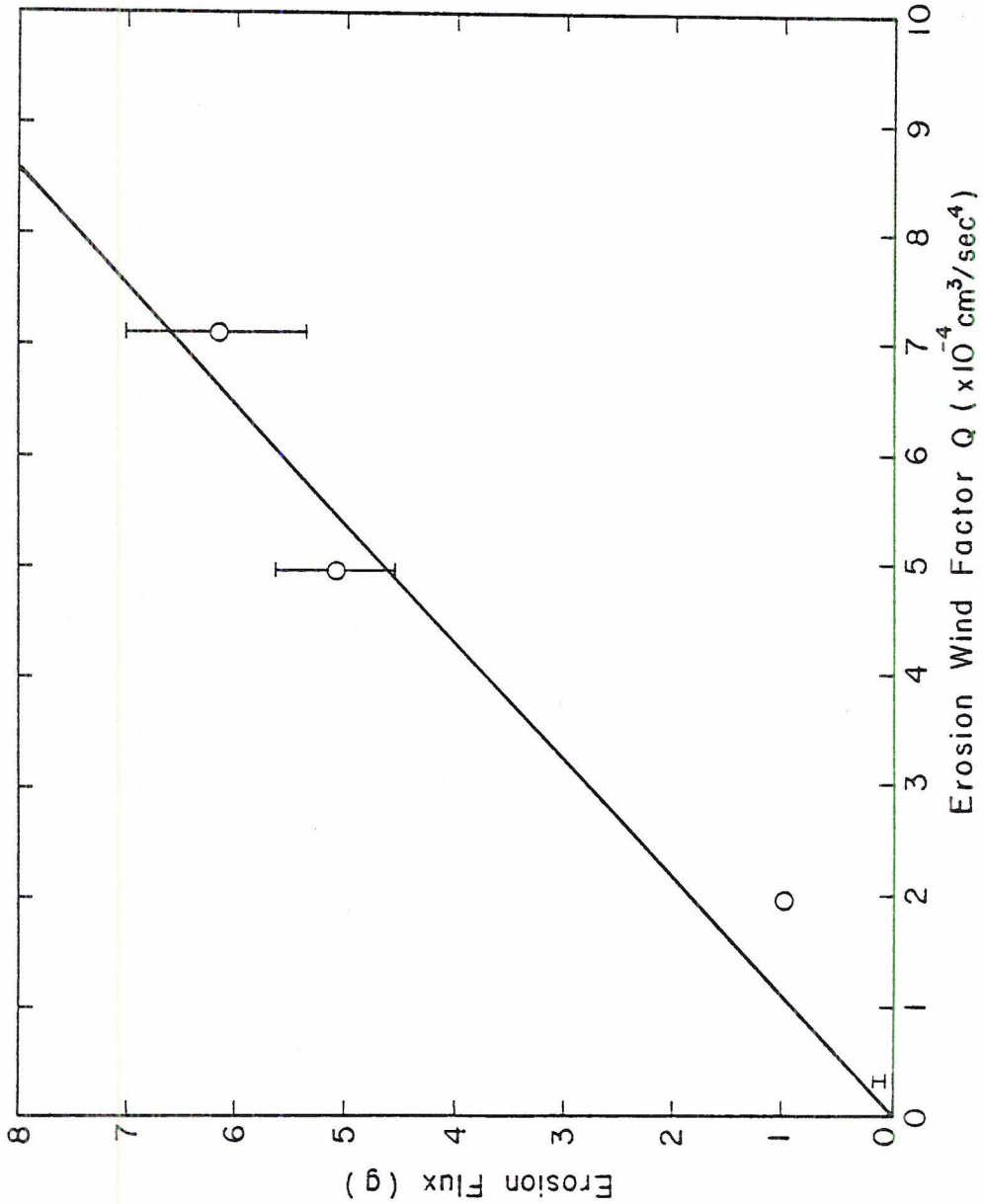

Fig. 21. Erosion Flux Equation Calibration

TABLE 7

SYSTRAC Station 15 Climatological Winds

	Frequency (%) Wind Speed Interval (kt)									
Month	0	1-4	5-9	10-14	15-19	20-29	30-39	40-49	>49	Average Speed (kt)
Jan.	18.6	57.2	14.1	5.4	2.6	1.9	0.14	0.0	0.0	3.8
Febr.	13.9	50.6	19.3	8.7	4.7	2.4	0.31	0.009	0.0	4.9
March	8.4	45.9	21.9	11.9	6.3	4.6	0.78	0.132	0.090	6.5
April	16.3	36.7	22.5	12.7	6.6	4.5	0.56	0.018	0.007	6.2
May	8.1	42.1	24.1	13.6	7.6	4.3	0.15	0.004	0.0	6.5
June	9.8	42.7	22.3	13.3	8.1	3.7	0.17	0.004	0.004	6.3
July	11.6	41.2	24.5	13.4	6.6	2.5	0.12	0.0	0.015	5.9
Aug.	16.3	45.5	21.9	10.1	4.7	1.4	0.05	0.007	0.003	4.8
Sept.	15.3	45.3	23.0	9.0	4.7	2.6	0.10	0.0	0.0	5.1
Oct.	12.9	52.5	19.8	8.5	4.2	2.0	0.14	0.009	0.031	4.7
Nov.	17.3	55.9	16.5	6.1	2.8	1.3	0.12	0.014	0.0	3.8
Dec.	14.4	55.3	16.1	7.1	4.0	2.9	0.23	0.0	0.0	4.6

TABLE 7 (cont'd)

Frequency (%)

Month	Wind Speed Interval (kt) 0	1-4	5-9	10-14	15-19	20-29	30-39	40-49	>49	Average Speed (kt)
Annual	13.8	47.5	20.5	10.0	5.2	2.8	0.240	0.017	0.012	5.2

(from Quiring, 1976)

Period of record is August 1969 - October 1976
Observations are 10 second averages
Sampling period was 5 minutes for first two years, 15 minutes thereafter
Missing data is 15% of possible data, occurs randomly

rainfall rate, estimated surface runoff and downward percolation, and a calculated evapotranspiration rate. The latter depends upon air temperature and humidity, solar radiation, and soil moisture. Unfortunately, these methods are only capable of calculating the total moisture content of a deep soil layer containing the available water, not the soil moisture right at the surface. It is the soil moisture of the very topmost layer that determines the erosion threshold. Accordingly, the problem is approached by following a suggestion of Philip (1957) who extensively studied atmospheric soil moisture relationships. He assumed a thermodynamic equilibrium at the air-soil interface between the relative humidity of the air (RH) and the moisture potential of the soil (Φ):

$$RH = \exp \{g\Phi/RT\} \qquad (7\text{-}4)$$

where R = thermodynamic gas constant. Φ has been determined as a function of soil moisture for many soils, among them sandy loams. Therefore, it should be theoretically possible to relate relative humidity to soil moisture. Unfortunately, these curves are accurate only for relatively large values of soil moisture, not for the low values found in the desert. However these arguments did suggest that some functional relationship should exist between surface soil moisture and relative humidity. Accordingly, the measured soil moisture is plotted against concurrently measured relative humidity (Fig. 22). Two values were discarded because they were measured during rainfall episodes. As might be expected, the graph exhibits considerable scatter because this attempts to grossly simplify a

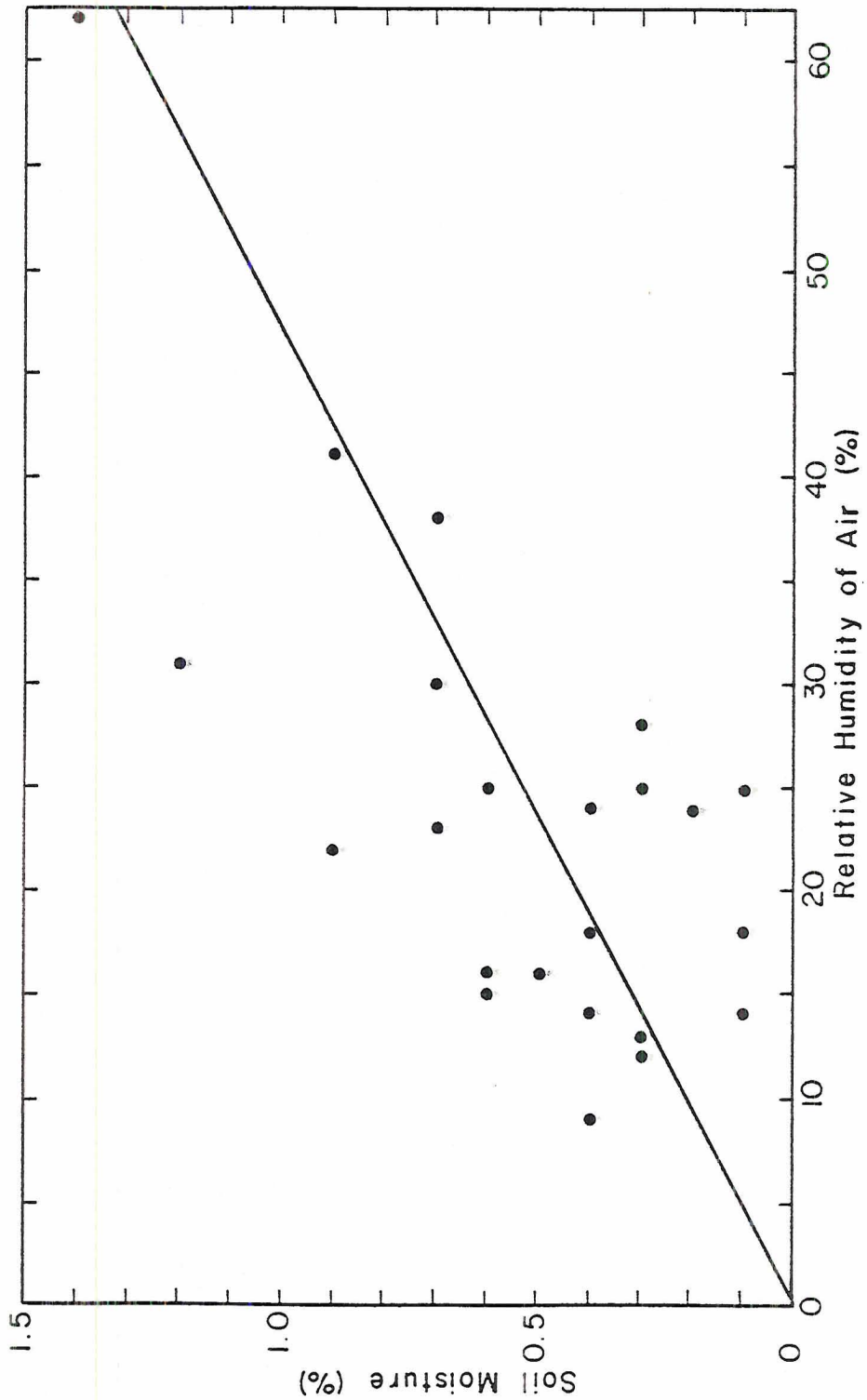

Fig. 22. Soil Moisture as a Function of Relative Humidity

complex process by assuming that equilibrium has been achieved. The correlation coefficient was only 0.69. Nevertheless, this method is believed to provide the best availabe estimate of the average monthly soil surface moisture from the available data.

The 10 year climatalogical summary for the Yucca Flat weather station ten miles north of GMX provides monthly mean air humidity values (Table 1). Because humidity varies diurnally, the 1600 hour values are used since the measurements used to derive Fig. 21 were also made around that hour. These average monthly humidity values may be converted into an estimated average soil moisture for each month using Fig. 22. U_t in Eq. (7-3) is then adjusted for soil moisture according to Eq. (7-2).

The erosion collectors only sampled the horizontal flux up to a height of 30.5 cm. Since the total erosion flux below bush height is required, a correction must be made for the flux not sampled due to the short height of the collector. Nemoto et al. (1969) have verified a theoretical prediction of Kawamura (1948) that the vertical concentration of saltating particles [C(z)] varies as:

$$C(z) \alpha \exp(-mz) \tag{7-5}$$

where m is an empirical constant. It is necessary to determine whether the GMX saltation data agrees with this equation. Since the saltation flux was collected over a finite vertical height, it is necessary to integrate Eq. (7-5) between the heights defining each of the four compartments:

$$SF = \frac{\int_{h_i}^{h_2} C(z)dz}{\int_{0}^{H_s} C(z)dz} = \frac{[\exp(-mh_1) - \exp(-mh_2)]}{[1 - \exp(-mH_s)]} \qquad (7\text{-}6)$$

where SF = calculated saltation fraction in one compartment
h_1, h_2 = heights of bottom and top of compartment respectively
H_s = height of saltation collector = 30.5 cm.

The m giving the best fit between calculated and measured fractions can be found for each of the six measurements. The average is 11.7 m^{-1} (σ = 2.2 m^{-1}) with an average correlation coefficient of 0.996. Thus Eq. (7-5) does accurately describe the vertical distribution of saltation flux. Integrating Eq. (7-5) from 30.5 to 100 cm, the calculated saltation flux from the top of the erosion collector to the average bush height was found to be only 2.9% of the saltation flux captured by the collectors. When the creep fraction is included, the flux below bush height not sampled by the collectors is found to be only 2.4% of the amount sampled. The major mass flux occurs very close to the surface.

An approximate correction will be made for rainy day episodes. When the soil is wetted, no erosion will take place until the surface moisture has dropped below M(15 atm). Under desert conditions, i.e. with a large solar radiation flux and generally windy conditions, the top surface will quickly dry. The exact time for which erosion is inhibited is unknown, for no studies have been made of the drying of the surface soil layer. Even theoretical discussions deal only with the drying of soil well below the top 0.5 cm.

Soil moisture transport is a complex subject involving the solution to differential equations whose coefficients are not constant

but are themselves functions of soil moisture. Computer simulations are usually required to solve soil moisture flow problems (Philip, 1975). The complexities increase greatly for the relatively dry soils characteristic of the desert. Parameters such as hydraulic conductivity change markedly for very dry soils, and quantitative results are not really available. Evaporation transport dominates the hydraulic transport under these conditions, and the former phenomenon has not been widely studied (Wang, 1963). Jackson et al. (1975) found that their computer model predictions of water flux agreed well with measurements in the modelled soil except in the first centimeter below the surface. It is known that where the surface evaporation rate is rapid, the capacity of the soil to deliver water upwards is usually exceeded. The exposed surface then dries quickly, but just how quickly is unknown. Continued evaporation then depends upon vapor flow through this dry layer, but since the vapor density is low the transfer process is slow, and it becomes slower as the dry layer depth increases. In this manner the desert traps its precious soil water at deeper levels. In fact, a paradox can result whereby the "water loss may be least when, by the usual standards, conditions are most favorable for evaporation" (Philip, 1957) due to this surface bottleneck. The basis for the "rainy day" correction will be taken from a discussion with Dr. A. Klute, CSU Department of Agronomy. His experiments with water saturated soil columns dried under high radiation and wind conditions led him to estimate that a wetted desert soil surface will dry out within one day after a rainfall, but exactly how much less than one day is uncertain. Accordingly, the calculated monthly flux

is decreased by 1/31 for each day that the rainfall exceeded 0.1 inch, based on 10 year climatalogical percipitation data. The 0.1 inch cutoff is chosen because a lesser amount of rain fall only wets the soil to a depth less than 0.7 cm and would be quickly evaporated. The resulting corrections vary from 3% to 19% (Table 8). The larger corrections occur in months where the estimated erosion flux is small, so the net effect of this "rainy day" correction is minor and it is not believed that any large error is introduced by this somewhat qualitative argument.

Combining the monthly erosion fluxes estimated from Eq. (7-3), the correction for erosion flux not captured by the collectors, and the rain day correction gives an estimated horizontal erosion flux below bush height of about 40 grams of soil per cm of flow width per year (Table 8). March, by far the windiest month, is responsible for a very large percentage of the total erosion. This erosion rate is very small. Chepil (1946) found erosion fluxes many times larger in his studies of eroding fields. But these agricultural fields had a loose soil structure and were not protected by vegetation. A very low erosion flux is reasonable for the GMX region because the soil surface consists of a well-developed cemented crust and is further protected by surface pebbles and sheltering vegetation. The combination produces a highly non-erodible soil. The observation that blowing dust and sand is seldom visible supports this conclusion; indeed, even the very strong winds produced by dust devils raise relatively little dust.

TABLE 8

GMX Monthly Erosion Estimates

Month	Average Relative Humidity (%) (A)	Estimated Soil Moisture (%) (B)	Moisture Correction to V_T (kt) (C)	SYSTRAC V_T (kt) (D)	Erosion Wind Factor Q (E)	Monthly Erosion (g) (F)	Average Days with >0.1 inch Precip. (A)	Net Monthly Erosion (g) (G)
Jan.	35	0.75	9.5	21.4	1.2×10^5	1.2	2	1.1
Febr.	32	0.69	8.8	20.7	2.0	1.9	3	1.7
March	23	0.51	6.5	18.4	12.7	12.3	3	11.1
April	21	0.47	6.1	18.0	6.6	6.4	3	5.8
May	17	0.39	5.0	16.9	4.5	4.3	2	4.0
June	14	0.33	4.3	16.2	5.0	4.8	3	4.3
July	15	0.35	4.6	16.5	4.2	4.1	6	3.3
Aug.	16	0.37	4.9	16.8	1.9	1.8	5	1.5
Sept.	17	0.39	5.1	17.0	2.7	2.6	4	2.3
Oct.	19	0.43	5.6	17.5	3.8	3.7	1	3.6
Nov.	31	0.67	8.5	20.4	1.3	1.3	3	1.2
Dec.	41	0.87	10.9	22.8	1.6	1.6	3	1.4

TABLE 8 (cont'd)

Month	Average Relative Humidity (%) (A)	Estimated Soil Moisture (%) (B)	Moisture Correction to V_T (kt) (C)	SYSTRAC V_T (kt) (D)	Erosion Wind Factor Q (E)	Monthly Erosion (g) (F)	Average Days with >0.1 inch Precip. (A)	Net Monthly Erosion (g) (G)
Annual	23	0.51	6.6	18.5	47.6×10^5	46	38	41

(A) From Table 1
(B) From Figure 19
(C) Using Equation (7-2)
(D) Based upon V_T = 11.9 kt for 0% soil moisture
(E) $Q = \Sigma_i n_i U_i^2 (U_i - U_t)$
(F) Using Equation (7-3) with $A = 9.65 \times 10^{-6}$ g/Q unit
(G) With correction for precipitation days

8. VEGETATIVE CAPTURE

8.1 Shrub Interception of Particles

The eroding soil does not pass unimpeded; sooner or later the erosion flux is intercepted by a bush. Although the creosote bushes are aerodynamically porous, they are nearly optically opaque horizontally. Therefore practically all of the surface creep and the eroding particles below bush height will eventually impinge upon a branch as they attempt to pass through the volume occupied by the shrub.

The saltating particles travel in ballistic trajectories with speeds close to that of the wind. The impact probability of a particle incident upon a branch represented by a cylinder can be calculated. For example, Figure 46 of Fuchs (1964) indicates that a relatively small particle ($d = 100\ \mu m$) encountering a $\frac{1}{2}$ cm diameter branch at the relatively slow speed of $\frac{1}{2}$ m/sec has an impact probability of 90%. The more usual circumstance, a larger particle and/or a higher incident velocity, has an even greater impact probability.

The branches are relatively soft; therefore, the intercepted particles will lose much of their horizontal momentum upon impact. The exact path of the particle after impact depends upon many factors--velocity, impact angle, and elasticity--but it may be assumed that the surface creep stops moving and the saltating particles essentially fall vertically. This assumption is justified because 1) the saltating particles are in close proximity to the ground (90% within 20 cm of the ground), 2) a particle takes a short time to fall such a

stress, since particle movement would then be initiated. Therefore it is necessary to estimate the ground stress inside a bush.

In well developed canopy flow with closely spaced elements the shear stress decreases greatly from the canopy top to the surface, resulting in negligible surface stress (Wright and Lemon, 1966; Kawatani, 1968). However, the creosote bush flow is not well developed, and the bushes themselves are aerodynamically porous, so these canopy results cannot be applied to the present case. One might still suspect this to be true, since Kawatani (1968) found that in the initial development zone of a roughness array the stress did decrease close to the surface. The effect of a mound is a further complication, since it will increase the surface stress of the air passing over it. Therefore it was necessary to obtain an estimate of the ground stress inside a bush; it could not be assumed to be small.

The ground stress inside the test bush was estimated using two different methods: 1) by assuming that an equilibrium layer exists within 4 cm of the ground, and 2) by assuming that the ratio $(U_*)_g/\sigma_u$ was a constant equal to its value outside the bush, where $\sigma_u = \{\overline{u^2}\}^{\frac{1}{2}}$.

The equilibrium layer assumption is discussed and justified in Appendix B. The four periods analyzed were those with high average velocities, for this method is more justifiable under such conditions. The dissipation determined $(U_*)_g$'s were adjusted to a reference velocity value by assuming that $(U_*)_g/U$ was constant. As shown in Table 9, the predicted ground friction velocity inside the bush for a 2 m reference velocity of 6 m/sec is 0.082 m/sec. For the same

short distance, and 3) the lower wind speeds inside the bush will not allow the intercepted particles to gain enough forward momentum to escape from the bush.

Once a hummock has started to build it will act to intercept saltating particles traveling within a mound height of the ground. The mound will also cause the particles in surface creep to lose energy as they roll up the slope. Particles moving slowly will be trapped on the upward slope of a large hummock. Therefore the upwind slope will be more gradual than the downwind slope, as is apparent in Fig. 8. The asymmetry of this figure shows that the intercepted particles do not fall completely vertically but also travel horizontally.

The above arguments indicate that nearly all of the particles incident upon a bush will not pass through it but will impact a branch or the hummock somewhere inside the shrub. More elaborate theories of vegetative interception of particles have been developed (e.g. Chamberlain, 1975; Bache and Uk, 1975), but they are required only for smaller particles ($d < 100$ μm) with much lower impact probabilities. Furthermore, they require a branch density parameter to be known. The simplified arguments used above are believed valid for the case of large particles with significant horizontal momentum encountering an optically opaque shrub. The filtering efficiency of a bush will not be perfect, but it will be very high.

8.2 Estimation of Ground Stress Inside the Test Bush

The particles building the wind hummock will not remain in place if the stress on the ground inside the bush exceeds the threshold

TABLE 9

$(U_*)_g$ Estimates Inside the Test Bush

A. From Dissipation Measurements

U (m/sec)	ε (m^2/sec^3)	$(U_*)_g$ (m/sec)(A)	$\frac{(U_*)_g}{U}$	$(U_*)_g$ for U (2 m) = 6 m/sec (m/sec)(B)
2.01	0.41	0.15	0.074	0.078
2.13(C)	0.46	0.19	0.087	0.092
2.13	0.41	0.18	0.084	0.089
1.74(C)	0.11	0.12	0.066	0.070
Average			0.078	0.082

(A) Using $(U_*)_g = [kz\varepsilon]^{1/3}$

(B) Where U = 1.06 m/sec

B. From Turbulence Intensity Measurements

U (m/sec)	$\overline{\sigma_u}$ (m/sec)(D)	$(U_*)_g$ (m/sec)(E)	$\frac{(U_*)_g}{U}$	$(U_*)_g$ for U (2 m) = 6 m/sec (m/sec)(B)
2.03	0.69	0.25	0.124	0.13
2.35(C)	0.61	0.22	0.095	0.10
2.33	0.63	0.23	0.099	0.10
1.89(C)	0.32	0.12	0.063	0.07
Average			0.096	0.10

(C) These measurements not made at center of bush spot, others are

(D) Based upon 5 second wind averages

(E) Using $(U_*)_g/\overline{\sigma_u} = 0.37$

conditions the ground friction velocity at an isolated spot would be 0.31 m/sec, thus $\{(U_*)_g$ (inside bush)$/(U_*)_g$ (outside bush)$\}$ = 26%.

The assumption of a constant $(U_*)_g/\bar{\sigma}_u$ is discussed in Appendix C. Intensity measurements made inside the bush were also adjusted to a 2 m reference velocity of 6 m/sec, predicting a ground friction velocity inside the bush of 0.10 m/sec (Table 9), or $\{(U_*)_g$ (inside bush$)/(U_*)_g$ (outside bush)$\}$ = 32%.

The two methods gave surprisingly similar results. Assuming the ground friction velocity to increase in proportion with the wind speed, the wind would have to increase to over three times the outside threshold value to move the soil inside the bush. Since the SYSTRAC average threshold speed is 21 kts, winds of over 70 kts would be required, a highly unlikely occurrance according to the climatalogical record (Table 1). Therefore, once the eroding particles are captured by the bush they may be adjudged to remain there.

An additional factor further increases the likelihood that the hummock soil particles will remain trapped. The soil inside a bush is not bare, the top layer containing much organic material. Soil particles settle below this debris and are partially sheltered from direct wind action. The type of organic material most easily disturbed is the seed pod sections, which have a very low density. Using Iversen et al.'s (1973) results and the measured density (ρ_p = 0.13 gm/cm^2) and approximate size (D ≈ 0.4 cm) of the pods, the calculated threshold friction velocity is 25 cm/sec. This value is greater than that for the soil alone; therefore, the organic material will not be removed at wind speeds when soil particles would be

moved. The sheltering action of the debris then makes the removal of soil from a hummock even more difficult.

8.3 Hummock Growth

A growing creosote bush initially has no wind hummock at its base. The number of branches, the optical density, and the filtering efficiency all increase as the shrub grows in height and diameter. However, any intercepted particles will not remain trapped if the surface stress inside the shrub is large enough to initiate saltation. Also, saltating particles intercepted by smaller shrubs may pick up enough horizontal velocity as they fall to escape from the shrub. The much smaller bursage plants were observed to possess no visible hummocks. Therefore there must be some critical shrub size below which the particles may be intercepted but not trapped.

As a creosote bush grows larger the airflow around and inside it is more affected by the increasing aerodynamic drag. The surface stress inside the bush decreases, increasing the entrapment efficiency. Furthermore, after a mound is formed it will also grow, intercepting more saltating particles directly and capturing more surface creep. Thus the volume growth rate of the hummock increases as the shrub enlarges, due both to the greater area swept out and the greater interception and entrapment efficiencies. The growing shrub will therefore become increasingly efficient at building a mound.

For a mature creosote bush such as the test bush, the interception efficiency is virtually 100% due to its optical opacity, and the low surface stress inside the bush allows entrapment of the intercepted

particles. The volume growth rate of the hummock is then essentially determined by the erosion flux and the shrub width.

As the mound grows the surface stress is affected by the hummock size. For an isolated hill, the surface stress increases from its upwind value to a maximum at the crest (Taylor and Gent, 1974; Jackson and Hunt, 1975). The surface stress on a mound covered by a bush should be similarly affected although it is apparent that the stress increase will be much less since the effect of the shrub on the airflow will dominate the effect of the mound. The results of the preceeding section indicate that even for a large mound the surface stress inside the shrub is a fraction of the stress outside. Therefore, the effect of the hummock on the surface stress may be considered negligible when compared to the effect of the shrub for the hummock sizes observed in the GMX area. Confirmatory evidence is given by Fuller (1975) who mentions that in areas of much greater erosion flux the hummocks may grow large enough to partially cover the creosote bushes. The erosion flux at the GMX site is so small that in the lifetime of an average shrub the mound height cannot grow large enough to increase the surface stress sufficiently to allow intercepted particles to escape. There the hummock growth is limited only by the life expectancy of a creosote bush.

If the initial growth period is neglected, the minimum age of a creosote bush can be estimated from the erosion flux and a measured mound profile. In performing this calculation it is assumed that the shrub size remains constant and that the shrub interception and trapping efficiencies are 100%. These assumption are valid for the bushes observed on the GMX site, but for smaller bushes which have

not reached mature size they are not. Unfortunately there are too many unknowns to enable the dependence of the capture efficiency upon the age of the bush to be computed. Therefore the above assumptions must be made, with the knowledge that the calculated age will be an underestimate.

The minimum age of the test bush will now be calculated. The measured volume of the mound profile (Fig. 8) is 2300 cm^3 per unit width. The estimated yearly erosion flux below bush height is 40 grams per unit width. Since the soil bulk density is 1.37 g/cm^3, the minimum age of the test bush is 80 years. This estimate seems reasonable, since the average lifetime of a creosote bush is about 100 years. Because the test bush had such a large hummock, it is presumed to be one of the oldest bushes in the area.

If the hummock profiles of the other bushes are assumed to be similar to that of the test bush, then the minimum age of a bush is proportional to its hummock height, assuming average upwind fetches. Using this criteria, any bush with a hummock height over 4 cm has existed since the GMX plutonium release 20 years ago. These shrubs have been collecting eroding radioactive soil for this entire period.

The maximum age of a creosote bush may be estimated by assuming that its particle capture efficiency is 0% until it reaches maturity and is 100% thereafter. Adding the maturation age to the minimum age determined above will then give the estimated maximum age. Since the maturation age is estimated as 50 years, the maximum age of the test bush is estimated to be 130 years.

8.4 Transport of Radioactivity

After the release of plutonium from ground zero at GMX, the radioactive particles settled on the soil surface. With weathering they migrated downward, but the highest activity is still found at the surface. The eroding soil comes from this surface soil. The erosion process strips the soil with the highest radioactivity from the desert pavement and deposits it in the hummocks. Thus the activity per gram of the hummock soil is greater than that of the desert pavement, as shown by Tables 3 and 4. The hummocks will be "hotter" than the surrounding soil.

This analysis predicts that the radioactivity of the desert pavement will be slowly collected by the wind hummocks and that its horizontal movement downwind will proceed very slowly. Thus vertical transport through resuspension will be the major process by which radioactivity escapes from the GMX area.

Because the GMX soil has a cemented surface crust and is protected by vegetation, horizontal soil movement is minimal, and therefore little radioactivity is transported by horizontal erosion. This circumstance is fortunate, for if the soil consisted of loose particles the radioactivity would spread much more rapidly from a contaminated site. Thus the GMX site is an excellent location for nuclear experiments involving surface release of radioactivity.

9. SUMMARY

This thesis investigated the airflow above and below shrub height and inside a bush. The yearly horizontal erosion flux below shrub height and the growth rate of wind hummocks inside the shrubs were both estimated.

Wind profiles obtained above shrub height allowed the calculation of the total stress and drag coefficient above the vegetated surface. The drag coefficient was found to decrease with increasing wind speeds.

Flow measurements below shrub height implied the existence of a logarithmic wind profile, ascribed to the development of an internal boundary layer downwind of the shrubs. Their wide spacing and high porosities made the airflow more representative of a flow over individual roughness elements than of a plant canopy flow. Ground stress estimates from a logarithmic wind profile and an equilibrium layer assumption both gave identical results under high wind conditions.

Velocity profiles measured near and inside a bush evidenced the great reduction in wind speed produced by bush drag. In adjusting to these velocity reductions, the flow seemed to diverge horizontally as much as it did vertically.

Measurements of the ground stress and the total stress above the vegetation enabled computation of the drag exerted by the vegetation. The calculated drag coefficient of a single bush implied that the bushes were aerodynamically very porous. Partitioning the total drag into the components due to the ground and to the bush demonstrated that the porosity of the shrubs cannot be ignored when estimating the extent of erosion protection provided by vegetation. Vegetation was found to

significantly reduce the surface stress, even for widely spaced and porous shrubs.

The threshold stress required to initiate saltation was determined to be close to, but slightly greater than, the minimum surface stress measured for individual particles forming a smooth surface. This threshold speed increase resulted from a combination of the cementation of the surface soil crust and the stress absorbed by surface projections such as pebbles.

The yearly horizontal aeolian transport below bush height was estimated from wind and soil moisture data, based upon actual field measurements. The very low value found, 40 grams per year per cm width, was ascribed to both the great stability of the cemented surface crust and the protective effect of the vegetation.

Arguments were presented supporting the assumption of a high filtering efficiency for creosote bushes, with the bushes sweeping out most of the eroding particles incident upon them. Surface stress estimates demonstrated that wind hummocks cannot grow large enough in their lifetime under the low erosion flux conditions of the GMX area to significantly affect the ground stress inside the bush. Therefore, the limitation to hummock growth was found to be the life span of the creosote bush. The estimated age of a bush based upon its hummock height was comparable to the creosote bush life span.

It is concluded that the aeolian horizontal soil erosion is mainly trapped by bushes in their hummocks, and this mode of radioactive transport over large distances is an extremely slow one. Thus the major escape of radioactivity from the GMX area must

be through the resuspension of small particles. These can be lifted high above the ground and horizontally transported by the wind large distances in a relatively short time.

BIBLIOGRAPHY

Allen, L.H. Jr., 1968: Turbulence and wind speed spectra within a Japanese Larch plantation. J. Appl. Meteor., 7, 73-78.

Anspaugh, L.R. and P.L. Phelps, 1974: Results and data analysis: Resuspension element status report. The Dynamics of Plutonium in Desert Environments, USAEC Report NVO-142, Nevada Operations Office, 265-297.

Anspaugh, L.R., P.L. Phelps, N.C. Kennedy, J.H. Shinn, and J.M. Reichman, 1976: Experimental studies on the resuspension of plutonium from aged sources at the Nevada Test Site. Atmosphere-Surface Exchange of Particulate and Gaseous Pollutants, Richland, Washington Symp., 727-743. (NTIS Accession No. CONF-740921)

Arya, S.P.S., 1975: A drag partition theory for determining the large-scale roughness parameter and wind stress on the arctic pack ice. J. Geophys. Res., 80, 3447-3454.

Bache, D.H. and S. Uk, 1975: Transport of Aerial Spray, II: Transport within a crop canopy. Agric. Meteor., 15, 371-377.

Bagnold, R.A., 1954: The Physics of Blown Sand and Desert Dunes. William Morrow, New York, 265 pp.

Barad, M.L., 1964: The vertical transfer of momentum and heat at and near the earth's surface. Trans. N.Y. Acad. Sci. Ser. II, 26, 830-844.

Barenblatt, G.I. and G.S. Golitsyn, 1974: Local structure of mature dust storms. J. Atmos. Sci., 31, 1917-1933.

Belly, P.Y., 1964: Sand movement by wind. Tech. Memo No. 1, U.S. Army Coastal Engineering Research Center, 80 pp.

Bliss, W. and L. Dunn, 1971: Measurement of plutonium in soil around the Nevada Test Site. Proc. Environmental Plutonium Symp., Los Alamos Scientific Lab., August 4-5, 89-92.

Bradley, E.F., 1968: A micrometeorological study of velocity profiles and surface drag in the region modified by a change in surface roughness. Quart. J. Roy. Meteor. Soc., 94, 361-379.

Bradley, E.F., 1972: The influence of thermal stability on a drag coefficient measured close to the ground. Agric. Meteor., 9, 183-190.

Bryson, M.C., 1973: Describing and testing for heavy-tailed distributions. Third Conference on Probability and Statistics in Atmospheric Science, Amer. Meteor. Soc., Boulder, CO, 118-121.

BIBLIOGRAPHY (cont'd)

Busch, N.E. and H.A. Panofsky, 1968: Recent spectra of atmospheric turbulence. Quart. J. Roy. Meteor. Soc., 94, 132-140.

Businger, J.A., 1973: Turbulent transfer in the atmospheric surface layer. Workshop on Micrometeorology, D.A. Haugen, Ed., Amer. Meteor. Soc., Boston, 67-100.

Businger, J.A., J.C. Wyngaard, Y. Izumi, and E.F. Bradley, 1971: Flux-profile relationships in the atmospheric surface layer. J. Atmos. Sci., 28, 181-189.

Castro, I.P., 1971: Wake characteristics of two-dimensional perforated plates normal to an air-stream. J. Fluid Mech., 46, 599-609.

Chamberlain, A.C., 1975: The movement of particles in plant communities. Vegetation and the Atmosphere, Vol. I, J.L. Monteith, Ed., Academic Press, New York, 155-203.

Champagne, F.H., C.A. Friehe, J.C. LaRue, and J.C. Wyngaard, 1977: Flux measurements, flux estimation techniques, and fine-scale turbulence measurements in the unstable surface layer over land. J. Atmos. Sci., 34, 515-530.

Chepil, W.S., 1941: Relation of wind erosion to the dry aggregate structure of a soil. Sci. Agric., 21, 488-507.

Chepil, W.S., 1945: Dynamics of wind erosion, I: Nature of movement of soil by wind. Soil Sci., 60, 475-480.

Chepil, W.S., 1946. Dynamics of wind erosion, V: Cumulative intensity of soil drifting across eroding fields. Soil Sci., 61, 257-263.

Chepil, W.S., 1956: Influence of moisture on erodibility of soil by wind. Soil Sci. Soc. Am. Proc., 20, 288-292.

Chepil, W.S., 1959: Wind erodibility of farm fields. J. Soil Water Conservation, 14, 214-219.

Chepil, W.S. and N.P. Woodruff, 1954: Estimation of wind erodibility of field surfaces. J. Soil Water Conservation, 9, 257-265.

Chepil, W.S. and N.P. Woodruff, 1963: The physics of wind erosion and its control. Advances in Agronomy, Vol. 15, Academic Press, New York, 211-302.

Chew, R.M. and A.E. Chew, 1965: The primary productivity of a desert shrub (Larrea tridentata) community. Ecol. Monographs, 35, 355-375.

BIBLIOGRAPHY (cont'd)

Cionco, R.M., 1965: A mathematical model for air flow in a vegetative canopy. J. Appl. Meteor., 4, 517-522.

Cionco, R.M., 1972: A wind-profile index for canopy flow. Boundary-Layer Meteor., 3, 255-263.

Counihan, J., 1975: Adiabatic atmospheric boundary layers: A review and analysis of data from the period 1880-1972. Atmos. Env., 9, 871-905.

Counihan, J., J.C.R. Hunt, and P.S. Jackson, 1974: Wakes behind two-dimensional surface obstacles in turbulent boundary layers. J. Fluid Mech., 64, 529-563.

Dalton, P.D. Jr., 1961: Ecology of the Creosote bush Larrea Tridentata (D.C.) Cov. Ph. D. Dissertation, University of Arizona, Tuscon, 161 pp.

Deacon, E.L., 1959: The measurement of turbulent transfer in the lower atmosphere. Advances in Geophysics, Vol. 6, Academic Press, New York, 211-228.

Eberhardt, L.L. and R.O. Gilbert, 1974: General statistical considerations in environmental Pu studies. The Dynamics of Plutonium in Desert Environments, USAEC Report NVO-142, Nevada Operations Office, 43-50.

Edling, W.H., 1974: Three-dimensional turbulent boundary layer flow on roughness strip of finite width. Ph. D. Dissertation, Colorado State University, Fort Collins, 245 pp.

Elliot, W.P., 1958: The growth of the atmospheric internal boundary layer. Trans. Amer. Geophys. Union, 39, 1048-1054.

Elliott, J.A., 1972: Microscale pressure fluctuations measured within the lower atmospheric boundary layer. J. Fluid Mech., 53, 351-383.

Fichtel, G.H. and G.E. McVehil, 1970: Longitudinal and lateral spectra of turbulence in the atmospheric boundary layer at the Kennedy space center. J. Appl. Meteor., 9, 51-63.

Fowler, E.B. and E.H. Essington, 1974: Soil element activities, October 1972-September 1973. The Dynamics of Plutonium in Desert Environments, USAEC Report NVO-142, Nevada Operations Office, 7-16.

Frost, W., W.L. Harper, and G.H. Fichtel, 1975: Analysis of atmospheric flow over a surface protrusion using the turbulence kinetic energy equation. Boundary-Layer Meteor., 8, 401-417.

BIBLIOGRAPHY (cont'd)

Fuchs, N.A., 1964: Mechanics of Aerosols. MacMillan, New York, 408 pp.

Fuller, W.H., 1975: Soils of the Desert Southwest. University of Arizona Press, Tuscon, 102 pp.

Gilbert, R.O. and L.L. Eberhardt, 1974: Statistical analysis of Pu in soil at the Nevada Test Site—some results. The Dynamics of Plutonium in Desert Environments, USAEC Report NVO-142, Nevada Operations Office, 51-90.

Gillette, D.A., 1976: Production of fine dust by wind erosion of soil: Effect of wind and soil texture. Atmosphere-Surface Exchange of Particulate and Gaseous Pollutants, Richland, Washington Symp., 591-609. (NTIS Accession No. CONF-740921)

Gillette, D.A., I.H. Blifford, Jr., and C.R. Fenster, 1972: Measurements of the aerosol size distributions and vertical fluxes of aerosols on land subject to wind erosion. J. Appl. Meteor., 11, 977-987.

Gillette, D.A., I.H. Blifford, Jr., and D.W. Fryrear, 1974: The influence of wind velocity on the size distributions of aerosols generated by the wind erosion of soils. J. Geophys. Res., 79, 4068-4075.

Good, M.C. and P.C. Joubert, 1968: The form drag of two-dimensional bluff-plates immersed in turbulent boundary layers. J. Fluid Mech., 31, 547-582.

Graham, J.M.R., 1976: Turbulent flow past a porous plate. J. Fluid Mech., 73, 565-591.

Grass, A.J., 1971: Structural features of turbulent flow over smooth and rough boundaries. J. Fluid Mech., 50, 233-255.

Hagen, L.J. and E.L. Skidmore, 1971: Windbreak drag as influenced by porosity. Trans. Amer. Soc. Agric. Eng., 14, 464-465.

Hanjalic, K. and B.E. Launder, 1972: A Reynolds stress model of turbulence and its application to thin shear flows. J. Fluid Mech., 52, 609-638.

Hess, G.D. and H.A. Panofsky, 1966: The budget of turbulent energy near the ground. Quart. J. Roy. Meteor. Soc., 92, 277-280.

Homan, D., 1976: Personal communication of erosion measurements made by J.M. Reichman, Lawrence Livermore Lab., Livermore, CA.

Inoue, E., 1963: On the turbulent structure of airflow within crop canopies. J. Meteor. Soc. Japan (Ser. II), Tokyo, 41, 317-326.

BIBLIOGRAPHY (cont'd)

Iversen, J.D., R. Greeley, J.B. Pollack, and B.R. White, 1973: Simulation of Martian eolian phenomena in the atmospheric wind tunnel. Proc. 7th Conf. Space Simulation, NASA SP-336, 191-213 (NTIS Accession No. N74-10232).

Iversen, J.D., R. Greeley, and J.B. Pollack, 1976: Windblown dust on Earth, Mars, and Venus. J. Atmos. Sci., 33, 2425-2429.

Izumi, Y. and M.L. Barad, 1970: Wind speeds as measured by cup and sonic anemometers and influenced by tower structure. J. Appl. Meteor., 9, 851-856.

Jackson, P.S. and J.C.R. Hunt, 1975: Turbulent wind flow over a low hill. Quart. J. Roy. Meteor. Soc., 101, 929-955.

Jackson, R.D., B.A. Kimball, R.J. Reginato, S.B. Idso, and F.S. Nakayama, 1975: Heat and water transport in a natural soil environment. Heat and Mass Transfer in the Biosphere (Part I), D.A. deVries and N.H. Afgan, Eds., Scripta Book Co., Washington, D.C., 29-38.

Kaimal, J.C., J.C. Wyngaard, Y. Izumi, and D.R. Coté, 1972: Spectral characteristics of surface layer turbulence. Quart. J. Roy. Meteor. Soc., 98, 563-589.

Kawamura, R., 1948: Sand movement by wind. Kagaku, 18, 24-30, in Japanese, cited by Nemoto, et al., 1969.

Kawatani, T., 1968: The structure of a canopy flow field. M.S. Thesis, Colorado State University, Fort Collins, 122 pp.

Klebanoff, P.S., 1955: Characteristics of turbulence in a boundary layer with zero pressure gradient. NACA Rep. No. 1053.

Kutzbach, J.E., 1961: Investigation of the modification of wind profiles by artificially controlled surface roughness. Annual Rept. 1961, Dept. of Meteorology, University of Wisconsin, Madison, 71-113.

Landsberg, J.J. and A.S. Thom, 1971: Aerodynamic properties of a plant of complex structure. Quart. J. Roy. Meteor. Soc., 97, 565-570.

Leavitt, V.D., 1974: Soil surveys of five plutonium-contaminated areas on the test range complex in Nevada. The Dynamics of Plutonium in Desert Environments, USAEC Report NVO-142, Nevada Operations Office, 21-28.

Lettau, H., 1969: Note on aerodynamic roughness parameter estimation on the basis of roughness-element description. J. Appl. Meteor. 8, 828-832.

BIBLIOGRAPHY (cont'd)

Lettau, H., 1973: Personal communication cited in Gillette, 1976.

McBean, G.A., 1971: The variations of the statistics of wind, temperature, and humidity fluctuations with stability. Boundary-Layer Meteor., 1, 438-457.

McBean, G.A., R.W. Stewart, and M. Miyake, 1971: The turbulent energy budget near the surface. J. Geophys. Res., 76, 6540-6549.

Malurkar, S.L. and L.A. Ramdas, 1931: Theory of extremely high lapse-rates of temperature very near the ground. Indian J. Physics, 6, 495-508.

Marshall, J.K., 1970: Ascessing the protective role of shrub-dominated rangeland vegetation against soil erosion by wind. Proc. 11th International Grassland Congr., Surfers Paradise, Australia, 19-23.

Marshall, J.K., 1971: Drag measurements in roughness arrays of varying density and distribution. Agric. Meteor., 8, 269-292.

Meroney, R.N., 1968: Characteristics of wind and turbulence in and above model forests. J. Appl. Meteor., 7, 780-787.

Morris, H.M., 1955: Flow in rough conduits. Trans. Amer. Soc. Civil Engrs., 120, 373-410.

Munroe, D.S. and T.R. Oke, 1973: Estimating wind profile parameters for tall, dense crops. Agric. Meteor., 11, 223-228.

Nemoto, S., M. Mitsudera, K. Takahashi, H. Uotsu, and S. Kobayashi, 1969: On the threshold friction velocity for saltation of sand. Papers in Meteorology and Geophysics, 20, 365-383.

O'Loughlin, E.M. and V.S.S. Annambhotla, 1969: Flow phenomena near rough boundaries. J. Hydraul. Res., 7, 231-250.

Owen, P.R., 1964: Saltation of uniform grains in air. J. Fluid Mech., 20, 225-242.

Panofsky, H.A., 1969: Spectra of atmospheric variables in the boundary layer. Radio Sci., 4, 1101-1109.

Paulson, C.A., 1970: The mathematical representation of wind speed and temperature profiles in the unstable surface layer. J. Appl. Meteor., 9, 857-861.

Perrier, E.R., R.J. Millington, D.B. Peters, and R.J. Luxmoore, 1970: Wind structure above and within a soybean canopy. Agron. J., 62, 615-618.

BIBLIOGRAPHY (cont'd)

Perrier, E.R., J.M. Robertson, R.J. Millington, and D.B. Peters, 1972: Spatial and temporal variation of wind above and within a soybean canopy. Agric. Meteor., 10, 421-442.

Philip, J.R., 1957: Evaporation and moisture and heat fields in the soil. J. Meteor., 14, 354-366.

Philip, J., 1975: Water movement in soil. Heat and Mass Transfer in the Biosphere (Part I), D.A. deVries and N.H. Afgan, Eds., Scripta Book Co., Washington, D.C., 29-47.

Plate, E.J., 1971: The aerodynamics of shelter belts. Agric. Meteor., 8, 203-222.

Plate, E.J. and C.W. Lin, 1965: The velocity field downstream from a two-dimensional model hill. Rept. CER65EJP14, Fluid Dynamics Diffusion Lab., Colorado State University, Fort Collins.

Pruitt, W.O., D.L. Morgan, and F.J. Laurence, 1973: Momentum and mass transfers in the surface boundary layer. Quart. J. Roy. Meteor. Soc., 99, 370-386.

Quiring, R.F., 1968: Climatalogical data--Nevada Test Site and Nuclear Rocket Development Station. ESSA Res. Lab. Tech. Memo., ERLTM-ARL7, 168 pp.

Quiring, R.F., 1976: Personal communication. ESSA Air Resources Lab., Las Vegas, NV.

Reichman, J.M., 1974: Saltation and creep sampler. The Dynamics of Plutonium in Desert Environments, USAEC Report NOV-142, Nevada Operations Office, 247-254.

Rhoades, W.A., 1974: Analysis of vegetation cover in certain Pu-contaminated areas using aerial photography. The Dynamics of Plutonium in Desert Environments, USAEC Report NVO-142, Nevada Operations Office, 119-134.

Romney, E.M., A. Wallace, R.O. Gilbert, S.A. Bamberg, J.D. Childress, J.E. Kunnear, and T.L. Ackerman, 1974: Some ecological attributes and plutonium contents of perennial vegetation in Area 13. The Dynamics of Plutonium in Desert Environments, USAEC Report NVO-142, Nevada Operations Office, 91-106.

Sadeh, W.Z., J.E. Cermak, and T. Kawatani, 1971: Flow over high roughness elements. Boundary-Layer Meteor., 1, 321-344.

Schlichting, H., 1968: Boundary Layer Theory. McGraw-Hill, New York, 747 pp.

BIBLIOGRAPHY (cont'd)

Schuepp, P.H. and K.D. White, 1975: Transfer processes in vegetation by electrochemical analog. Boundary-Layer Meteor., 8, 335-358.

Seginer, I., 1972: Windbreak drag calculated from the horizontal velocity field. Boundary-Layer Meteor., 3, 87-97.

Seginer, I., 1974: Aerodynamic roughness of vegetated surfaces. Boundary-Layer Meteor., 5, 383-393.

Seginer, I., 1975: Atmospheric-stability effect on windbreak shelter and drag. Boundary-Layer Meteor., 8, 383-400.

Seginer, I. and R. Sagi, 1972: Drag on a windbreak in two-dimensional flow. Agric. Meteor., 9, 323-333.

Sellers, W.D., 1965: Physical Climatology. University of Chicago Press, Chicago, 272 pp.

Shreve, F. and A.L. Hinkley, 1937: Thirty years of change in desert vegetation. Ecology, 18, 463-478.

Sinclair, P.C., 1976 : Vertical transport of desert particulates by dust devils and clear thermals. Atmosphere-Surface Exchange of Particulate and Gaseous Pollutants, Richland, Washington Symp., 497-527. (NTIS Accession No. CONF-740921)

Smith, D.D., 1974: Grazing studies on selected plutonium-contaminated areas in Nevada. The Dynamics of Plutonium in Desert Environments, USAEC Report NVO-142, Nevada Operations Office, 151-162.

Tamura, T., 1974: Distribution and characterization of plutonium in soils from Nevada Test Site. The Dynamics of Plutonium in Desert Environments, USAEC Report NVO-142, Nevada Operations Office, 29-42.

Taylor, P.A. and P.R. Gent, 1974: A model of atmospheric boundary-layer flow above an isolated two-dimensional "hill". Boundary-Layer Meteor., 7, 349-362.

Taylor, R.J., 1961: A new approach to the measurement of turbulent fluxes in the atmosphere. J. Fluid Mech., 10, 449-458.

Tennekes, H., 1968: Outline of a second-order theory of turbulent pipe flow. AIAA Journal, 6, 1735-1740.

Tennekes, H., 1973a: The logarithmic wind profile. J. Atmos. Sci., 30, 234-238.

BIBLIOGRAPHY (cont'd)

Tennekes, H., 1973b: Similarity laws and scale relations in planetary boundary layers. Workshop on Micrometeorology, D.A. Haugen, Ed., Amer. Meteor. Soc., Boston, 177-216.

Thom, A.S., 1971: Momentum absorbtion by vegetation. Quart. J. Roy. Meteor. Soc., 97, 414-428.

Townsend, A.A., 1951: The structure of the turbulent boundary layer. Proc. Comb. Phil. Soc., 47, 375-398.

Townsend, A.A., 1961: Equilibrium layers and wall turbulence. J. Fluid Mech., 11, 97-120.

Townsend, A.A., 1965: Self-preserving flow inside a turbulent boundary layer. J. Fluid Mech., 22, 773-797.

Uchijima, Z. and J.L. Wright, 1964: An experimental study of air flow in a corn plant-air layer. Bull. Nat. Inst. Agric. Sci. Ser. A (Japan), 11, 19-66.

van Eimern, J., R. Karshon, L.A. Razumova, and G.W. Robertson, 1964: Windbreaks and shelterbelts. WMO Tech. Note 59, 188 pp.

Wang, J.Y., 1963: Agricultural Meteorology. Pacemaker Press, Milwaukee, WI, 693 pp.

Wilson, N.R. and R.H. Shaw, 1976: A higher closure model for canopy flow. Journal Paper No. 6493, Purdue University Agricultural Experimental Station, W. Lafayette, IN, 34 pp.

Wooding, R.A., E.F. Bradley, and J.K. Marshall, 1973: Drag due to regular arrays of roughness elements of varying geometry. Bound.-Layer Meteor., 5, 285-308.

Woodruff, N.P., D.W. Fryrear, and L. Lyles, 1963: Engineering simlitude and momentum transfer principles applied to shelterbelt studies. Trans. Amer. Soc. Agric. Eng., 6, 41-47.

Wright, J.L. and E.R. Lemon, 1966: Photosynthesis under field conditions, VIII: Analysis of windspeed fluctuation data to evaluate turbulent exchange within a corn crop. Agron. J., 58, 255-261.

Wyngaard, J.C. and O.R. Coté, 1971: The budgets of turbulent kinetic energy and temperature variance in the atmospheric surface layer. J. Atmos. Sci., 28, 190-201.

Zingg, A.W. and W.S. Chepil, 1950: Aerodynamics of wind erosion. Agric. Eng., 31, 279-284.

APPENDIX A

EFFECT OF MEAN AND FLUCTUATING VERTICAL VELOCITY ON MEASURED HORIZONTAL VELOCITY

A hot wire anemometer measures the velocity of moving air in a plane perpendicular to the wire axis. With the axis oriented horizontally the vector sum of the horizontal and the vertical velocities (U_{meas}) will be measured:

$$U_{meas} = \sqrt{(U + u)^2 + (W + w)^2}. \tag{A-1}$$

In the data reduction process, a voltage was first converted into an equivalent U_{meas} and the measured velocities were averaged into a mean measured velocity $\overline{U}_{meas}$:

$$\overline{U}_{meas} = U\left[1 + \frac{2u}{U} + \frac{u^2}{U^2} + \frac{W^2}{U^2} + \frac{2Ww}{U^2} + \frac{w^2}{U^2}\right]^{\frac{1}{2}}. \tag{A-2}$$

Since:

$$[1 + r]^{\frac{1}{2}} = 1 + \frac{1}{2}r - \frac{1}{8}r^2 + \frac{1}{16}r^3 + \ldots$$

then neglecting higher order terms:

$$\overline{U}_{meas} \simeq U\left\{1 + \frac{W^2}{U^2}\left[\frac{1}{2} - \frac{1}{8}\left(\frac{W^2}{U^2}\right) - \frac{(\overline{u^2} + 3\overline{w^2})}{4U^2}\right] + \frac{1}{U^2}\left[\frac{\overline{w^2}}{2} - \frac{W\overline{uw}}{U}\right]\right\}. \tag{A-3}$$

A.1 Error Due to Non-zero Mean Vertical Velocity

If turbulent fluctuations are neglected, Eq. (A-3) becomes:

$$\overline{U}_{meas} \simeq U\left\{1 + \frac{W}{U^2}\left[\frac{1}{2} - \frac{1}{8}\left(\frac{W^2}{U^2}\right)\right]\right\}. \tag{A-4}$$

The velocity profiles taken upwind, downwind, and inside of the test bush can be used to estimate the mean vertical velocity. If the volume occupied by the branches is much less than the bush volume, then the continuity equation becomes:

$$\frac{\partial U}{\partial x} + \frac{\partial V}{\partial y} + \frac{\partial W}{\partial z} = 0 . \qquad \text{(A-5)}$$

The $\partial V/\partial y$ term will be neglected, resulting in a maximum vertical velocity estimate (W_{max}) from finite differences:

$$W_{max} = \int_0^z - \left(\frac{\Delta U}{\Delta x}\right) dz . \qquad \text{(A-6)}$$

Using the velocity profiles to measure $\Delta U/\Delta x$, the largest value of W_{max}/U is found to be 0.15. Substitution in Eq. (A-4) results in $\overline{U}_{meas} = 1.01\ U$. Therefore, the effect of the mean vertical velocity on the measured horizontal velocity may be neglected.

A.2 Error Due to Vertical Velocity Fluctuations

If $W = 0$, Eq. (A-3) becomes:

$$\overline{U}_{meas} \simeq U \left[1 + \frac{\overline{w^2}}{2U^2}\right] . \qquad \text{(A-7)}$$

Assuming $\overline{w^2}/\overline{u^2} = 0.27$ (Frost et al., 1975), then the largest turbulent intensity observed, $\sqrt{\overline{u^2}}/U = 0.7$, gives $\overline{U}_{meas} = 1.07\ U$. The more normal turbulent intensity of 0.3 results in $\overline{U}_{meas} = 1.01\ U$. Thus under all but the most extreme conditions this source of error is negligible.

APPENDIX B

STRESS ESTIMATION FROM AN EQUILIBRIUM LAYER ASSUMPTION

As defined by Townsend (1961), an "equilibrium layer" is a region where equilibrium exists between the local rates of energy production and dissipation. In general the turbulent kinetic energy of a flow may depend as much on transport processes from remote locations as on the local production and dissipation. Near a rigid boundary, however, the flow is often virtually unaffected by the flow in adjacent areas. Equilibrium, or quasi-equilibrium, layers have a universality of structure independent of the history of the flow, resulting in a simple dependence of the mean velocity gradient on the Reynolds stress and distance from the boundary, i.e. apparent validity of the mixing length momentum transfer theory. The most familiar equilibrium layer is a constant stress region which has a logarithmic velocity profile. However in flows with an adverse pressure gradient the constant stress region forms only a small part of the total equilibrium layer (Townsend, 1961).

Laboratory experiments examining the flow near both smooth and very rough walls have shown the production and generation terms to greatly exceed the other terms of the turbulent energy equation near the wall (Hanjalic and Launder, 1972; Klebanoff, 1955; Townsend, 1951). This equilibrium region where the production and dissipation terms balance covered 1/5 of the boundary layer depth, or about 10 times the height of the roughness elements for a rough surface. Both terms increased greatly close to the solid boundary.

An equilibrium region has also been found close to the wall downwind of a model windbreak (Good and Joubert, 1968).

The use of an assumed equality between mechanical energy production and dissipation to calculate the momentum flux in the atmosphere was first proposed by Deacon (1959) and demonstrated by Taylor (1961). Under neutral conditions with locally isotropic, horizontally homogeneous, and stationary turbulence, the turbulent energy equation reduces to:

$$-\overline{uw}\,\frac{\partial U}{\partial z} = \varepsilon \qquad \text{(B-1)}$$

and gives:

$$u_* = (kz\varepsilon)^{1/3} \qquad \text{(B-2)}$$

when a logarithmic velocity profile is assumed.

In the following sections the use of Eq. (B-2) to measure the ground friction velocity will be justified for the flow both outside and inside a bush at a height of 4 cm. In both cases, the assumption is made that the shear stress measured very near the ground is equal to that at the ground itself. This is valid for a spot between shrubs, but less apparent for bush flow. Support for the latter case does come from Wilson and Shaw (1976) whose model for canopy flow found little shear stress variation close to the ground.

While the equilibrium between production and dissipation is more fully realized closer to the ground, it does not extend to the viscous region where the turbulence Reynolds number is so small that viscous effects become important and local isotropy no longer exists. The equilibrium depends upon fully turbulent (high Reynolds number) flow, but this is certainly the condition at a 4 cm height.

To use Eq. (B-2) a velocity spectrum density function was found by Fourier transformation of the hot wire anemometer data. For the inertial subrange, the velocity spectral density function $[S_u(n)]$ is:

$$S_u(n) = (U/2\pi)^{-2/3} \alpha_1 \varepsilon^{2/3} n^{-5/3} \qquad \text{(B-3)}$$

where α_1 = one-dimensional Kolmagorov constant
n = frequency

so a straight line with a slope of -5/3 was fit by eye to the inertial subrange of a $\ln [S_u(n)]$ vs. n curve, from which ε could be calculated using a value of 0.5 for α_1.

B.1 Flow Between Shrubs

In this section the use of Eq. (B-2) will be justified for flow outside a bush. Some disagreement has been voiced over whether the turbulent energy equation equilibrium is between the dissipation term and the total (mechanical and bouyancy) production terms (Busch and Panofsky, 1968) or just the mechanical production term (Fichtel and McVehil, 1970). In the most complete study to date, Wyngaard and Cote´ (1971) showed that the dissipation exceeds the total production slightly for non-neutral conditions (Fig. 23). Therefore the magnitude of the bouyancy term can be important and must be estimated. The bouyant production term $g\ \overline{\theta w}/T$ cannot be computed directly from the available data. An indirect approach using similarity theory results will be utilized.

The extensive investigation of the atmospheric energy budget conducted by Wyngaard and Cote´ (1971) found an empirical expression

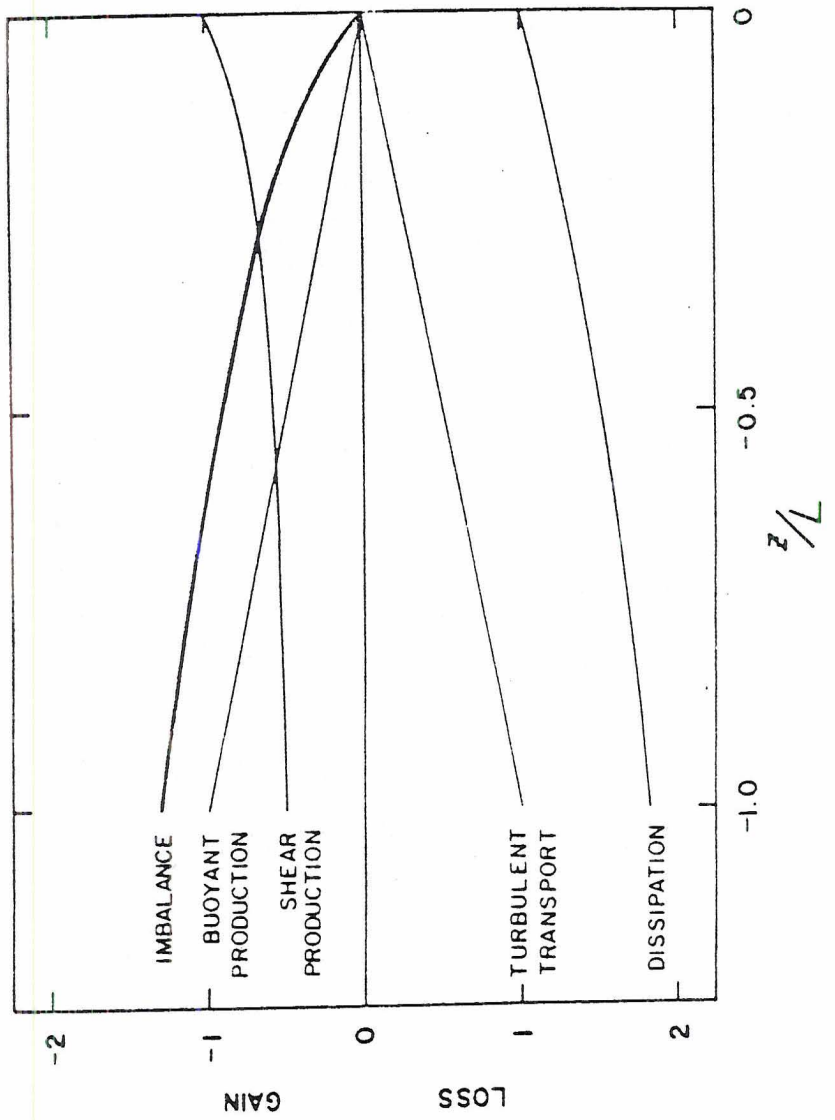

Fig. 23. Relative Magnitude of Terms in the Turbulent Kinetic Energy Equation (after Wyngaard and Coté, 1971)

for the imbalance between mechanical turbulent energy production and dissipation:

$$\overline{uw}\,\frac{\partial U}{\partial z} + \varepsilon = I \qquad \text{(B-4)}$$

where the imbalance term I is a function of ζ. This imbalance results from the sum of the bouyant production, the pressure transport, and the turbulent transport terms of the turbulent kinetic energy equation. Elliott (1972) measured the pressure-velocity correlation directly and concluded that below 5 m this term is negligible under neutral conditions. The term is small in itself and it is also partially balanced by the turbulent transport terms. Thus the imbalance term is mainly due to bouyancy production. Combining Eq. (B-4) with the diabatic velocity gradient expression of Businger, et al. (1971), Champagne, et al. (1977) derived the result:

$$u_* = \gamma(kz\varepsilon)^{1/3} \qquad \text{(B-5)}$$

where γ = diabatic correction factor = $[1 + 0.5\,|\zeta|^{2/3}]^{-3/2}$. They obtained good agreement between indirect measurements of u_* using Eq. (B-5) and direct measurements using $\overline{uw}$ at a 4 meter height in a Minnesota field.

To estimate the diabatic correction factor γ at a 4 cm height for the isolated spot, ζ must first be estimated. A derivation results in:

$$\zeta = \frac{z}{L} = \frac{gk^2z^2(K_h/K_m)(\frac{\partial T}{\partial z} + \Gamma)}{u_*^2 T} \,. \qquad \text{(B-6)}$$

For $z = 4$ cm, and assuming:

1) $K_h/K_m \rightarrow 1.35$ as $\zeta \rightarrow 0$ (Businger, 1971)

2) $\partial T/\partial z >> \Gamma$ very close to the ground

3) $(U_*)_g = 0.114\ U(4\text{ cm})$

4) $U(4\text{ cm}) = 1$ m/sec and $T(4\text{ cm}) = 42°C$

5) $\partial T/\partial z \simeq -0.67°C/\text{cm}$ @ 4 cm, based upon a fit of the observed temperatures to the temperature profile equations of Malurkar and Ramdas (1931).

The computed values are $\zeta = -0.050$ and $\gamma = 0.97$.

Therefore, the mechanical production dominates the bouyant production of turbulent kinetic energy at this height, i.e. the velocity gradient near the bounary dominates the temperature gradient in producing turbulent kinetic energy. For all practical purposes, therefore, Eq. (B-2) can be used to estimate $(U_*)_g$ from the dissipation, i.e. to a good approximation $\gamma = 1$ very close to the ground. This result is supported by Hess and Panofsky (1966) and Elliott (1972), who both found that the equilibrium of the production and dissipation terms of the turbulent kinetic energy equation is not significantly affected by bouyancy within 6 m of the ground, even for quite unstable conditions. $(U_*)_g$ calculated by this method for an isolated spot is found to be a function of wind speed, approaching under high wind conditions the 0.114 value derived by assuming a logarithmic wind profile below bush height (Table 10, Fig. 11). This result lends credence to the arguments presented above, since the assumptions required for both a logarithmic wind profile and Eq. (B-2) are better met at higher wind speeds, and therefore the two methods of estimating $(U_*)_g$ should approach each other under such conditions.

TABLE 10

$(U_*)_g/U$ and $(U_*)_g/\overline{\sigma_u}$ Between Shrubs at 4 cm Height

U (m/sec)	$\overline{\sigma_u}$ (m/sec) (A)	ε (m^2/sec^3) (B)	$(U_*)_g$ (m/sec) (C)	$\frac{(U_*)_g}{U}$	$\frac{(U_*)_g}{\overline{\sigma_u}}$
1.40	0.57	0.47	0.20	0.14	0.35
0.98	0.43	0.29	0.17	0.17	0.38
0.46	0.34	0.20	0.15	0.32	0.44
0.92	0.49	0.91	0.24	0.27	0.50
1.49	0.63	0.87	0.24	0.16	0.38
1.87	0.83	2.00	0.32	0.17	0.38
2.14	0.68	0.83	0.24	0.11	0.35
2.01	0.61	0.96	0.25	0.12	0.41
1.69	0.66	1.01	0.25	0.15	0.38
1.91	0.72	0.78	0.23	0.12	0.32
2.01	0.67	0.92	0.25	0.12	0.37
2.03	0.80	1.26	0.27	0.13	0.34
2.28	0.86	1.89	0.31	0.14	0.37
1.87	0.80	0.83	0.24	0.13	0.30
2.56	0.90	1.67	0.30	0.12	0.33
2.23	0.90	1.45	0.29	0.13	0.32
1.74	0.70	0.94	0.25	0.14	0.35
1.68	0.83	1.91	0.31	0.19	0.38
1.94	0.78	1.55	0.29	0.15	0.37
2.11	0.78	1.85	0.31	0.15	0.40
2.07	0.77	1.17	0.27	0.13	0.35
2.51	0.85	1.42	0.28	0.11	0.33

TABLE 10 (cont'd)

U (m/sec)	$\overline{\sigma_u}$ (m/sec)(A)	ε (m^2/sec^3)(B)	$(U_*)_g$ (m/sec)(C)	$\frac{(U_*)_g}{U}$	$\frac{(U_*)_g}{\overline{\sigma_u}}$
2.24	0.89	1.07	0.26	0.12	0.29
1.77	0.86	2.85	0.36	0.20	0.42
Average				0.15	0.37
				σ = 0.05	σ = 0.05

(A) Based upon 5 second wind averages

(B) From velocity spectrum measurements

(C) Using $(U_*)_g = [kz\varepsilon]^{1/3}$

B.2 Flow Inside a Bush

The conditions for an equilibrium layer inside a bush are difficult to establish theoretically and must be estimated from experimental measurements. Before making these calculations, some results from experiments in vegetative canopies will be mentioned. Cionco (1965) derived the mixing length variation with height from vegetative canopy wind measurements. He found a constant proportion between the mixing length and height for the lower quarter of a canopy, the proportionality constant being close to the von Karman constant. Above this region the roughness element effect upon the flow was evident, as the mixing length remained constant with height. Uchijima and Wright (1964) found similar results up to half the canopy height for a corn crop of relatively sparse spacing, while Schuepp and White (1975) found a logarithmic velocity region up to one-tenth the height of their model canopy of closely spaced elements. Wilson and Shaw (1976) used a turbulence closure scheme canopy flow and found the dissipation to balance the production up to 0.15 the canopy height. These results imply that the lower layer is an equilibrium region. The depth of the equilibrium region may depend upon the spacing of the branches in the canopy.

The necessary equilibrium layer conditions will now be estimated for a creosote bush from field measurements. The bouyancy term will be neglected, as the last section found it to be negligible. The condition that the transport terms be much less than the production terms is satisfied, assuming two-dimensional flow and neglecting buoyancy production, when:

$$U \frac{\partial q}{\partial x} + W \frac{\partial q}{\partial z} << -\overline{uw} \frac{\partial U}{\partial z} . \qquad (B-7)$$

The following assumptions are made:

1) $q \approx \overline{u^2}$

2) $(U_*)_g$ inside bush $\approx 0.3\ (U_*)_g$ outside, based upon the results of surface stress predictions

3) $\partial U/\partial z = (U_*)_g/kz$

4) $-\overline{uw} = (U_*)_g^2$.

Measurements, adjusted by assuming that U and u are proportional to a reference velocity at a 2 m height, give:

1) U(4 cm)(inside bush) = 0.176 U(2 m)

2) $(U_*)_g$(outside bush) = 0.054 U(2 m)

3) $\Delta(\overline{u^2})/\Delta x = -(5.2 \times 10^{-4})\ U^2(2\ m)$

4) W(4 cm) = 0.0015 U(2 m), based upon continuity equation calculations in Appendix A

5) $\Delta(\overline{u^2})/\Delta z = 0.054\ U^2(2\ m)$

and Eq. (B-6) then becomes:

$$[-9\text{x}10^{-5}]U^3(2\ m) + [8\text{x}10^{-5}]U^3(2\ m) << [26\text{x}10^{-5}]U^3(2\ m). \qquad (B-8)$$

This condition appears to be well met, but only because the two advection terms cancel each other out. There is no doubt that this is qualitatively true, for the horizontal velocity flow travels from a higher turbulence region to a lower one while the vertical velocity flow does the opposite. But while the horizontal advection term estimate is based upon adequate measurements, the magnitude of the vertical advection is based on measurements with a vertical spacing so large that the calculated value can only be considered a rough estimate.

A second criteria that must be met is for the diffusion terms also to be much less than the production terms, i.e.:

$$\frac{\partial}{\partial z}\left[\overline{qw} + \overline{pw}\right] << -\overline{uw}\,\frac{\partial U}{\partial z} \,. \qquad \text{(B-9)}$$

Estimating the diffusion terms directly is not possible, but Townsend (1961) states that they are usually of the order $(q)^{3/2}$, which for the present case is about 0.010. Eq. (B-9) then becomes 0.010 << 0.086, so this condition is also reasonably well met.

Since both conditions are met, it is assumed that the local turbulent kinetic energy production equals the local dissipation inside the bush at a height of 4 cm. Therefore Eq. (B-2) can be used to estimate $(U_*)_g$ inside the bush.

APPENDIX C

STRESS ESTIMATION FROM TURBULENCE INTENSITY MEASUREMENTS

Many investigators have empirically estimated stress by assuming $u_* \propto \sigma_u$ or $u_* \propto \sqrt{q}$. This assumption is based upon experimental data. For example, Hanjalic and Launder (1972) found the ratio between u_* and $\sqrt{q}$ to be constant for an extensive depth in flow over a rough surface.

Unfortunately the proportionality constants obtained show considerable scatter, even when plotted against stability (ζ). Panofsky (1969) states that there is little reason to expect u_*/σ_u to be a "universal" function of ζ due to the lack of similarity between differing sites. For neutral atmospheric conditions u_*/σ_u values of 0.40 (Frost, et al., 1975), 0.43 (McBean, 1971), and 0.56 (Kaimal et al., 1972) have been reported. Laboratory experiments for homogeneous shear flows reported $u_*/\sqrt{q}$ values from 0.52 to 0.57 (Hanjalic and Launder, 1972), where $\sqrt{q} \simeq \sigma_u$. Wilson and Shaw's (1976) turbulence closure theory for a canopy predicted $u_*/\sigma_u = 0.53$ close to the ground.

Measurements of $(U_*)_g/\overline{\sigma_u}$ taken at a 4 cm height at the bush site, using $(U_*)_g$ values determined from dissipation measurements, averaged to 0.37 ($\sigma = 0.05$) for 24 measurements (Table 10), somewhat lower than the values quoted above. However, Grass (1971) has shown that for flow over a rough boundary this ratio is not really a constant but decreases close to the surface. Therefore, the calculated ratio was believed to be valid. This ratio obtained for a spot far removed from the bushes was used to estimate surface stress near and inside the bush.

BIBLIOGRAPHIC DATA SHEET	1. Report No. Atmospheric Science Paper#310	2.	3. Recipient's Accession No.
4. Title and Subtitle Aeolian Transport and Vegetative Capture of Particulates			5. Report Date Fall 1977 6.
7. Author(s) John W. Glendening			8. Performing Organization Rept. No. CSU AS Paper #310
9. Performing Organization Name and Address Colorado State University Dept. of Atmospheric Science Fort Collins, Colorado 80523			10. Project Task/Work Unit No. 11. Contract/Grant No. LLL Subcontract #5594605
12. Sponsoring Organization Name and Address Lawrence Livermore Laboratory Livermore, California 94550			13. Type of Report & Period Covered 14.

15. Supplementary Notes

16. Abstracts

Aeolian (wind-blown) transport of soil particles to which plutonium is attached is responsible for the escape of radioactivity beyond the boundaries of the Nevada Test Site. This thesis concerns the horizontal aeolian erosion of the large particles, which travel close to the ground. They are captured by desert creosote bushes, building radioactive wind hummocks around the shrub bases.

The airflow above and below the average shrub height and inside a bush is investigated. The drag coefficient above the vegetation is found to decrease with increasing wind speed. Below the shrub height, the development of an internal boundary layer results in a logarithmic velocity profile. The bushes are widely spaced and aerodynamically very porous, producing a flow more typical of individual roughness elements than of a plant canopy. Partitioning the total drag above the vegetation into ground drag and bush drag contributions illustrates the dominant role of the vegetation in producing drag and thereby controlling soil erosion.

17. Key Words and Document Analysis. 17a. Descriptors

Wind erosion, air flow within vegetation

17b. Identifiers/Open-Ended Terms

17c. COSATI Field/Group

18. Availability Statement	19. Security Class (This Report) UNCLASSIFIED	21. No. of Pages 149
	20. Security Class (This Page UNCLASSIFIED	22. Price